This document is downloaded from DR-NTU (https://dr.ntu.edu.sg)
Nanyang Technological University, Singapore.

Novel properties and applications of carbon nanodots

Xiao, Lian; Sun, Handong

2018

Xiao, L., & Sun, H. (2018). Novel properties and applications of carbon nanodots. Nanoscale Horizons, 3(6), 565-597. doi:10.1039/C8NH00106E

https://hdl.handle.net/10356/107579

https://doi.org/10.1039/C8NH00106E

© 2018 The Royal Society of Chemistry. All rights reserved. This paper was published in Nanoscale Horizons and is made available with permission of The Royal Society of Chemistry.

Downloaded on 27 Aug 2022 21:56:27 SGT

Novel Properties and Applications of Carbon Nano-dots

Lian Xiao[a], Handong Sun[a b c]*

[a] *Division of Physics and Applied Physics, School of Physical and Mathematical Sciences, Nanyang Technological University,* 21 *Nanyang Link, Singapore 637371*
[b] *Centre for Disruptive Photonic Technologies (CDPT), School of Physical and Mathematical Sciences, Nanyang Technological University, Singapore 637371*
[c] *MajuLab, CNRS-UCA-SU-NUS-NTU International Joint Research Unit, Singapore*

Abstract

In recent decade, carbon dots have drawn intensive attention in its own right and triggered substantial investigation. Carbon dots manifest superior merits including excellent bio-compatibility for both in vitro and in vivo, resistance to photo-bleaching, being easy to surface functionalization and bio-conjugation, outstanding colloidal stability, eco-friendly synthesis, and low cost. All of these endow them the high potential to replace the conventional unsatisfied florescent heavy meal contained semiconductor quantum dots or organic dyes. Even though the picture of their photoluminescence mechanism is still controversial, carbon dots have already exhibited versatile applications. In this article, we summarize and review the recent progress achieved in the field of carbon dots, where we provide the comprehensive summary and discussion on synthesis methods and emission mechanisms in section 2 and 3 respectively. We also present the applications achieved from carbon dots in bio-imaging, drug-delivery, microfluidics, light emitting diode (LED), sensing, logic gates, and chiral photonics *etc.*. Some unaddressed issues, challenges, and prospects of carbon dots are discussed and displayed in the last section. We envision that carbon dots will eventually go to market and become a strong competitor to some currently used fluorescent materials. It is our hope that this review can provide insight into both the fundamental research and practical applications of carbon dots.

Outline of the review

Lian Xiao received his Bachelor's degree in Physics from Sichuan University, China, in 2014. He is currently a year 4 Ph.D. student in the School of Physical and Mathematical Sciences, Nanyang Technological University, Singapore. His research interests include nanomaterials, optical spectroscopy, semiconductor physics and micro-fluidics.

Handong Sun is currently an Associate Professor in the School of Physical and Mathematical Science, Nanyang Technological University. He received his bachelor's degree in physics from Dalian University of Technology, and his master's and Ph.D. degrees from Huazhong University of Science and Technology, and Hong Kong University of Science and Technology, respectively. He was elected to be a Fellow of the American Physical Society in 2016. His research interests cover optoelectronic materials and devices, semiconductor physics, optical spectroscopy, nanomaterials and applications in microfluidics.

1. Introduction

Carbon dots have become the topic of numerous scientific studies since their discovery[1, 2] due to the obvious advantages over the conventional semiconductor quantum dots whose notable toxicity and environmental hazard are well-documented[3-6]. Both in vitro and in vivo toxicity evaluation have demonstrated that carbon dots exhibit excellent bio-compatibility, which along with the photo-stability, chemical inertness, ease of surface function group modification and low cost endow carbon dots vast scope of applications in various fields[2, 7, 8]. The exploration of stable, fast, low-cost synthesis approach is the pre-requisition to make use of carbon dots, and fortunately numerous breakthroughs have been achieved during the past decade. Consequently, carbon dots have become the center of significant research efforts to develop the alternative to replace the unsatisfied traditional florescent materials, and the publications about carbon dots continuously increase since 2006 as seen in figure 1 (The dates are generated from web of science until April-16-2018, search criteria: topic "carbon dots" or "C-dots" or "carbon nanodots" or "graphene quantum dots", database: Web of Science Core collection). Carbon dots synthesized from different approaches share some similar features such as less than 10 nm size, bright fluorescent emission, rich hydrophilic surface groups which endow carbon dots excellent water solubility, bio-compatibility and so on. However, some contradictory behaviors like, non-photo blinking[2, 9] and photo blinking[10-12], pH stable[13] and pH dependent PL[14, 15], carbon dots size dependent[13, 16-18] and size independent PL[19, 20], excitation dependent[20] and independent PL[13, 21] *etc.* have been reported by different research groups. All of these attributes indicate that carbon dots represent a much complex system than expected. It seems that the diverse behaviors of carbon dots result from the different synthesis approaches, namely, different synthesis methods will result in different types of carbon dots [21]. Therefore it is necessary to provide the synthesis method when talking about carbon dots. Thus prior to discussion about the optical properties and applications, we first present the synthesis approaches of carbon dots adopted during the past decades in section 2 of this review. After more than 10 years of efforts, numerous synthesis methods including several intriguing one-step approaches have been discovered by researchers. Generally, carbon dots synthesis methods can be divided into two categories: top down and bottom up, and each of them contain many sub-categories which will be shown in detailed in section 2. What is exciting for carbon dots is that researchers have successfully explored the highly luminescent carbon dots whose quantum yield is up to 80%[22], which is comparable to the conventional semiconductor quantum dots and the emission range can be tuned from deep UV to near IR by proper choosing synthesis approaches and precursors[13, 17, 23-28].

To make better use of carbon dots and tune the optical properties, a full understanding of carbon dots emission is essential. Ironically, the actual emission mechanisms of carbon dots are still controversial even though some breakthroughs have been obtained in recent years. In section 3, we summarize and display the emission models proposed by different authors and also provide the key evidences for each emission mechanism. Some of the mechanisms are mutually complementary, while some of them are in sharp conflict. We speculate that different emission mechanisms may be applied to one or more kinds of carbon dots, but cannot be valid to all kinds of carbon dots.

The applications of carbon dots are exhibited in section 4. In this review, we focus on the optical and optoelectronic applications including bio-imaging, drug delivery, microfluidic application, light emitting diode (LED), sensing especially for the high resolution ratiometric sensing, chemical logic gates and chiral photonics. Carbon dots demonstrate good performances in all of the above applications. In the last section, we will show a brief summary and discuss on the challenges and prospects of carbon dots in further exploration. This article is not intended to be a comprehensive review (or a complete list of published results) in the research field of carbon dots, but rather some selective helpful insights chosen from our direct experience as well as the recent literature of the subject. We hope that this review article can present a clear picture for carbon dots from synthesis, characterization to applications, and give valuable insight into both fundamental physics and practical applications. In addition, we also hope to offer some perspectives and clues to further improve the optical properties and explore more far-reaching applications of carbon dots.

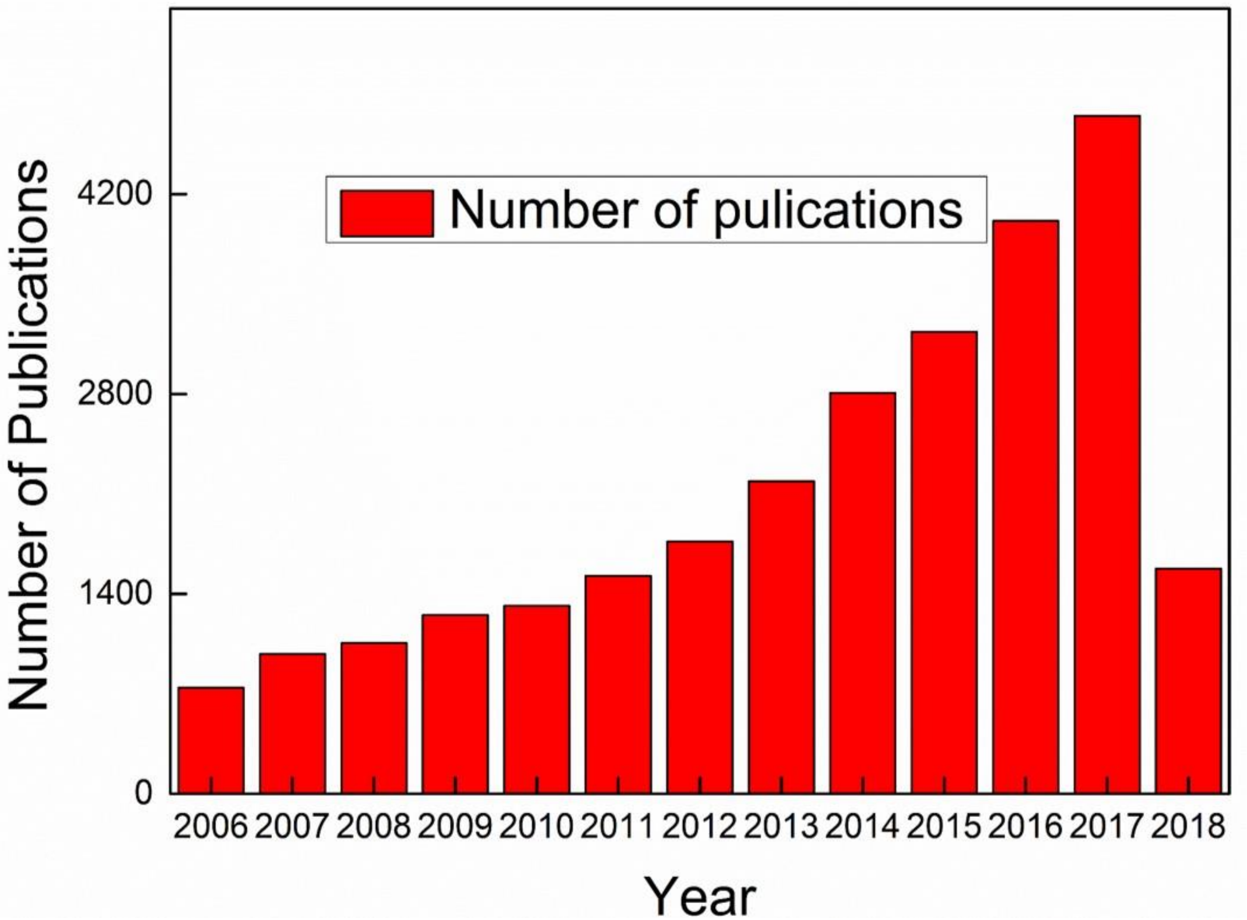

Figure 1 Number of publications about carbon dots since 2006. Dates are generated from web of science until April-16-2018, search criteria: topic “carbon dots” or “C-dots” or “carbon nanodots” or “graphene quantum dots”, database: Web of Science Core collection.

2. Synthesis approaches

Since discovered fortuitously by Xu *et al.* in 2004[1], later named by Sun *et al* in 2006[2], researchers have paid numerous attention to carbon dots because of their striking advantages. However, the stable, economic, easy and fast synthesis method is the prerequisite to further explore the properties and applications of carbon dots. Overall, carbon dots synthesis methods can be divided into two categories, either top down or bottom up, based on the starting carbon source. Top down method is realized by directly exfoliating the bulk carbon source such as graphite, graphene, carbon fibre *etc.* into nano-scale carbon dots, followed by surface treatment. Opposite to direct exfoliation, bottom up methods synthesize carbon dots from carbon element contained small molecules such as glucose, citric acid *etc.* In this part, we will review the main progress of carbon dots synthesis achieved by researchers for both top down and bottom up approaches. To improve and tune the optical properties such as quantum yield, emission wavelength, photo-stability *etc.*, surface passivation and hetero-atom doping have always been employed during the carbon dots synthesis process, which are also displayed in each synthesis method separately. We want to emphasize that it's not reasonable to evaluate which method is the best synthesis approach. As we discussed in the section 1, different kinds of carbon dots exhibit different and even opposite properties, thus we suggest that the choice of the synthesis method depends on the applications and requirement.

2.1 Top down approach of fabricating carbon dots

2.1.1 Arc-discharge method

In 2004[1], *Xu et al.* utilized the preparative electrophoresis method to purify the arc-discharged single welled carbon nanotube soot. After purification, the crude nanotube soot segregated into three isolated parts: long nanotubes, short tubular materials and a new kind of nanodots which was located at the fast moving band. Surprisingly, the nanodots could emit bright light under 365nm light excitation. Further elution separated the mixed florescent band into green-blue, yellow and orange sub-emission bands. The molecular weights of these three kinds of nanodots were determined to be 3K-10K, 10K-30K, 30-50K NMWL (nominal molecular weight limit) by means of Centricon filtration devices. Element analysis indicated that these kinds of nanodots only contained C (55.93%), H (2.65%), N (1.2%) and O (40.33%), and no heavy metal components were included.

2.1.2 Laser ablation/irradiation approach

Later, In 2006[2], Sun *et al.* proposed a new approach to synthesize fluorescent carbon based nanomaterial and termed it as carbon dots. Briefly, A Q-switched Nd:YAG laser (1064 nm, 10 Hz) has been utilized to ablate a carbon target which was fabricated by hot-pressing of graphite and cement. The flowing acidic treatment was accomplished by 2.6 M nitric acid solution with refluxing for another 12h. There was no detectable PL emission from the acidic treatment sample. However, once the simple molecular was linked to surface of the dots by surface treatment, bright luminescence could be observed from the carbon dots. The authors demonstrated that both diamine-terminated oligomeric poly (ethylene glycol) $H_2NCH_2(CH_2CH_2O)_nCH_2CH_2CH_2NH_2$ (average n ~ 35, PEG_{1500N}) and poly(propionylethyleneimine-co-ethyleneimine) (PPEI-EI) could be used to surface passivate the acidic treated carbon nanoparticle. In the typical surface treatment process, the mixture of the acid treated carbon particles and small molecules (PEG_{1500N} or PPEI-EI) was heated to 120 °C for 72 h. The resultant carbon dots had an average diameter of 5 nm and showed bright photoluminescence (PL) with the quantum yield reaching to 10% when excited by a 400 nm laser, as illustrated in figure 2a-c. The PL spectra would change when excitation wavelength were different, termed as excitation dependent PL, as depicted in figure 2b and 2c. Besides, carbon dots exhibited much stable emission under continuous photo-excitation for several hours.

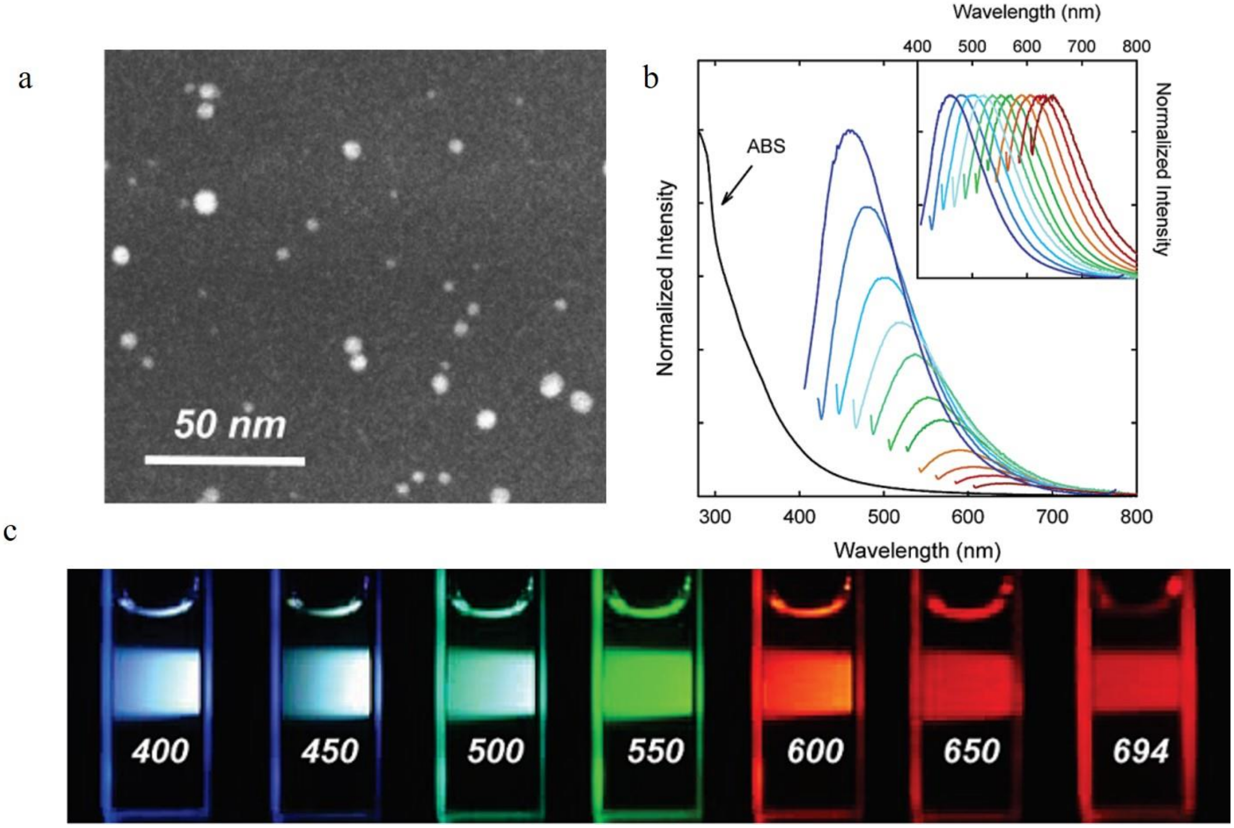

Figure 2 a). STEM imagine of PEG_{1500N} surface passivated carbon dots. b) Absorption and the emission spectra for different excitation wavelength from 400 nm to 600 nm with an increase step of 20 nm. c) The photograph when excited by different excitation wavelength as indicated in the figures. a–c) Reproduced with permission[2]. Copyright 2006, American Chemical Society.

Later, the amended approaches by combining the laser ablation and surface modification process into one procedure were also reported[7, 20, 29, 30]. The authors used a Nd:YAG pulsed laser (wavelength of 1.064 μm and power density $6.0 * 10^6$ W/cm^2) to irradiate the mixture of graphite and organic solvent resulting in the carbon dots synthesis and surface modification accomplished simultaneously. Besides, the researchers also proposed that the emission properties of carbon dots could be tuned by properly choosing the organic solvent such as, PEG_{2000N}, diamine hydrate, diethanolamine *etc.*

2.1.3 Electrochemical approach

The electrochemical approach to synthesizing blue carbon dots from multi-walled carbon nanotubes (MWCNT) was first suggested by Ding's group[31]. The MWCNT, fabricated by scrolling the layered graphene on carbon paper by chemical vapor deposition (CVD), was used as working electrode in an electronchemical cell which comprised a Pt wire counter electrode and an Ag/$AgClO_4$ reference electrode. The degassed acetonitrile solution which included 0.1 M tetrabutylammonium perchlorate (TBAP) was prepared as the supporting electrolyte solution. After certain cycles with applied potential from -2 to 2 V at a scan rate 0.5V/s, the colourless electrolyte solution changed to dark brown which indicated the formation of carbon dots. The obtained carbon dots sample were purified by evaporating the acetonitrile, re-dissolving in water, and dialyzing with cellulose ester membrane bag. The purified carbon dots shown a narrow size distribution being 2.8 ± 0.5 nm with a lattice spacing about 3.3Å. When excited by a 340 nm light source, the carbon dots emitted bright blue light with the quantum yield of 0.064.

Li and co-workers[32] also employed the electrochemical approach to synthesizing carbon dots, while they used the graphite as both the anode and cathode with the current intensity in the range of 10-200 mA/cm^{-2}. They have demonstrated that the electrolyte environment played an important role for the carbon dots formation. When the electrolyte was alkaline (for example NaOH/EtOH), carbon dots could be synthesized successfully, while the acid electrolyte (for example H_2SO_4/EtOH)) could not form the carbon dots. (HR)TEM analysis shown that the synthesized carbon dots had the diameter within 4 nm with the lattice spacing around 0.32 nm.

In addition to the graphite and carbon nanotube, other bulk carbon source such as graphene film, carbon fiber *etc.*[33-35] have also been employed to synthesize carbon dots by means of electrochemical approach.

2.1.4 Chemical exfoliation method

Liu and co-workers [19] were the first to employ the oxidative acid to synthesize carbon dots from bulk candle soot which was prepared from the smoldering candles. They refluxed the candle soot with 5M HNO_3 and followed by centrifugation and neutralization. Polyacrylamide gel electrophoresis (PAGE) was also utilized to further purify and separate the different component of the soot mixture. The electrophoresis results indicated that the soot mixture was consisted of three kinds of species: fast-moving fluorescent band, slow-moving non-florescent band, and agglomerated band. The fast emission band could further separate into 9 sub-bands located at different position of the column, all of them were eluted from gels and dialyzed against distilled water for several times. The obtained carbon dots had the similar height about 1 nm revealed by AFM, while the emission spectra were different for different column band carbon dots.

In addition to candle soot, carbon dots synthesized from chemical exfoliation of carbon fibers was reported by Ajayan's group[18]. The mixture of concentrated H_2SO_4 and HNO_3 was prepared to exfoliate the carbon fiber. The carbon fiber was added to the concentrated acid followed by 2 h sonic treatment. After that, the mixture was heated to a certain temperature for 24 h with vigorous stirring. The synthesized carbon dots exhibited a relatively narrow size distribution (diameter was between 1-4 nm) with a lattice parameter of 0.242 nm. The authors also demonstrated that the optical properties (absorption and PL) of carbon dots could be tuned by simply controlling the reaction temperature which shall yield different size of carbon dots. Later Ye and co-workers[36] also employed concentrated H_2SO_4 and HNO_3 to exfoliate coal to synthesize carbon dots.

2.2 Bottom up approach of fabricating carbon dots

2.2.1 Thermal Pyrolysis approach

The one step thermal pyrolysis method was first discovered by Emmanuel P. Giannelis's group[37]. Different ammonium citrate salts have been utilized to synthesize carbon dots, where the citrate part provided the carbon source while organic ammonium part served as the surface modifier. And both organophilic and hydrophilic carbon dots could be achieved by choosing proper surface modifier *e.g.* octadecyl ammonium ($C_{18}H_{37}NH_3^+$) citrate salt for organophilic and 2-(2-aminoethoxy)-ethanol ($OHCH_2CH_2OCH_2CH_2NH_3^+$) salt for hydrophilic carbon dots respectively. Even for both kinds of carbon dots, the linkage between the organic corona and cores were accomplished through covalently amide linkages which were formed by the thermal dehydration of ammonium carboxylate moieties, while the sample preparation avenues for organophilic and hydrophilic carbon dots were different. Specifically, the organophilic carbon dots were synthesized by directly calcining the pretreatment citric acid monohydrate in air at the temperature 300°C for 2h with a heating rate of 10°C/min, however in the case of hydrophilic carbon dots synthesis, the mixture of citric acid monohydrate (2 g, 9.5 mmol) and $HOCH_2CH_2OCH_2CH_2NH_2$ (1.3 g, 12.4 mmol) was dissolved in 10 ml water, and dried at 65°C resulting in thick syrup. Teflon equipped stainless steel autoclave has been utilized to heat the thick syrup at temperature of 300°C for 2 h. For both kinds of carbon dots, the relative low melting point of the ammonium citrate salt guaranteed the uniform growth of carbon dots from liquid phase. TEM analysis showed that organophilic carbon dots revealed mono-disperse dots of near spherical shape with an average diameter of 7 nm, while hydrophilic carbon dots revealed less mono-disperse distribution with an average diameter of 7 nm.

Later Emmanuel P. Giannelis's group[38] did a comprehensive investigation of carbon dots pyrolysis process. Citric acid monohydrate ($C_6H_8O_7$) and ethanolamine (C_2H_7ON) were employed to synthesize carbon dots in different pyrolysis temperature in the absence of solvent and under reflux in air. The authors demonstrated that on the condition of low temperature such as pyrolysis at 180°C for 30 min (termed as CNP180), the pyrolysis resulted in carbon dots precursors, and the strong PL emission originated from organic fluorophores. There were several evidences which supported the molecular assumption: 1. No carbon dot particles have been observed by either DLS or TEM. 2. The sample showed excitation independent PL with a remarkable quantum yield of 50%. More specifically, the authors suggested[38] the amide related molecular contributed to the emission of carbon dots molecular precursor, which was verified by FTIR, XPS and ^1H & ^{13}C

NMR. To further confirm the amide related functional groups, amide was also synthesized by alternative approach using citric acid monohydrate ($C_6H_8O_7$) and ethanolamine (C_2H_7ON) as the row materials, the results showed that the amide and the carbon dots precursor exhibited similar optical behaviors which validated the mechanism.

Higher temperature (*e.g.* at 230℃ for 30 min, CNP230) pyrolysis triggered the carbon dots formation, which have been verified by TEM analysis where the carbon dots shown a spherical morphology with an average size of 19 nm. The authors claimed[38] that the carbon dots formation was the result of extensive crosslinking reactions and the appearance of interchain imide bonds substantiated by the FTIR spectrum. Element analysis showed that the hydrogen component of CNP230 (44.85% C, 5.75% H, 10.85% N) decreased compared to CNP180 (41% C, 7.8% H, 11.7% N). The PL quantum yield of CNP230 decreased to 15%, while the excitation dependent PL started to appear.

Increasing the temperature to 300℃ resulted in darkening of the sample and the synthesized carbon dots had an average size of 8 nm. TGA-MA analysis uncovered[38] that some CO_2 emanated from the mixture during the pyrolysis which contributed to the decrease of size of carbon dots. Element analysis exhibited an increased C component (50.5% C, 3.7% H, and 13.1% N) which indicated the further carbonization. Different from CNP180 and CNP230, CNP300 displayed distinct excitation dependent PL with the quantum yield about 4%. Further increasing the pyrolysis temperature to 400℃ resulted in cluster and nonuniform particle with the size reach to several hundred nanometer caused by the aggregation. Even though the resultant carbon dots could still emit light, the intensity was very low.

Later, Fu Wang *et al*[39] synthesized carbon dots by means of pyrolyzing the citric acid in molten $LiNO_3$ with the argon as the protecting gas. Compared to solid $LiNO_3$, the molted alkali metal nitrates could endow the nitrate anion with the ability to form an anion O_2 or an oxygen atom O, which could serve as the oxidizing condition. Also the surface passivation could strongly improve the emission intensity. In a typical experiment, the mixture of carbon dots and PEG_{1500N} were dissolved into the mixture of water and toluene. The surface passivation was started by separating the water from the mixture through a water segregator, the reaction was finished when the water was totally removed from the mixture. The passivated carbon dots had increased diameter of about 5-8 nm with the PL quantum efficiency reaching 10%.

Beside the citric acid salt, other small molecular such as ethylenediamine-tetraacetic acid salts, synthetic polymer *e.g.* epoxy-enriched polystyrene (PS), natural materials such as hair, green tea, konjac flour, paprika *etc.*[40-47] have also been employed to synthesize carbon dots by means of thermal pyrolysis approach.

2.2.2 Hydrothermal method

Carbon dots synthesized from hydrothermal method was reported in 2011[48]. Briefly speaking, glucose and monopotassium phosphate (KH_2PO_4) were mixed with a certain molar ratio and dissolved into DI water. Nitrogen has been employed to remove the oxygen dissolved in water. Then the sealed Teflon-lined autoclave chamber was transferred to an oven and reacted at 200℃ for 12 h. After that, the mixture was centrifuged at 9000 rpm to separate the precipitate, the upper supernatant was gathered and freezing dried, followed by re-dissolving the carbon dots into ethanol to form a suspension. After 2 h hours standing, the salt would precipitate from the solution and was removed by a PTFE syringe filter with pore size of 1 μm. Further purification was finished by Spectra/Por dialysis membrane whose cut-off molecular weight was 100 g/ mol. The advantage of this approach is that the carbon dots formation and surface treatment are accomplished simultaneously. Furthermore, the PL properties of carbon dots could be tuned by altering the concentration of KH_2PO_4[48]. When the molar ratio of glucose/KH_2PO_4 was 1/36, the synthesized carbon dots emitted blue light when excited by UV light, while a molar ratio of 1/26 of glucose/KH_2PO_4 resulted in green emission. TEM analysis indicated that the average diameter was 1.83 nm for 1/36 molar ratio blue and 3.38 nm for 1/26 molar ratio green carbon dots. The observation of $\mathrm{C=C}$ by the FTIR spectroscopy in both carbon dots implied the occurrence of carbonization[48] during the hydrothermal process. In addition, the surface passivation occurred by means of oxidation of –OH groups.

In addition to glucose, natural bio-resources[14] *e.g.* orange juice have also been utilized to synthesize carbon dots by means of hydrothermal treatment at relative low temperature about 150°C. The authors[14] proposed that the carbon dots emission was the result of hydrothermal carbonization of organic component in orange juices such as sucrose, glucose, fructose, citric acid *etc.* TEM images showed that carbon dots have spherical morphology with a narrow diameter distribution between 1.5 and 4.5 nm with a lattice spacing of 0.18 nm. XPS and FTIR analysis disclosed the existence of many hydrophilic function groups such as -OH, -COOH *etc.,* which endowed carbon dots excellent solubility in water. The intriguing features of this approach is that neither post surface passivation treatment nor expensive chemicals are needed, thus this work triggered continuous exploration about bio-resources based carbon dots synthesis in one-step[49, 50].

Later on, Pin-Che Hsu and co-workers[51] proposed that organic molecules which contained amino and carboxylic acid groups such as 2-amino-2-hydroxymethyl-propane-1,3-diol (TRIS), ethylenediaminetetraacetic acid (EDTA), glycine, *etc.* could benefit the carbon dots formation. They claimed that carbon dots formation underwent four steps: dehydration, polymerization, carbonization and passivation. Hydrogen bond played a key role during the molecular assemble, heating leaded to polymerization happen, resulting in the single burst of nucleation. Finally, the solutes reached to the surface of the nuclei through diffusion, resulting in the growth of carbon dots.

Until now, by choosing proper organic molecules and adjusting the reaction environment (such as alkaline or acidic) with controlled surface function groups by means of hydrothermal method, it is possible to synthesize carbon dots with emission wavelength covering the whole visible range [17, 48, 52-55].

2.2.3 Microwave heating method

The intriguing microwave assisted carbon dots synthesis approach was discovered and demonstrated by Yang's group[56]. This method possesses numerous merits such as less time consumption, homogeneous heating, low cost *etc.* Briefly, poly (ethylene glycol) (PEG-200) and saccharide (glucose, fructose *et al.*) were dissolved into DI water to form a transparent mixture. A microwave oven was utilized to heat the solution at the power of 500 W for 2-10 min. The carbon dots was formed once the transparent solution was changed to dark brown mixture. The carbon dots exhibited different average diameter size as the reaction time varied *e.g.* 2.57 ± 0.45 nm for 5 min heating, 3.65±0.6 nm for 10 min heating. X-Ray photoelectron spectroscopy (XPS) unveiled that the main components of carbon dots were carbon and oxygen, and the existence of the rich hydrophilic function groups endowed carbon dots good water solubility, allowing carbon dots for the bio applications. The PL quantum yield of the sample displayed excitation dependent behavior varying from 6.3% to 3.1%.

This novel approach open a new avenue to synthesize carbon dots[57], *e.g.*, Sourov *et al* [58]and Qu *et al*[59] fabricated the green emission carbon dots with relative high quantum yield separately; blue emission carbon dots with high quantum yield of 44.9% (excited by 360 nm) was reported by Jiang *et al*[60]. What's more, Tang *et al* [26]and Sun *et al* [61] achieved even deep UV and near IR emission from carbon dots by using microwave approach.

2.2.4 Anchor/Support based approach

Silica spheres have been employed by Liu's group as the carrier to synthesize carbon dots[62]. The silica spheres could supply anchors which accelerate the polymerization of carbon source. In addition, the aggregation of carbon dots was also suppressed by the spheres during high temperature pyrolysis, which further benefited carbon dots formation. Briefly, the silica surface was first treated by amphiphilic triblock copolymer F127 ($EO_{106}PO_{70}EO_{106}$, Mw = 12600; EO = ethylene oxide, PO =propylene oxide). The surface treatment of silica by F127 surfactant was the prerequisite to synthesize carbon dots. The surfactant F127 could trigger the micellization-like self-assembly happening on the sphere surface. After interaction with water, the copolymer chains of F127 shall extend on the surface of the sphere, resulting in the core-shell silica-F127 surfactant structure. The opened F127 shell contributed to the carbon source enter into the shell layer, which benefited for the molecular loading and polymerization. More specifically, the hydrophilic part of F127 (also called PEO blocks) offered more anchors for resol molecules and strong hydrogen bond interaction, which contributed to the polymerization of resol molecules, resulting in the construction of polymer/F127 surfactant /Silica sphere composites. After the surface treatment of silica, prepared resols as the carbon source was added to the suspension for the polymerization.

To further facilitate polymerization and dehydrogenating the resols, calcination method of these polymer/F127/silica structure has been utilized at temperature 900℃ for 2 h with the Ar as the protection gas. In addition, the surfactant f127 also totally released during the calcination process. After that, the carbon dots was released from the silica sphere by etching with NaOH solution. The surface passivation was still crucial for achieving bright photoluminescence. The post surface treatment was carried out by heating the mixture of carbon dots solution and diamine-terminated oligomeric poly (ethylene glycol), $H_2NCH_2(CH_2CH_2O)_nCH_2CH_2CH_2NH_2$ (PEG_{1500N}) at 120℃ for 72 h. Element analysis exposed that the carbon dots contained C 64.65 wt.%, H 7.67 wt.%, N 1.13 wt.%, and O (calculated) 26.55 wt.%. The average size of carbon dots was in the range of 1.5-

2.5nm. The absence of discernible lattice structure indicated that this kind of carbon dots were amorphous. The carbon dots could emit bright PL with a quantum yield 14.7% when excited by 360 nm light source.

In addition to silica, NaY zeolite have also been employed as the supports to synthesize carbon dots[63, 64]. The authors demonstrated that the anchor assisted carbon dots shown similar PL behaviors with the non-support approach synthesized carbon dots.

2.2.5 MOF template based approach

To achieve the uniform, ultra small carbon dots, Zhi-Gang Gu and co-workers[65] made use of well-defined pore size of metal–organic frameworks (MOFs) as the template to synthesize carbon dots. One of the motivations of this approach is that MOFs possess rich isoreticulars whose pore size vary from 1 nm to 10 nm, which offer the opportunity to synthesize carbon dots with controlled size and morphology. The MOF powder was synthesized using solvothermal method. The glucose (carbon souse) was loaded inside the MOF pore by easily immersing the MOF power into the mixture of glucose and EtOH/H_2O (9:1). The different weight of HKUST-1 MOF samples before (1.00 g) and after (1.13 g) loading confirmed the successful loading of glucose. Glucose started to decompose when the loaded MOF power was heated to 200℃, while the MOF template was still stable even the temperature was as high as 280℃, which was confirmed by the Thermogravimetric (TG) analysis. PXRD analysis demonstrated that the structure of the MOF was not destroyed during calcination. The prominent color changed from blue to green signified the carbon dots formation, the considerable decreasing of N_2 adsorption ability from 130 cm^3/g for pristine MOF to 5 cm^3/g for calcinated MOF indicated the successful filling of MOF pore by carbon dots.

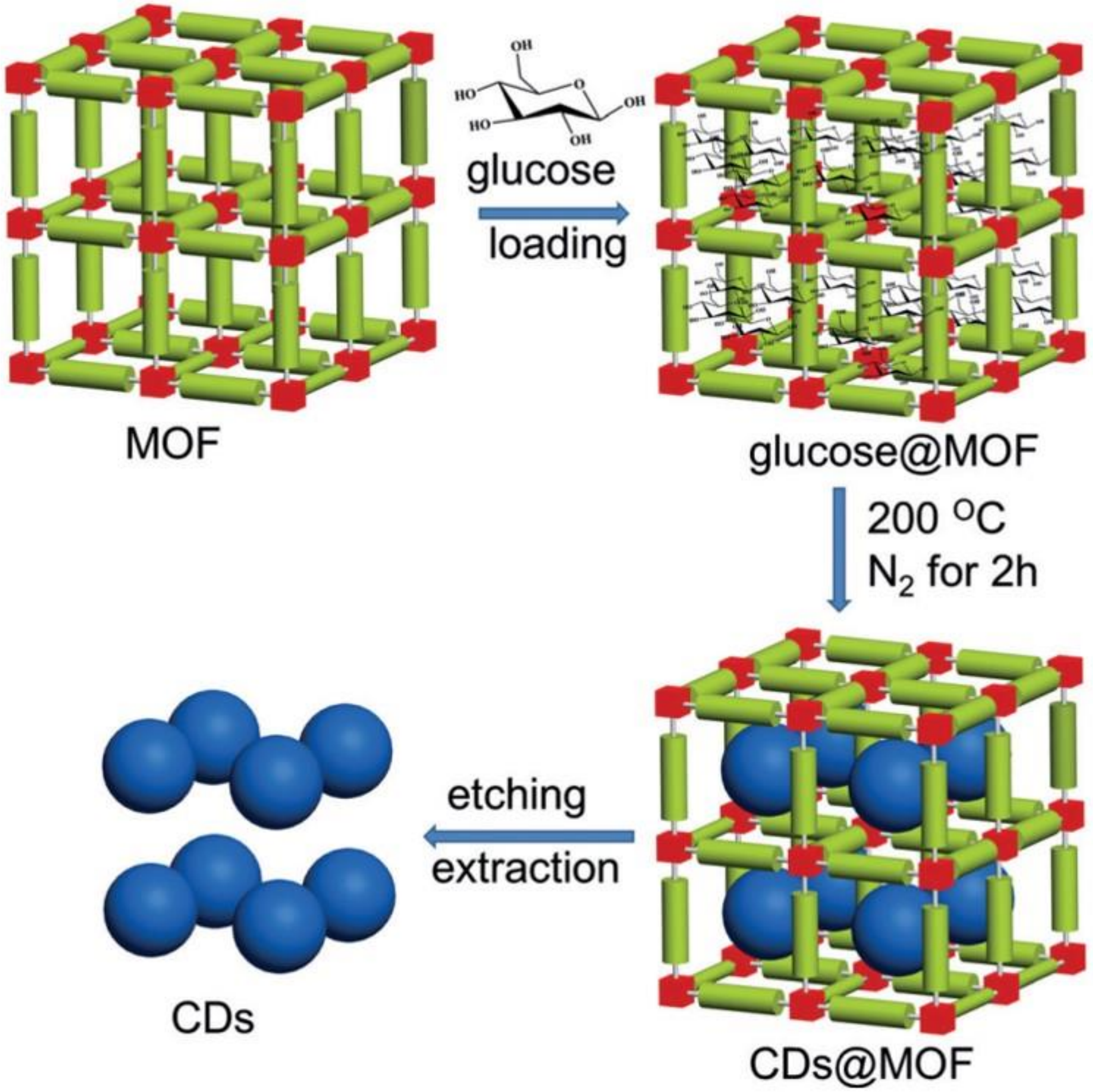

Figure 3 Illustration of carbon dots prepared by using the MOF pore as template. Reproduced with permission[65]. Copyright 2017, Wiley-VCH.

To release the carbon dots from the MOF temperate, aqueous KOH solution was utilized by the authors[65] to dissolve the template, the whole procedure is illustrated in figure 3. After purification, the carbon dots exhibited rather narrow size distribution with an average diameter of 1.5 nm. Actually, this size was close to the large pore size inside the HKUST-1 MOF (HKUST-1 contain 3 kinds of pore: 1.35 nm, 1.1 nm, 0.5 nm), this was the results of the preference to form carbon dots nuclei in the largest pores as proposed by the authors[65]. By choosing different MOFs as templates with different pore sizes, the authors synthesized different sizes of carbon dots, such as, HKUST-1 MOF for 1.5 nm carbon dots with largest pore size 1.35 nm, ZIF-8 MOF for 2.0 nm carbon dots with largest pore size 1.9 nm, MIL-101 MOF for 3.2 nm carbon dots with largest pore size 3.4 nm. However, carbon dots synthesized from MOF template absence method shown a nonregular size distribution with an average diameter of 4.5 nm. All of the results suggested the size and morphology controllability offered by the MOF template. The PL of the carbon dots showed redshift as the size increased from 1.5 nm to 4.5 nm excited by UV light.

Due to the intriguing controllability in size and morphology[66, 67], other template such as mixed soft template (copolymer Pluronic P123) and hard template (ordered mesoporous silica (OMS) SBA-15) also employed by Yang *et al*[68] to develop carbon dots with uniform morphology.

The above mentioned approaches are the most general bottom up methods widely utilized by researchers to synthesize carbon dots. The discovery of versatile bottom up approaches, especially the fast and simple one-step synthesis methods ensure the prerequisite of pushing carbon dots into practical applications. What's more, in addition to the general bottom up methods, researchers also proposed some unusual approaches[69, 70] for example, Liu *et al*[70] demonstrated the avenue which using catalase enzyme to decompose graphitic carbon nitride to synthesize carbon dots at room temperature.

3 Emission mechanism

3.1 Band gap emission and quantum confinement effect

By proper controlling of the reaction precursor and time, Yuan *et al.*[13] claimed that they have synthesized the band gap edge emission carbon dots, and the different color emission originated from the different size effect. All of the different emission carbon dots were synthesized by hydrothermal method. Hydrothermal treatment of the mixture of CA (citric acid) and 2,3-diaminonaphthalene ethanol solution for 4h and 9h resulted in the blue and green emission carbon dots, while hydrothermal treatment of CA and 1,5-diaminonaphthalene ethanol solution for 4h and 9h shall form yellow and orange carbon dots, finally, the red emission carbon dots could be achieved by hydrothermal treatment of the mixture of CA, 1,5-diaminonaphthalene and concentrated sulfuric acid. The wavelength of absorption peaks of the blue (B), green (G), yellow (Y), orange (O) and red (R) carbon dots were located at 350 nm, 390 nm, 415 nm, 480 nm, 500 nm respectively as illustrated in figure 4a, which displayed continuous increase. The corresponding PL peaks were located at 430 nm, 513 nm, 535 nm, 565 nm and 604 nm for B, G, Y, O and R respectively as seen in figure 4b. Different from the previous reported carbon dots, all of the carbon dots here exhibited excitation independent PL, and the PLE peaks coincided with the absorption peaks, both of which indicated that

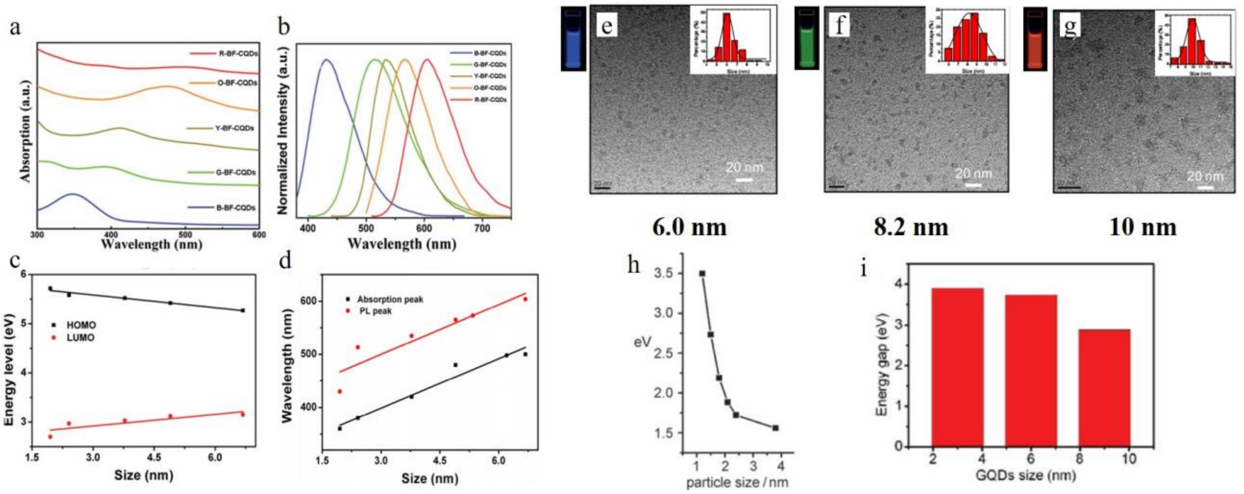

Figure 4 a,b) The absorption and PL spectra of B-, G-, Y-, O-, R- emission carbon dots. c) HOMO and LUMO energy for different size of carbon dots, obtained from UPS spectroscopy. d) The corresponding absorption and emission peaks for different size of carbon dots. e-g) 6 nm, 8.2 nm and 10 nm size carbon dots (synthesized by Jiang et al.) emit blue, green and red light respectively, excitation wavelength 365 nm. h, i) Relationship between carbon dots size and band gap value for Li *et al*'s sample and Peng et al's samples respectively. a-d) Reproduced with permission[13]. Copyright 2016, Wiley-VCH. e-g) Reproduced with permission[17]. Copyright 2015, Wiley-VCH. h) Reproduced with permission[32]. Copyright 2010, Wiley-VCH. i) Reproduced with permission[18]. Copyright 2012, American Chemical Society.

these carbon dots emission originated from the band emission. TEM analysis evinced that the size of the carbons dots were 1.95 nm (B-), 2.41nm (G-), 3.78 nm (Y-), 4.90 nm (O-), and 6.68 nm (R-) respectively, in addition, the high degree of the crystallinity feature for all carbon dots were exposed by the HRTEM, thus the authors claimed[13] that the carbon dots emission originated from the band edge emission. The different color emission was the result of different effective band gaps: 3.02 eV (B-), 2.61 eV (G-), 2.49 eV (Y-), 2.30 eV (O-) and 2.12 eV (R-), where the band gaps were obtained from the absorption peaks (see figure 4d). The band gap emission results were also confirmed by the UPS spectroscopy which measure HOMO and HOMO values of carbon dots and were given in figure 4c. Combined with the TEM analysis, the authors claimed[13] that the different band gaps resulted from the different quantum confinement/size effect. All of the carbon dots exhibited pH-stable (pH value vary from 2 to13) emission peaks, which, combining with the monoexponential decay of PL lifetimes, further confirmed that carbon dots emission originated from the band-emission, instead of surface states emission. In addition, all the excitation independent emission carbon dots possessed relative high quantum yield: 75% (B), 73% (G), 58% (Y), 53% (O), and 12% (R).

The quantum confinement induced PL spectral shift of carbon dots was also claimed by several other groups. Jiang *et al.* [17] synthesized 6.0 nm, 8.2 nm, and 10.0 nm size carbon dots by hydrothermal treatment method, which shown blue, green and red emission respectively (figure 4 e-g). In addition to the hydrothermal method, carbon dots synthesized by other approaches[16, 17] can also exhibit size dependent PL. Li *et al*[32] and Peng *et al.*[18] synthesized carbon dots by utilizing the alkali-assisted electrochemical and chemical exfoliation separately, while both of them observed the size dependent PL spectral shift from their carbon dots, as can be seen figure 4h and 4i.

3.2 Surface states emission

To explore the emission mechanism of carbon dots, the purification of carbon dots is the pre-requisition. Ding *et al.*[25] have employed the silica column chromatography technique to purify carbon dots synthesized by hydrothermal treating of urea and p-phenylenediamine at 160℃ for 10 h. The purified carbon dots emitted blue, green, yellow and red light respectively, labeled as A, B, C and D. The UV-visible absorption spectra of the purified carbon dots displayed distinct absorption peaks in the longer wavelength region located at 383, 410, 488, and 528 nm respectively, and the PLE spectra of each carbon dot samples also exhibited only one peak close to the corresponding absorption bands. Differ from the ensemble carbon dots which presented excitation dependent PL, the purified carbon dots disclosed excitation independent PL behavior, as can be seen in figure 5a-d. What's more, time-resolved spectroscopy evinced that all carbon dots samples possessed analogous mono-exponential decay process with the lifetime about 9 ns. All of these suggested that the purified different carbon dots samples manifested the uniformity in optical properties. While (HR) TEM analysis unveiled that all the carbon dots samples showed similar size distribution with an average diameter of 2.6 nm. In addition to the size, the lattice constant of all carbon dots also shown the same values about 0.21 nm, as seen in figure 5a-d, lower parts, thus it became clear that the different color emission of carbon dots were not originate from the size effect or quantum confinement.

FTIR spectroscopy analysis signified that as the carbon dots emission changed from blue to red (sample A to sample D), the degree of the oxidation continued to increase, which was substantiated by the enhanced COOH bond signal located at 1759 cm^{-1}. Besides, compared to the blue and green carbon dots, the yellow and red carbon dots appeared to hold a more broad O-H band distribution which suggested higher polarity, consistent with column chromatography results. The increased degree of oxidation was also verified by the XPS, where both the component of the carboxyl groups (represented by the intensity of the 289.0 eV signal) and the O element continuously increased from blue to red emission carbon dots.

Based on the theory proposed by Chen *et al.*[71] that the COOH groups on the sp^2-hybridized carbons will generate local distortions, leading to the decreasing of the energy gap, the authors[25] recommended the following emission mechanism: the emissive center is located at the surface of the carbon dots, mainly constituted by the conjugated carbon atoms and bonded oxygen atoms, thus the energy difference between the HOMO and LUMO of the carbon dots is intensely related to the degree of oxidation. More specifically, the increased oxidation or O component leaded to the decreased band gap, so the red shift of the PL of carbon dots originated from the increased surface oxidation, as represented at figure 5e. The PL spectra of red emission carbon dots exhibited red shift in acidic condition also supported the surface states emission. The authors attributed[25] the pH triggered PL intensity decrease and peak shift to the protonation-deprotonation induced surface charge modification.

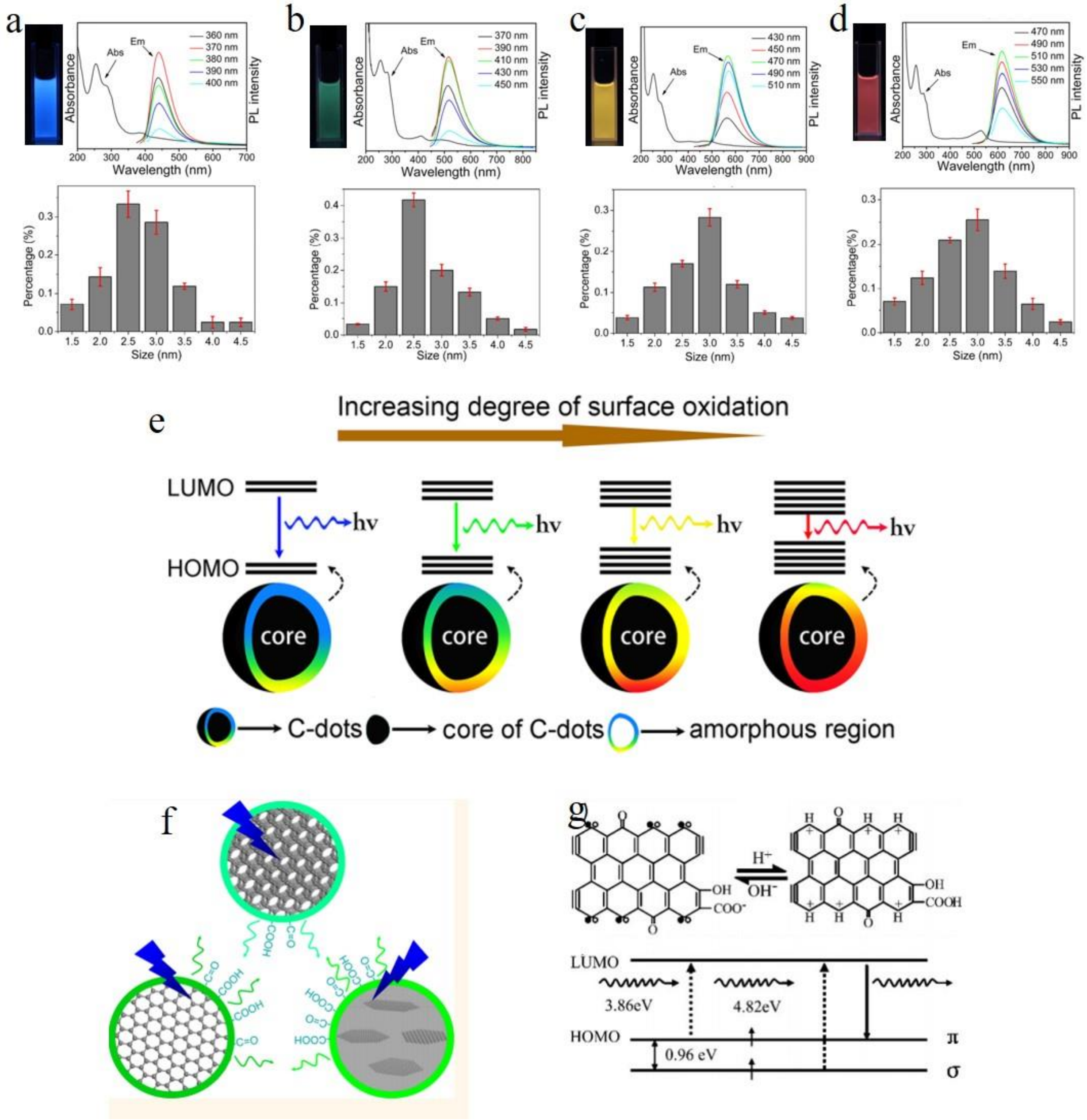

Figure 5 a,b,c,d) The photograph under UV light, absorption and PL spectra, the size distribution for blue, green, yellow, and red emission carbon dots respectively. All the purified carbon dots exhibited excitation independent PL and shown a similar size distribution with an average diameter of 2.6 nm. e) Model for the tunable PL of carbon dots. The band gap decreased with the increasing of degrees of surface oxidation, resulting in the red shift of carbon dots emission. f) Wang *et al*[72] suggested that the green emission of carbon dots originated from hydroxyl and carboxyl surface function groups. g) Pan *et al* proposed that the blue emission of carbon dots originated from surface zigzag sites which possessed a carbene-like triplet ground state, donated as s^1p^1. a-g) Reproduced with permission[25]. Copyright 2016, American Chemical Society. f) Reproduced with permission[72]. Copyright 2014, American Chemical Society. g) Reproduced with permission[52]. Copyright 2010, Wiley-VCH.

The mechanism of surface states emission was also adapted by Wang *et al.*[72] to interpret the carbon dots emission in their samples. They even assigned the surface states emission to the common origin of green light emission. They employed three kinds of carbon dots to explore the green emission of carbon dots, namely carbon dots synthesized by electrochemical treatment of graphite rod, microwave heating of citric acid and urea and hydrothermal treatment of graphene oxide DMF solution. The three kinds of carbon dots displayed similar green emission spectra when excited by 400 nm even though the absorption spectra were different. By combining the transient absorption and time resolved spectroscopy, the authors suggested[72] that the photo excited hot carriers were first located at the carbon core, followed by leaking fast to the emissive center and non-radiative traps. In other words, the graphitic carbon core did not contribute to the carbon dot emission but played the role of temporary hot carrier reservoir. To identity the emission center on the surface, $NaBH_4$ was utilized to achieve the surface chemical reduction for all three kinds of carbon dots, which resulted in different emission spectra. FTIR spectra analysis implied that the C=O function groups, especially the hydroxyl group and carboxyl group were the main function groups for both before and after surface reduced carbon dots, thus they attributed[72] the carbon dots green emission to the hydroxyl and carboxyl surface function groups, the different quantity of carboxyl surface function groups before and after surface reduction resulted in different green PL spectra of carbon dots. In addition, the authors also claimed[72] that the hybridization/interaction between the carbon core structure and C=O function groups was pre-requisition for the carbon dots emission as the pure C=O could not contribute to the green emission.

The surface states emission origination of carbon dots was also accepted by many researchers[12, 20, 24, 26, 52, 73-75] although the actual emission fine structures on the surface of carbon dots are still controversial, e.g. Pan *et al*.[52] argued that the blue carbon dots emission originate from the surface zigzag sites which possessed a carbene-like triplet ground state (figure 5g), donated as s^1p^1.

3.3 Molecular fluorophores and carbogenic core

Emmanuel P. Giannelis's group[38] has proposed that for the thermal pyrolysis approach synthesized carbon dots, the emission mechanism was related to the pyrolysis temperature. Briefly speaking, the mixture of citric acid monohydrate ($C_6H_8O_7$) and ethanolamine (C_2H_7ON) with a molar ratio 1:3 has been heated at certain temperature for 30 min under reflux in air. The authors propounded that when the pyrolysis temperature was low (*e.g.* 180°C), it could not form carbon dots, but instead form carbon dots precursor. The precursor contained some organic molecular fluorophores which contributed to the emission with a PL quantum efficiency of 50%. The claim of the molecular fluorophore emission was based on the following experiment observations: 1. No carbon dots particle have been observed by either DLS or TEM. 2. The sample showed excitation independent PL. To further identify the molecular structure, the authors employed[38] the FTIR, XPS, ^1H and ^{13}C NMR spectroscopy to study the chemical bond of the carbon dots precursor. The results suggested that the amide related fluorophore molecular were accounted for the precursor emission. Moreover, amide synthesized by an alternative approach using citric acid monohydrate ($C_6H_8O_7$) and ethanolamine (C_2H_7ON) as the raw materials demonstrated similar optical behaviors to carbon dots precursor, which validated the mechanism.

Increasing pyrolysis temperature to 230°C resulted in the PL quantum yield decreasing to 15% and the appearance of excitation dependent PL. Further increasing the temperature to 300°C or even 400°C also resulted in different PL quantum yield. Element analysis evinced that the carbon component continued increase with a concomitant decrease in hydrogen component. Thus the authors claimed[38] that carbon dots underwent further carbonization as the temperature increased. The carbonization shall generate carbogenic cores at the cost of the carbon dots precursor or molecular fluorophores. Both carbon core and amide-containing molecular fluorophores could contribute to the light emission. This model has been illustrated in figure 6a[38]. When temperature was low, the emission was from molecular fluorophores, while the carbogenic cores shall become the main emission mechanism if the temperature was too high (*e.g.* 400℃). Both molecular fluorophores and carbogenic cores contributed to the carbon dots emission if the pyrolysis temperature was moderate.

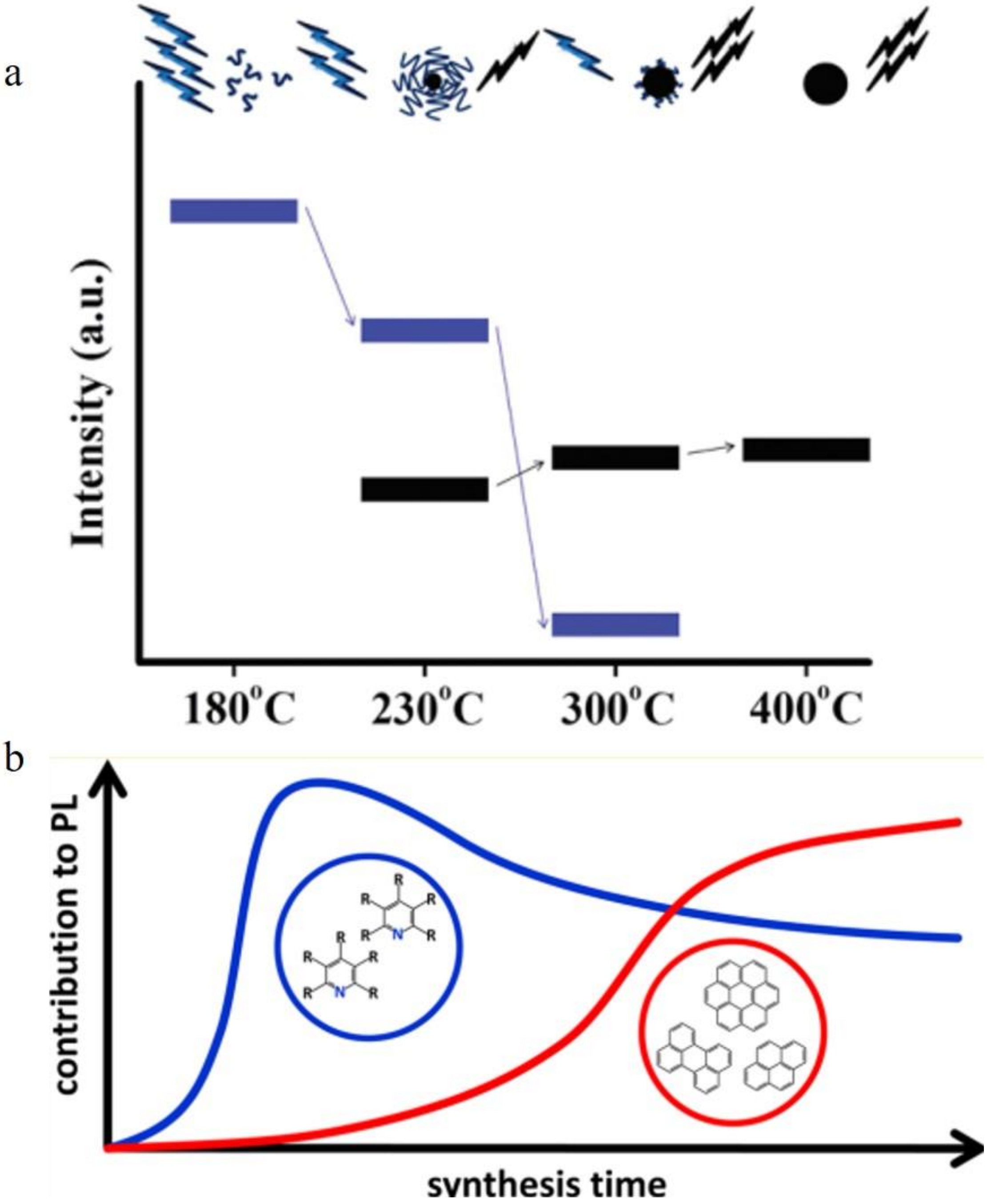

Figure 6 a) During pyrolysis, the molecular fluorophores (blue groups) were expended to generate carbogenic core (black sphere), as seen in the upper illustration. So as the temperature increased, the PL intensity which corresponds carbon core (bold black line, lower part) increased at the cost of the molecular fluorophores (blue line), thus along with the decrease of the precursor emission (bold blue line, lower part). Reproduced with permission[38].Copyright 2012, American Chemical Society. b) When the hydrothermal reaction time was short (e.g. less than 30 min), the emission center was main molecular fluorophores e.g. 2-pyridone derivatives, while as the reaction time increased, the carbon core which contained aromatic domain appeared and shall play a more important role for carbon dots emission. Reproduced with permission[76].Copyright 2017, American Chemical Society.

Differ from the high temperature pyrolysis method, Ehrat *et al.*[76] synthesized carbon dots from citric acid and ethylenediamine by means of hydrothermal treatment. However, they proposed a similar molecular fluorophores and carbogenic core model to interpret the carbon dots emission (figure 6b). When the hydrothermal reaction time was short (*e.g.* less than 30 min), the emission center was main molecular fluorophores *e.g.* 2-pyridone derivatives, while as the reaction time increased, the carbon core which contained aromatic domain appeared and shall play a more important role for carbon dots emission.

3.4 Polycyclic Aromatic Hydrocarbon molecular emission

Following the molecular emission[38], Alexander's group[9] proposed the Polycyclic Aromatic Hydrocarbon florescent molecular emission. The carbon dots utilized in the experiment was synthesized by hydrothermal treatment of citric acid and ethylenediamine, which showed a diameter between 2 to 5 nm. The authors claimed carbon dots were a kind of organic molecular nano-crystal based on the following evidences: 1. XPS spectroscopy indicated that there existed sp^2 (*e.g.* C=O bond) and sp^3 (*e.g.* C-C bond) hybrid bonds. 2. C 1s XPS spectra shown dramatic change after treated by Ar-ion sputtering. Specifically, the authors declared that carbon dots contained many

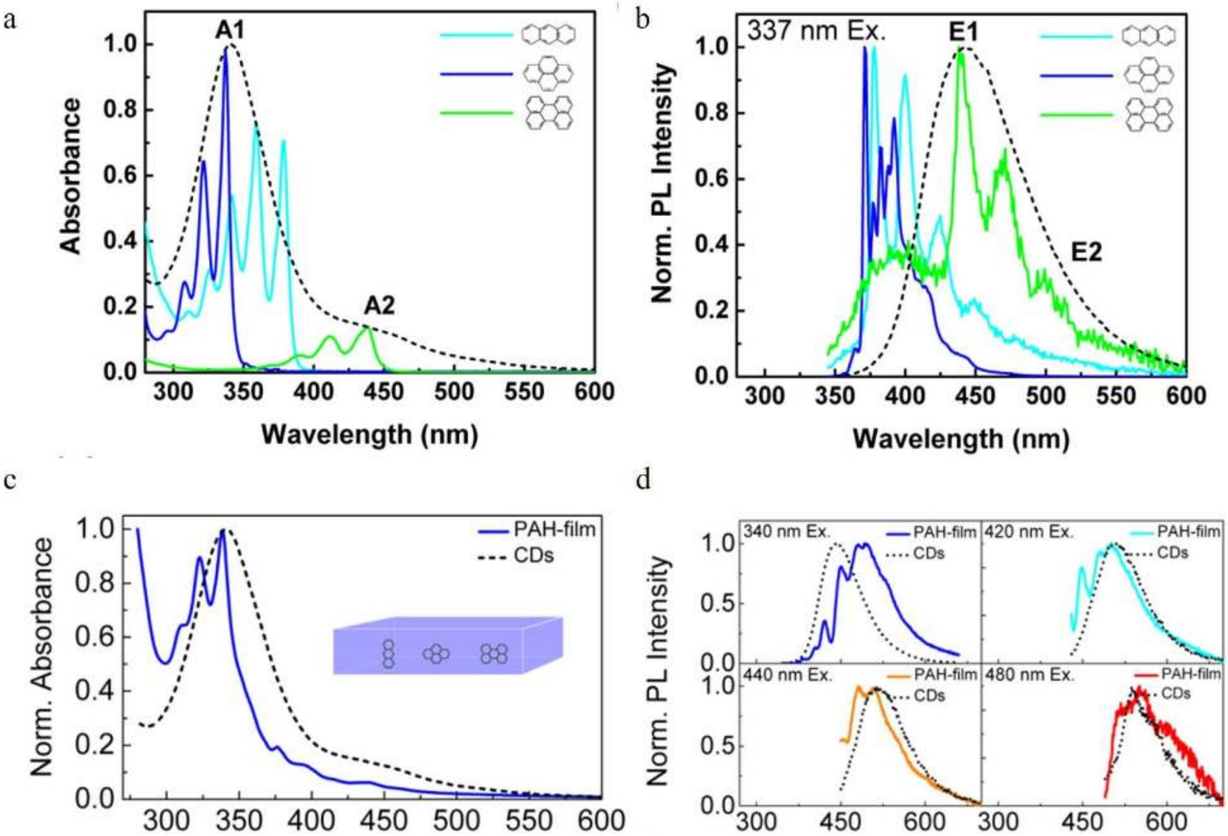

Figure 7 a,b) Absorption and normalized PL spectra of anthracene (light blue), pyrene (dark blue), perylene (green) in a PMMA matrix (concentration: 0.01 mol %) and CDs aqueous solution (black dashed line). c) Absorption spectra of a PMMA film containing three PAHs (blue) (molecular ratio: anthracene/pyrene/perylene/PMMA 10:10:1:20) and CDs aqueous solution (black dashed line) d) PL spectra of the film stimulated by different wavelength, CD PL spectrum (black dashed line) also given by a reference. a-d) Reproduced with permission[9]. Copyright 2015, American Chemical Society.

sp^2 carbon domains which were embedded in a sp^3 hybridized carbon matrix. Single particle measurement on carbon dots still exhibited excitation dependent PL, indicating that there exist multi-chromophores in one carbon dots. As a result, the authors employed[9] three basic polycyclic aromatic hydrocarbon (PAH), anthracene(3 rings), pyrene (4 rings), and perylene (5 rings), to mimic the emission nano-domain, chosen poly(methyl methacrylate) (PMMA) as the sp^3 hybridized matrix. The authors have stated that they chose these PAHs because 1. The absorption and PL spectra of these PAHs overlapped with those of the carbon dots, see figure 7a and 7b. 2. Their structure were relatively simple. After optimization, the fixed molecular ratio of 10:10:1:20 for anthracene/pyrene/perylene/PMMA has been utilized to mimic carbon dots. The results are reproduced in figure 7c and 7d, the absorption spectra of the PAH films and carbon dots displayed a similar shape, A redshift was observed for PL spectra when excited by 340 nm, while the PL line-shape and width were similar. Increasing the excitation wavelength resulted in the PL spectra changed, but in the condition of 420 nm, 440 nm and 480 nm excitation, the PAH films PL spectra matched very well with the carbon dots emission. Based on the model, the authors[9] gave the following picture: when excited by short wave length (< 400 nm), the PAHs which have larger bandgap (*e.g.*, anthracene and pyrene) were mainly excited (the authors claimed that the smaller band gap PAH, such as perylene did not absorb strongly at shorter wavelengths), which could emit light directly contributing to the main peak emission, or transfer energy to the smaller bandgap PAHs (*e.g.* perylene) resulting in the longer wavelength emission. While when the excitation wavelength was greater than 400 nm, both kind of PAHs (large and small band gap PAHs) could be exited directly, resulting in the redshift of carbon dots emission. Continuously increasing the excitation wavelength leaded to the small band gap PAHs absorption increased and large PAHs band gap decreased, contributing to the PL spectra of carbon dots continual redshift. Finally, the authors also stated[9] that there most likely existed other PAHs which were involved in the carbon dots optical process in addition to the above mentioned three PAHs.

3.5 Slowed solvent relaxation or solvatochromic shift

Apart from the electronic structure of carbon dots itself, the effect of the surrounding solvent molecular of carbon dots was also considered by Khan *et al*[77]. The diagram is illustrated in figure 8a. Different from the solid sample, the carbon dots aqueous solution have two kinds of decay processes after photo excitation (time scale about 10^{-15} s) occurring simultaneously. 1. Hot carriers (*e.g.* elections, holes *etc.*) vibrational relaxation, which results in the well-known stokes red shift. 2. Solvent relaxation or dipolar reorganization which takes place at the band edge, leading to the further redshift of emission spectra, commonly termed as solvatochromic shift[77]. According to Lippert-Mataga theory[78, 79], the greater polarity of solvent will lead to larger red shift of emission spectra. The authors[77] assumed that the hot carrier variation time is much less than the fluorescent lifetime τ_f, thus only the solvent relaxation effect (solvent relaxation lifetime:τ_r) was considered. When $\tau_f \gg \tau_r$, which means fast solvent relax, the solvent relaxation is fully finished before the light emission, resulting in the solvatochromic shift redshift, also called homogeneous broadening; when $\tau_f \ll \tau_r$, which is the case of much slow solvent relation, there is no solvent relaxation effect during the PL; while when the florescent lifetime and solvent relaxation time are the same order of magnitude *e.g.* $\tau_f \cong \tau_r$, a set of sub-states will be formed, all of the sub-states can contributed to emission maximum of carbon dots. This condition will lead to broadened band emission called inhomogeneous broadening. Both temperature, solvent dipole moment and fluorophore dipole moment can affect the inhomogeneous broadening, which is governed by the following equation[80]: $\delta_{\upsilon} = \delta_{\mu}\, a^{-\frac{3}{2}}(kT)^{1/2}$, where a is the Onsagar sphere radius. Considering the dynamics of the relative slow solvent relaxing *e.g.* $\tau_f \cong \tau_r$ process, the initial energy sates will migrated to lower energy states during the PL lifetime, which results in two effects: 1. The time resolved emission spectra will red-shift as time increases. 2. The time integrated PL spectra will red-shift as the excitation wavelength increases. More specifically, the center of mass of the time integrated spectra caused by the solvent relaxation is determined by the following equation[81]: $\upsilon = \upsilon_{t=\infty} - (\upsilon_{t=0} - \upsilon_{t=\infty})\tau_r/(\tau_f + \tau_r)$ where $\upsilon_{t=\infty}$ is the PL peak when time is long enough, $\upsilon_{t=0}$ represents the instant that the PL occurs. It is obvious that $\upsilon = \upsilon_{t=\infty}$ for $\tau_f \gg \tau_r$, $\upsilon = \upsilon_{t=0}$ for $\tau_f \ll \tau_r$, and in both two cases, the emission spectra are independent on the detection time. Only when the two time constants are of the same order, the time dependent emission spectra appears.

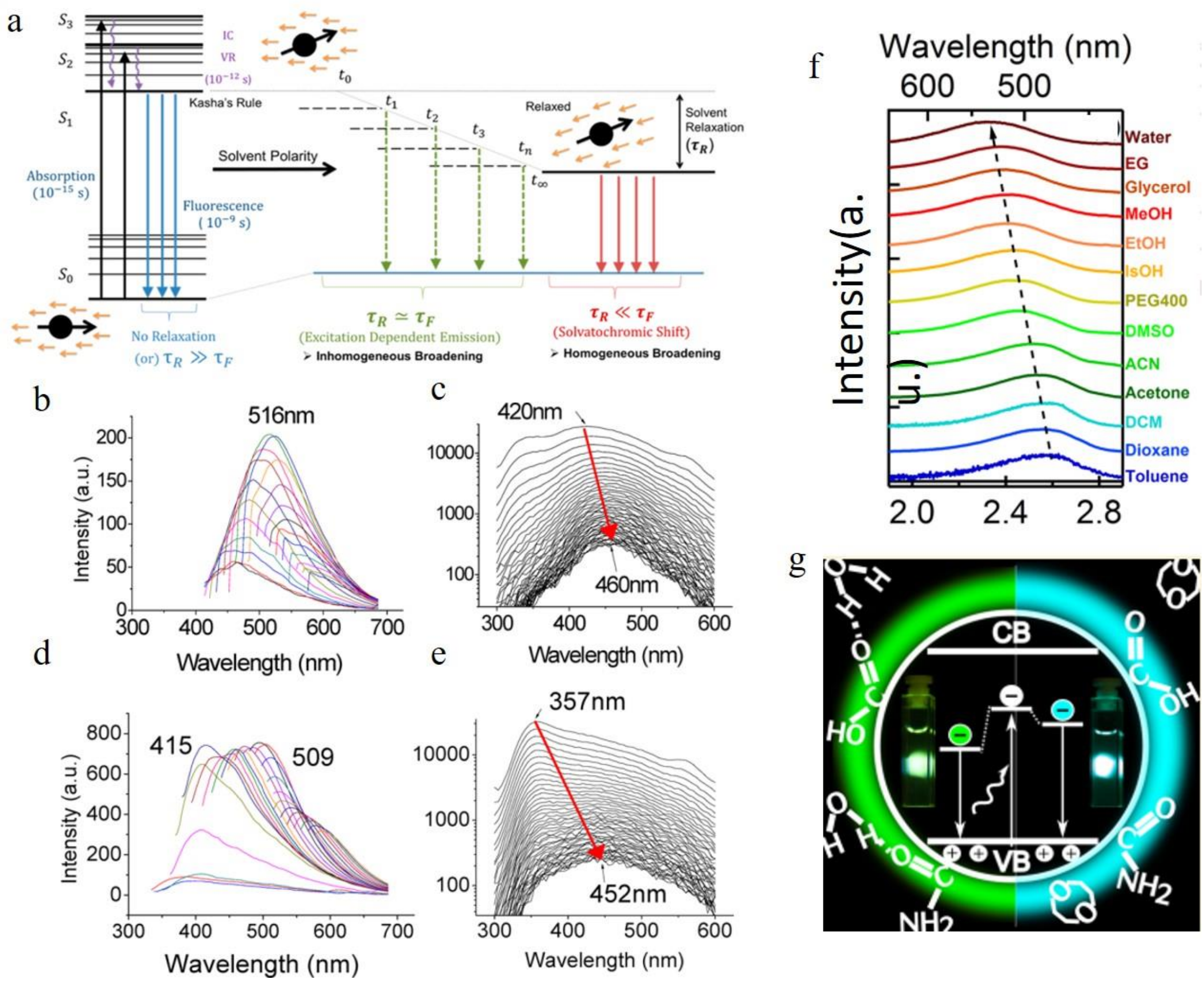

Figure 8 a) Illustrating of solvent relaxation. (Fluorescent lifetime τ_f, solvent relaxation lifetime:τ_r). b-e) Function of solvent dipole moment. b, c) Time integrated PL spectra and time resolved PL spectra as the function of time of carbon dots in water. d, e)

Time integrated PL spectra and time resolved PL spectra as the function of time of carbon dots in dimethylformamide (DMF). The red arrow indicated that as the time increased, the emission spectra redshift. The wavelength migration during the lifetime was 40 nm for water, while reached to 100 nm for DMF. f) Solvent dependent spectral shift. g) The recombination of the electrons located at the surface with valance band holes in the carbon dots crystalline core contributing to the carbon dots emission. a-e) Reproduced with permission[77]. Copyright 2015, American Chemical Society. f-g) Reproduced with permission[82]. Copyright 2016, American Chemical Society.

The carbon dots employed by the authors[77] were synthesized by means of microwave assisted method. They synthesized different carbon dots from different starting materials (carbon dots 1 from Chitosan and PEG, carbon dots 2 from Adenine sulphate, carbon dots 3 from sodium citrate and sodium thiosulphate, carbon dots 4 from Potato-dextrose agar) and all of the carbon dots exhibited similar behaviors, thus the authors carried out the analysis by using carbon dots 1 as the example. Further purification of carbon dots 1 was achieved by column-chromatographic, which resulted in two kinds of carbon dots with different polarity: less polar carbon dots presented blue light emission, higher polarity carbon dots showed longer wavelength emission. Water and dimethylformamide (DMF) which have different dipole moment have been adapted by the authors[77] to dissolve carbon dots to explore the solvent polar effect. Both of the water and DMF carbon dots solution demonstrated the time integrated excitation dependent PL and time resolved PL spectra migration, as described in figure 8b-e. The results indicated that the solvent relaxation time was the same order of the PL lifetime, and the excitation dependent PL was the result of solvent relaxation. Compared to water, DMF hold higher dipole moment, which leaded to more populated sub-states, resulting in the larger time resolved emission spectra migration reach to 100 nm (see figure 8e) (while only 40 nm emission migration for carbon dots aqueous solution).

The two kinds of carbon dots purified from the column-chromatographic also displayed different time resolved emission spectra migration due to the different polarity properties, which was consist with the author's model[77]. The less oxidized and polar fraction carbon dots demonstrated less or no time resolved emission spectra red-shift, which could be interpreted by the faster photon emission before a significant relaxation happens. While the highly oxidized and high polarity carbon dots fraction were considered to hold higher lifetime value and shown clear time resolved PL spectra migration, as the high polarity carbon dots sustained significant solvent relaxation during the PL lifetime, which resulted in the population of the sub-states, contributing to the red-shift edge effect and time resolved spectra migration.

Time resolved anisotropic analysis estimated[77] the rotational time of dipole in carbon dots to be in the range of 0.61 to 1.51 ns (for PH=7. The values varied for different emission wavelength), the same order to the PL lifetime (several ns) of carbon dots, consistent with the relative slowed solvent relaxation assumption. Combined with the pH dependent measurement, carbon dots concentration dependent measurement and single step photo-bleaching, the authors[77] claimed that carbon dots emission neither from the quantum confinement nor particle heterogeneity, instead they proposed that carbon dots was a kind of single emitter, and the excitation dependent PL was the slowed solvent relaxation or solvatochromic red shift. What's more, based on the observation of the blue shift of carbon dots in high pH (>10) condition, the authors claimed[77] that the emission center was located at the surface of carbon dots.

Even though the polar solvent effect has been observed by some other groups[82, 83], the slow relaxation of polar solvents mechanism was argued by some researchers[82]. The appearance of PL tunability even in the apolar solvents combined with the disappearance of the spectral migration during the PL lifetime of carbon dots (synthesized by thermal pyrolysis of citric acid monohydrate and urea) in all solvent contradicted to the slow relaxation of polar solvents mechanism. Instead, the researchers[82] attributed the solvation dependent PL to the surface function groups of carbon dots. The observation of the solvent effect was more efficient for excited sates than ground states combined with the fact that the amide and carboxylic surface groups were assumed not undergo any transitions at the 2-3 eV energy range, guiding the researchers to propose that carbon dots emission was the result of recombination of the electrons located at the surface with valance band holes in the carbon dots crystalline core[82], as illustrated in figure 8f and 8g . The inhomogeneous broadening of PL spectra was the result of size distribution, specifically, the size distribution affected the core band gap, resulting in the different efficient "energy band gap" between the valance band and the surface energy states.

3.6 Self-trapped exciton emission

Carbon dots (synthesized by microwave heating of glucose and urea) PL spectra manifested two distinct features[84]: 1. When exited by 442 nm, the emission wavelength started nearly from the excitation wavelength 450 nm with a broadened emission spectra over 1 eV. 2. The emission intensity of the whole spectra were the same of magnitude, which was contrary to band edge emission where the majority of emission intensity was located at the band edge. Based on these observations, it's reasonable to speculate that carbon dots emission originate from the localized emission. To verify this assumption, Xiao *et al.*[84] have employed the polarization spectroscopy to do comprehensive investigation and uncovered the emission mechanism of carbon dots. Polarization spectroscopy can provide the information of the energy and momentum relaxation dynamic, which is closely related to the electronic structure and emission mechanism[85, 86]. Linear polarized light will align the momentum of the photo-generated hot carriers (hot electrons and holes), the corresponding principles are ruled by the transition density matrix combined with the angular momentum distribution under dipole approximation[87]. The radiative recombination of carriers with aligned momentum will emit linear polarized light as the selection rules are the same for photo excitation and emission. However, the decay process of the hot carriers will randomize the aligned momentum, resulting in the isotropic momentum distribution of the ensemble carriers by means of collision and/or phonon emission[85]. As a result, the linearly polarized florescence can only be obtained from the hot carrier recombination where the momentum alignment/anisotropy excited by the linear excitation light is totally/partially conserved, on the contrary, the thermalized carriers which exhibit isotropic momentum distribution can only emit un-polarized light. Thus, the appearance of linearly polarized light unambiguously indicates the momentum alignment, which is the result of hot carrier property. The linearly polarized emission of carbon dots[84] are depicted in figure 9. Carbon dots shown distinct emission anisotropy as seen in figure 9a (the vertical axis was the angle between the polarization of the excitation and emission light with the excitation polarization fixed) and linear polarized emission. To quantitatively analyze the emission anisotropy, degree of linear polarization was defined as $P = (I_{\parallel} - I_{\perp})/(I_{\parallel} + I_{\perp})$ where $I_{\parallel}$ and $I_{\perp}$ were the parallel (0°) and perpendicular (90°) emission compared to excitation light respectively. Carbon dots exhibited extremely high linear polarization at the instant of excitation reached to 0.5, and continuously decreased as the emission energy decreased, as seen in figure 9b. However, there was still a large polarization value for carbon dots (about 0.25 for 690 nm) even if the energy difference between the excitation and emission light was more than 1 eV, which unambiguously - implied the hot carrier properties. Based on the observations, the authors claimed[84] that the carbon dots emission originated from the localized emission, where the momentum, energy and vibrational relaxation were strongly suppressed due to the existence of strong local potential field. As a result, the momentum relaxation time became comparable or even longer that the florescent lifetime, contributing to the highly polarized emission, therefore carbon dots emission was totally different from the band edge emission where the fluorescence lifetime of band edge emission is much longer than the momentum and energy relaxation time (several order of magnitude longer), consequently the emission is from the isotropic momentum distrusted and thermalized carriers.

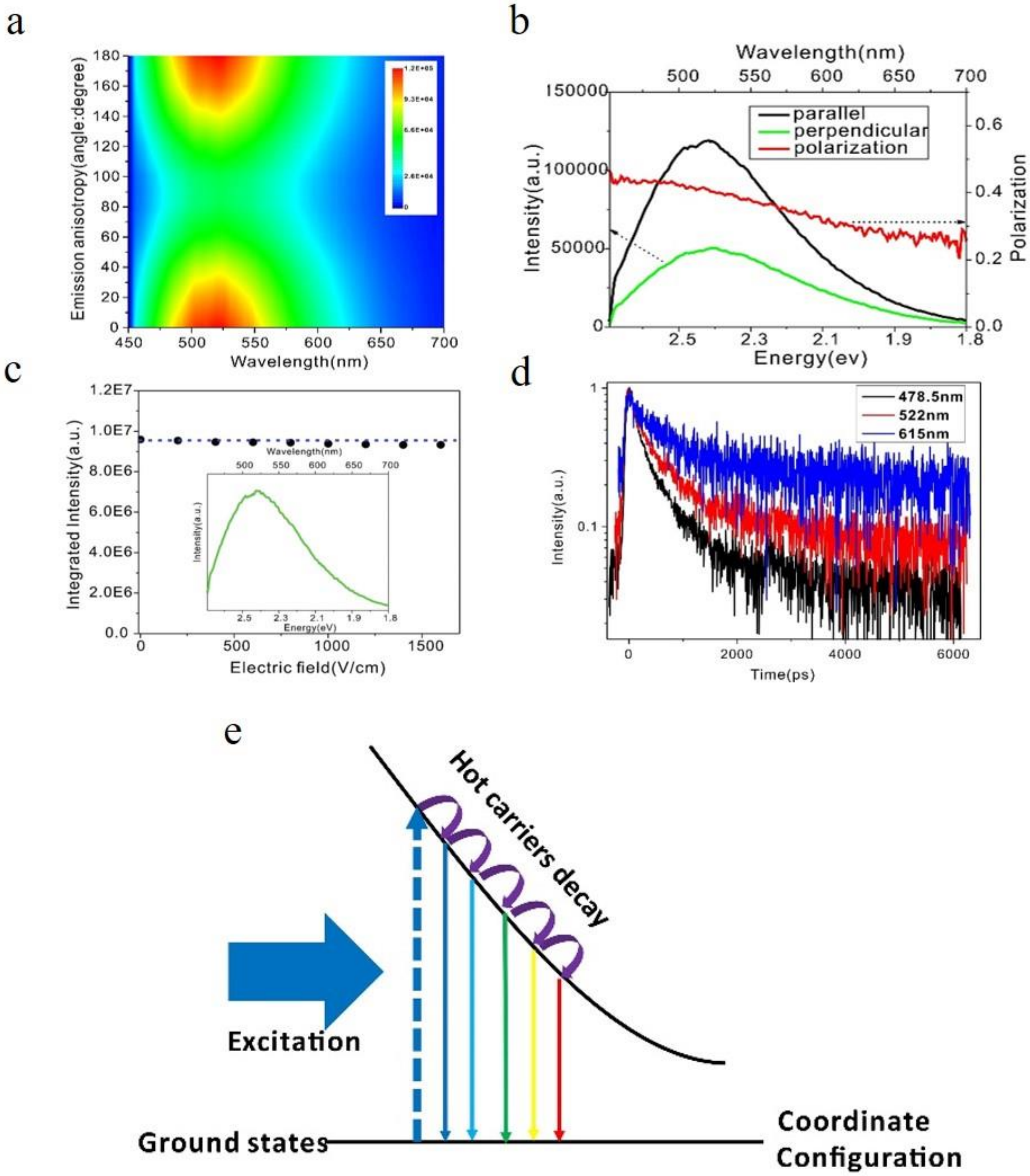

Figure 9 a,b) Emission anisotropy and degree of linear polarization of carbon dots. c) Electric filed modulation of carbon dots emission. d) Time-resolved spectroscopy for different emission wavelength. e) The electronic structure of self-trapped exciton which contribute to carbon dots emission. Excitation wavelength: 442 nm. a-e) Reproduced with permission[84]. Copyright 2017, Royal Society of Chemistry.

The localized emission was further confirmed by the electric-filed modulation experiment[84], as can be seen in figure 9c. Both the line-shape and the intensity of carbon dots PL were stable even if the electric field was as high as 1500 V/cm, which was consistent with the localized emission assumption: the strong local potential field in carbon dots protected the hot carriers against the quenching/tuning effect by the high external electric field[88, 89]. Power dependent PL experiments showed that the emission intensity of carbon dots exhibited a linear relationship to the excitation power even if the excitation power density was up to 1800 mw/cm^2, which implied that carbon dots emission originated from self-trapped exciton rather than defect[90, 91]. The self-trapped exciton property was further validated by the time-resolved spectroscopy[84]. For self-trapped excitons, the smaller charge distance r possesses larger wave function overlap and the transition matrix, and they recombine first[92]. As a consequence, the emission will shift to longer wavelength as the time increases, so the increased lifetime for the longer emission wavelength can be predicted. The time resolved experiment results demonstrated that as the emission wavelength increased from 478 to 615 nm, as seen in figure 9d, the PL lifetime also continuously increased, which corroborated the self-trapped exciton emission. By combining photo-excitation, relaxation and polarization emission, the energy diagram contributing to carbon dots emission was given by the authors[84], as illustrated in figure 9e, where the horizontal axis was the coordinate distance which represent the relative distance r between the hot carrier pairs. As the time evolution after the photo excitation, the larger distance self-trapped exciton states shall be activated and emit longer wavelength because they underwent the relaxation process. The excitation dependent PL of carbon dots could be also interpreted by the self-trapped exciton model, monochromatic light source excited the self-trapped exciton states with the energy equal to the excitation photon energy. The subdued decay process resulted in the emission starting from the excitation wavelength. When the excitation wavelength changed, the photons shall excite different self-trapped exciton states determined by the excitation photon energy, and the suppressed decay process performed in the same way as shown before. As a result, the emission started from the new excitation wavelength and the spectra also shifted, as observed by the experiment[84]. Another predicted phenomenon was the reduced linear polarization in the same fluorescence rang as the excitation energy increased. As reported by the authors[84], compared to 442 nm excitation, the linear polarization decreased for the 325 nm excitation in 460-690 nm range, which was the result of further relaxation and momentum randomization for 325 nm excitation.

3.7 Surface dipole emission centre

To reveal the single particle emission mechanism and its structure information, combined spectroscopic technique has been adopted by Ghosh *et al*[93]. By combining the high resolution transmission electron microscopy (HRTEM) with PL imaging spectroscopy, they achieved the correlative measurement of PL, crystal structure, and shape of a single carbon dots. The carbon dots were synthesised by the microwave assisted method with sucrose as the carbon source and PEG as the passivation agent. The combined HRTEM disclosed that there existed two kinds of carbon particles. One was onion like structure with an amorphous carbon shell, as seen in the left part of figure 10a. EDX analysis indicated that the amorphous shell mainly contained oxygen and carbon elements. The diameter of the onion like carbon dots varied from 7 to 20 nm, but with the same lattice constant about 0.35 to 0.36 nm. The other structure was a kind of fully crystalline carbon dots with the diameter range from 2 to 5 nm and a lattice constant of 0.24 nm, which was presented in the right part of figure 10a. All individual single carbon dots exhibited much narrower PL spectra compared to ensemble carbon dots and displayed a longer wavelength tail, thus the author suggested that there exist two splitting bands in carbon dots. By using two Gaussian functions to fit the emission spectra of single carbon dots, the authors claimed[93] that the splitting energy was in the range of 70 to 150 meV and showed no relationship to the emission peak. Based on the crystal structures of single carbon dots provided by HRTEM and the energy splitting information, the authors calculated the optical phonons which contribute to the carbon dots emission by using density-function tight-binding method. Three optical phonons have been proposed[93] to be involved in the carbon dots emission: 98 meV phonon for onion-shaped structure carbon dots, 112, and 113 meV for fully crystallized carbon dots, thus the longer wavelength PL peak was the result of the coupling between the radiative carriers with the optical phonons. The interaction between the electrons and lattice vibrations (phonons) leaded to a coupled states which possessed lower energy.

Focused or defocused imaging with an azimuthally polarized laser beam (APLB), which can measure and provide the information of excitation or emission transition dipole moment (TDM) respectively[94-96], has also been employed by the authors[93] to uncover the emission mechanism of carbon dots. The results are illustrated at figure 10b. Both the excitation and emission TDM patterns exhibited two nearby bright spots of elliptical shape, indicating the fixed linear excitation and emission TDM. The TDM projection to surface of a glass cover slide was shown by the white arrows which clearly shown that the excitation and emission TDM were oriented parallel to each other[93] for the same carbon dots and the projection perpendicular to the surface could not be detected. The fixed excitation and emission TDM suggested that carbon dots behaved as a dipole for both excitation/absorption and emission. Single step PL intermittency and bleaching between the on-off states, and monoexponential decay of the lifetime have been observed for a single carbon dots, which indicated that carbon dots was a kind of a single quantum emitter. To further confirm the single emitter property of single carbon dots, the authors checked[93] whether the PL spectra of carbon dots shall change when excited by different wavelength. The results are displayed in figure 10c. There was no difference in PL spectral shape for all the five individual single carbon dots when excited by 467 nm (red curve) and 488 nm (black curve) laser. The results indicated that individual carbon dots was a kind of single emitter, and the excitation dependent PL of carbon dots was the result of heterogeneity. The authors also measured[93] the PL quantum yield for different single carbon dots by means of nanocavity-based method, the results demonstrated that different single carbon dots possessed different quantum yield within the main range of 0-0.3, which was consistent with the single quantum emitter assumption. Considering that the different crystal structures did not present distinct PL properties, the authors speculated[93] that the defect emission centre was located at the surface of carbon dots rather than its core. The surface emission centre was also supported by the ion quenching experiments. In addition, the homogeneous distributed PL peak and lifetime values indicated that the all PL spectra originated from the similar defect emission centres.

Based on the all observations, the following emission mechanism was suggested by the authors[93]. Single carbon dots is a single emitter with the defect emission centre located at the surface of the carbon dots, where the strong coupling between the charged carriers with the lattice vibrational (phonon modes) results in the longer wavelength emission, and excitation dependent PL in carbon dot ensemble originates from the different carbon dots heterogeneity.

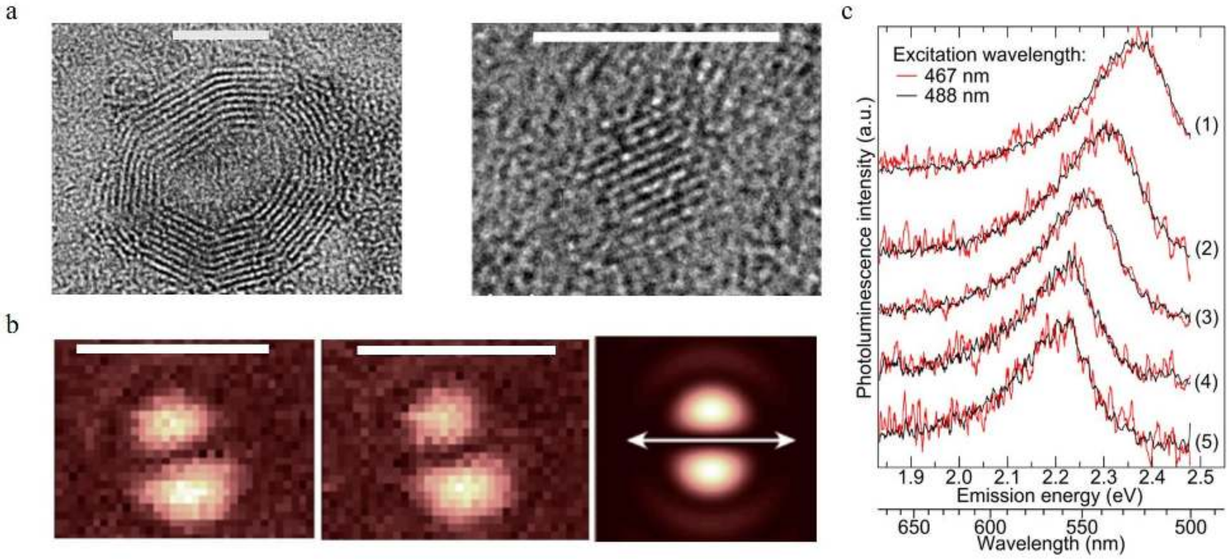

Figure 10 a) Two types of carbon dots. Left: The onion like shape structure, right: full crystalline structure. Scale bar 5 nm B) Consecutive imagines of the excitation TDM for the same carbon dots particle, the third one present a theoretically calculated excitation pattern, where the orientation of the dipole is indicated by the white double arrow. Scale bar 1 µm. c) Normalized PL spectra of different single CNDs (5 single carbon dots) on the surface of a glass cover slide stimulated by 467 nm (red) and 488 nm (black) laser line. The results shown that the emission spectra were various for different single carbon dots, while each single carbon dots presented same PL spectra even the excitation wavelengths were different. a-c) Reproduced with permission[93]. Copyright 2014, American Chemical Society.

3.8 Aggregate emission centre

Following the model of single surface dipole emission centre[93], researchers continued to explore the details of the structure which contribute to carbon dots emission[97]. The absorption of light happened by the coupling between the photons and aromatic species in carbon dots, thus the two general energy coupling approaches have been considered. One is the excitonic coupling between the π electronic systems in carbon dots, which is efficient in the condition of near contact. The other is dipole–dipole resonance (also called Förster Resonance Energy Transfer (FRET)) which possesses longer interaction distance. While the observed parallel orientated excitation and emission transition dipole moment (TDM) in single carbon dots[93] demonstrated that it's the excitonic coupling rather than the dipole–dipole interaction, as the dipole–dipole interaction will rotate the orientation of the emission TDM from the absorption TDM direction[97].

According to the theory proposed by Kasha[98], only two kinds of aggregate conditions can contribute to the excitonic coupling effect for molecular complexes, namely J and H aggregates. Parallel aligned molecular dipoles can constitute J-Aggregates which has distinct absorption and PL spectra features[99]. Compared to molecular monomer, both PL and absorption spectra of J-aggregates are narrow and shift to longer wavelength. What's more, the Stokes shifts between the excitation and emission is small, and all of the properties of J-aggregates are contradictory to the observation form the single carbon dots. The other type of π–π stacked H-aggregates possess opposite properties with the large energy shifted absorption spectra compared to molecular monomer and large Stokes shift between the excitation and PL, consistent with experiment observation. The energy diagram was given by Alexander P. Demchenko[97] as illustrated in figure 11a, the π–π-stacked aggregates lead to the dimer excited state split into two energy states, consisting of a higher energy excitonic state and a lower excitonic state. According to the classic theory proposed by Kasha[98], the relaxation to the lower excitonic states is forbidden, which means that the pure π–π-stacked H-aggregates are non-emissive centres, which is also contradict to observed bright emission from carbon dots. Considering recently observed bright emission from H-aggregates from other materials[100, 101], the authors rationalized[97] the optical spectroscopic observations from carbon dots within the concept of excition theory. Different from J-aggregates, the excitonic coupling in H-aggregates could occur by co-facial stacking alignment determined by weak van der Waals interactions. As a result, a slight rotation of the coupled monomer in H-aggregates could result in a non-zero transition probability from the excited states to the lower excitonic states which is the emission centre, thus even small structure disorder could lead to the transformation of non-emissive H-aggregates to highly emissive H-aggregates. The H-aggregates formed by different mono-chromophores (*e.g.* number, size, shape, surface *etc.*) exhibited different absorption and emission properties, which interpreted the heterogeneity of lifetimes and PL spectra for different single carbon dots, the energy decay process lead to the hot carriers decay to the lower excitonic states which contributed to the large Stokes shift.

Different from the dyes' molecular or supramolecular H-aggregates, the authors suggested[97] that the H-aggregates in carbon dots were assembled during the synthesis process by means of regular packing of graphene sheets. Accepting the assumption proposed by Siddharth Ghosh et al[93], the authors suggested[97] that the cofacial positions of chromophores were located at the surface of carbon dots, and the surface functional polar groups such as C=O and C=N could modify the optical properties of H-aggregates contained carbon dots.

The aggregates triggered emission was also adopted by several research groups[102-106], but with some modifications. Arjun Sharma *et al.* [103] have synthesised carbon dots by directly heating citric acid and urea. However, unlike the pure H-aggregates emission centre, they proposed that carbon dots emission originated from the discrete multiple electronic states and ascribed the PL excitation band of 350 nm, 450 nm and 520 nm to the carbon dots monomers, H-aggregates (see figure 11b, red arrow) and J-aggregates (see figure 11b, blue arrow) respectively. The corresponding emission bands were 460 nm, 540 nm and 600 nm, which means that both H and J aggregates contributed to the carbon dots emission. What's more, H and J aggregates manifested different PL response for increased temperature, PL intensity of H-aggregates will increase with the temperature increase as the thermal activated higher excitonic states are emissive, while the J aggregates display decreased PL intensity as the thermal activated states will return to the vibrational states, which is non-emissive. Therefore, the authors also carried out the temperature dependent PL[103], the results were as follows: H aggregated band (450 nm/ 540 nm excitation/emission band) presented increased emission intensity as temperature increased, while J aggregated band (520 nm/ 600 nm excitation/emission band) exhibited decreased PL intensity as temperature increased, which was consistent with the authors' claims.

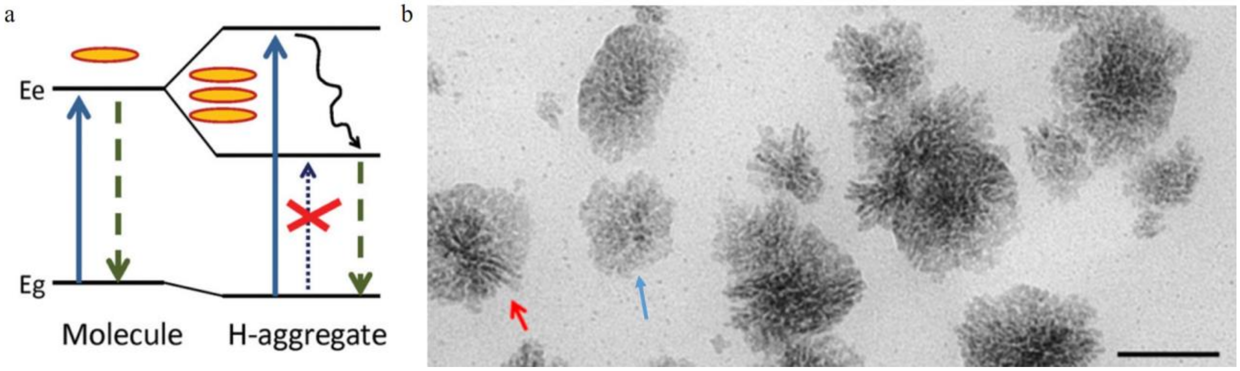

Figure 11 a) The H-type aggregates were formed by the $\pi - \pi$ stacking or side-to-side stacking of the chromophores, the resulted dimer excited states will split into the higher energy and lower energy excitonic states. The disorder in the H-aggregates leaded to the non-emissive lower excitonic states transfer to the emissive excitonic states, which contributed to the carbon dots emission and large Stokes shift. Reproduced with permission[97]. Copyright 2016, Royal Society of Chemistry. b) Not only H type aggregates, the authors[103] proposed that both the H (rod like, as indicated by red arrow) and J (flake like, as indicated by blue arrow) aggregates contribute to carbon dots emission. Reproduced with permission[103]. Copyright 2016, American Chemical Society.

4 Applications

4.1 Bio-imaging

Compared to florescent organic dyes and genetically engineered fluorescent proteins, carbon dots excel themselves with significant advantages like high PL quantum yield, photo-stability, resistance to metabolic degradation and so on, which endows the huge potential of carbon dots based bio-applications. While the toxicity evaluation of carbon dots is necessary and the pre-requisition for exploring the bio-applications of carbon dots, human breast cancer MCF-7 cells and human colorectal adenocarcinoma HT-29 cells have been employed by Yang *et al*[7] to assess the in vitro toxicity of carbon dots synthesised by laser ablation of graphite powder and cement using PEG_{1500N} as surface passivation agent. All the observations of cell proliferation, mortality, and viability from both two cell lines indicated that carbon dots exhibited superior biocompatibility even if the concentration of carbon dots was up to 50μg/ml which is much higher than the practical application demand, for example living cell-imaging. Additionally, the in vivo toxic evaluation was also carried out by the authors using the male CD-1 mice[7]. Two group mice were intravenously injected with carbon dots in the concentration of 8 mg/kg and 40 mg/kg separately, the third group mice was injected with 0.9% NaCl aqueous solution as the nontoxic control. During the four weeks of the experiment, the behaviours of all the mice were normal, neither violent nor lethargic behaviour was observed. In addition, all experiment mice exhibited no clinical anorexia or symptoms such as hair loss or scab. Serum biochemistry assays uncovered that both the hepatic injury indicators alanine amino transferase (ALT) & aspartate amino transferase (AST) and kidney injury indicators uric acid (UA), blood urea nitrogen (BUN) & creatinine (Cr) displayed similar levels for the carbon dots injected mice and control group mice, which indicated that carbon dots were non-toxic to mice. Histopathological analyses showed that carbon dots shall not cause the structure change of hepatic, splenic and kidneys sections. All of the above observations unambiguously demonstrated the nontoxicity of carbon dots in both in vitro and in vivo. Besides the mice evaluation, similar results were also observed from the zebrafish experiment[107], which also exhibited the excellent bio-compatibility of carbon dots.

Moreover, the plane cell toxicity of the carbon dots (synthesized by microwave heating of citric acid and urea) was also verified by Qu *et al*[59]. Carbon dots aqueous solution with a concentration of 1.5 mg/ml were adopted to grow the bean sprouts, the results indicated that carbon dots could be ingested by the plant cells, thus resulting in the bight emissive bean sprouts, and also no obvious toxicity and plant growth prevention were observed.

Due to the excellent bio-compatibility and bright fluorescence, carbon dots are naturally considered to be used in bio- and clinical applications. Ya-Ping Sun *et al*. have done the pioneer work for carbon dots bio-imagining[2]. They first employed carbon dots (synthesized by laser ablation) to label the E. coli ATCC 25922 cells, as depicted in figure 12 a-d, the cells displayed different colours when the excitation wavelength changed. Later, the same group also demonstrated the in vivo imaging of carbon dots[108], as can be seen in figure 12 e-i. The female DBA/1 mice (~25 g) were injected with 30 µg carbon dots (dissolved in 30 µL aqueous solution) via subcutaneous injection. As seen from figure 12f and h, subcutaneously injected mice shown bright green emission when stimulated by 470 nm, and the red light emission was observed for 525 nm excitation. Following the author's in vitro and in vivo imaging demonstration, various cell lines[7, 14, 17, 30, 62, 109-113] (such as HeLa cells, MG-63 cells and *etc.*) and animals[8, 107, 114, 115] (such as mice, zebra-fish and *etc.*) have been also imaged using diverse fluorescent carbon dots.

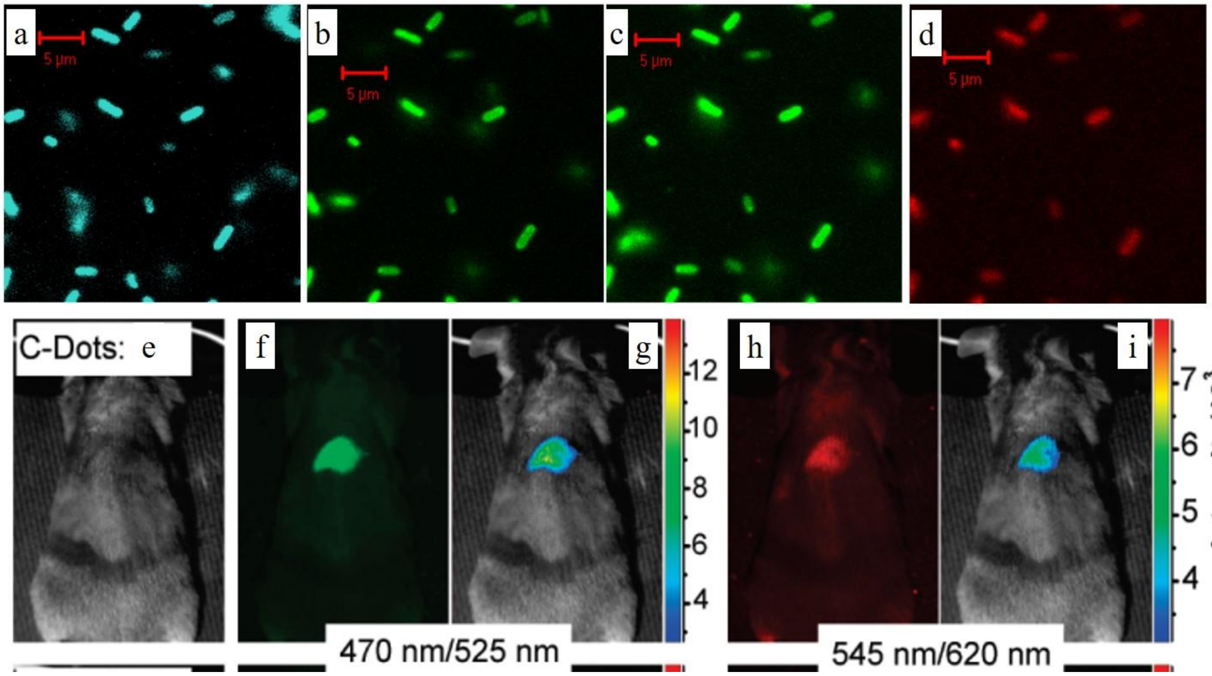

Figure 12 a-d) Confocal microscopy images of E. coli ATCC 25922 cell lines using carbon dots as the fluorescent material. a) 465 nm excitation, b) 477 nm excitation, c) 488 nm excitation, d) 514 nm excitation. e-i) In vivo imaging. e) Bright field image. f, h) In vivo fluorescent imaging for 470 nm excitation/525 nm emission and 545 nm excitation /620 nm emission respectively. g, i)

color-coded images for (b, d) respectively. The carbon dots were subcutaneously injected into the mice. a-d) Reproduced with permission[2]. Copyright 2006, American Chemical Society. e-i) Reproduced with permission[108]. Copyright 2009, American Chemical Society.

For further preclinical and potential clinical applications, carbon dots must meet the requirement of U.S. Food and Drug Administration (FDA) where the agents injected into human body must be removed entirely in a reasonable period of time[116], thus the injected agents cannot accumulate in the body and their circulation time should be optimized. The bright emissive carbon dots could be used as the in vivo bio-imaging, thus also endow the possibility to explore the biodistribution and clearance in animals. A main challenge for the carbon dots[8] (synthesized by laser ablation of carbon target, followed by PEG_{1500N} surface passivation) in vivo bio-imaging is the relative low quantum yield in the near-infrared (NIR) wavelength range of 650-900 nm. The in vivo imaging possess the high quality in the near-infrared (NIR) region as both the tissue absorption and scattering are supressed in these region. To overcome this issue, near-infrared dye ZW800 (emission wavelength about 795 nm) has been employed by Huang and co-workers[8] to link to the carbon dots by means of conjugating the dye NHS ester with amino groups on the C-dots. The resulted ZW800-carbon dots shown two absorption peaks at 420 nm and 770 nm and two emission peaks at 510 nm and 800 nm, corresponding to the carbon dots and dye ZW800 respectively. Various biological fluids (fetal bovine serum (FBS), blood, urine, and tissue lysate) tests demonstrated that the ZW800-carbon dots exhibited photo-stability, chemical stability and low emission background.

The carbon dots in-vivo dynamics was explored by means of three different injection routes: intravenous (iv), subcutaneous (sc), and intramuscular (im). The blood circulation behaviours of carbon dots were revealed by the relative PL intensity in the venous blood, which was analysed by the Maestro all-optical imaging system. The results demonstrated that different injection routes resulted in opposed carbon dots concentration dynamics. For iv injection approach, the carbon dots concentration in blood continued decrease after post-injection. Quantitative analysis disclosed that the PL intensity of the blood after 1 min of post-injection was about 17.3 times higher than 1 h. While for the subcutaneous (sc), and intramuscular (im) injection routes, the carbon dots concentration gradually increased and reached to the maximum value after post injection of 30 and 20 min respectively, as indicated by the increased blood PL intensity. These blood circulation behaviours were observed by both carbon dots part (420 nm excitation) and ZW800 component (770 nm excitation) emission. In addition to the blood circulation, the clearance or accumulation of carbon dots was evaluated by the authors[8]. Generally, nano-materials are cleared from body via two major approaches, namely the liver which convert it into bile and the kidneys which convert it into urine. Organs ex vivo imaging analysis demonstrated that for all three types of injection, most of the carbon dots were gathered by the kidneys after 1 h of post-injection. And the accumulation rate displayed the following sequence: im > sc > iv, on the contrary, only a small amount of carbon dots were collected by liver. However, when the time increased to 24 h, no obvious PL signal could be detected regardless of the injection approaches as illustrated in figure 13a, all of the observations ambiguously implied that carbon dots were totally removed from the body. Beside the ex vivo imaging, the authors[8] also employed the positron emission tomography

(PET) imaging technique, which shown similar results, which thus further confirmed the low accumulation of carbon dots in body. Further urine clearance evaluation was analysed by the in vivo bladder imaging analysis. Bladder red emission imaging demonstrated that intravenous (iv) injection exhibited fast clearance and reached to the maximum after 10 min of injection, subcutaneous (sc), and intramuscular (im) displayed a much lower urine clearance rate within 10 min as indicated by the relative low emission intensity. More specifically, the urine clearance rate of the three injection routes followed the sequence of iv > im > sc, which was in accordance with the carbon dots ZW800 clearance rate from the blood. The carbon dots ZW800 clearance mechanism was also confirmed by the carbon dots emission, while the strong background of urine in the visible range caused the contrast much lower. Besides, positron emission tomography (PET) imaging results also suggested the same urine clearance mechanism. We want to emphasize that different carbon dots sample may show different in vivo dynamics. Hong Bi's group[117] have demonstrated that carbon dots synthesized from thermal pyrolysis of konjac flour accumulated in both kidney and liver after 4 h of intravenous injection. While after 24h of the injection, all carbon dots are cleared from the mice, thus no PL signal can be detected from the organs.

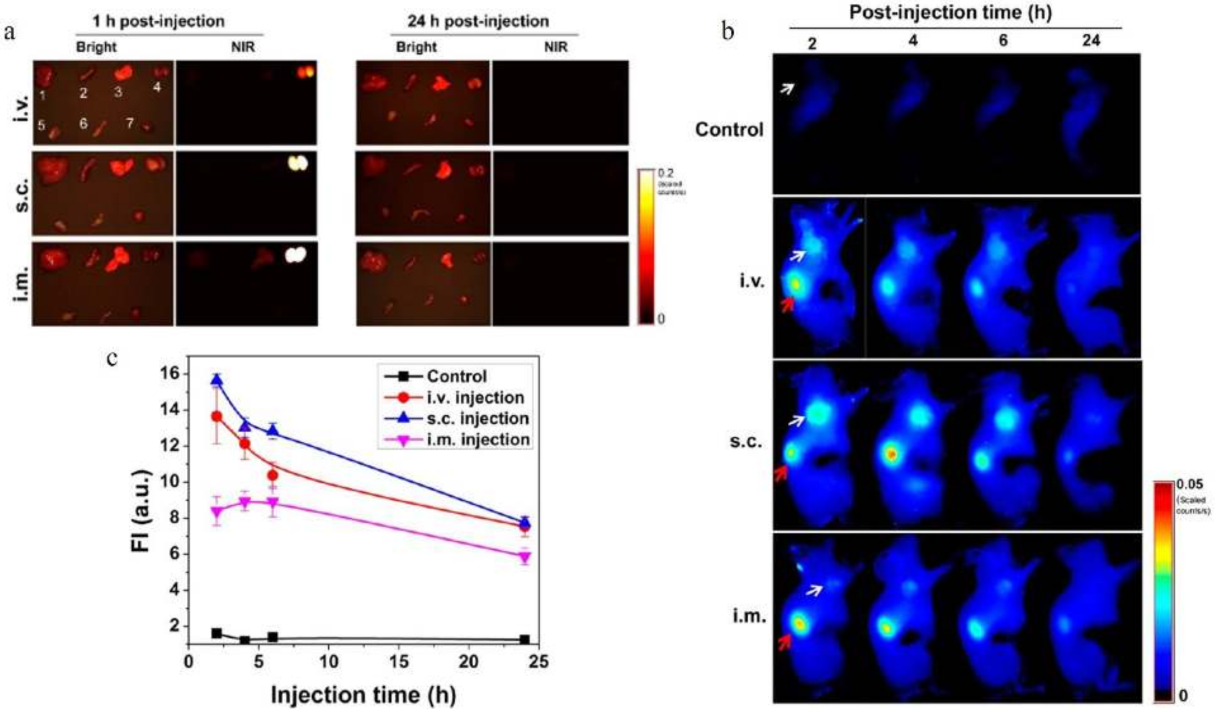

Figure 13 a) Ex vivo imaging of biodistribution of C-dot particles. After injection of ZW800-carbon dots, the major organs and tissues were collected from Balb/C mice at 1h (left) and 24 h (right), and subsequently, the bright field and NIR imaging were obtained using a Maestro imaging system. Top, iv injection ; Middle, sc injection ; Bottom, im injection ; Bright field numbers: 1, liver; 2, spleen; 3, lung; 4, kidneys; 5, muscle; 6, intestine; 7, heart. b) Tumor accumulation of ZW800-carbon dots for different injection approaches. In vivo fluorescence images of SCC-7 tumor bearing mice acquired after 2, 4, 6, and 24 h injection: control (without injection); iv; sc; im (white arrow labels tumor; red arrow labels kidney). c) Tumor florescence intensity analysis. a-c) Reproduced with permission[8]. Copyright 2013, American Chemical Society.

Another fascinating discovery by the authors[8] was that the prominent and prolonged ZW800-carbon dots uptaken by tumor. Athymic nude mice bearing subcutaneous SCC7 tumor were employed as the tumor model. All ZW800-carbon dots injected by three routes manifested accumulation around the tumor, resulting in the bright red light emission, thus the tumor became distinguishable from the surrounding normal tissue. In addition to the tumor accumulation, the remaining carbon dots exhibited no accumulation for other normal organs and was totally removed via kidneys (red arrow), which was uncovered by the in vivo imaging analysis using Maestro all-optical imaging system. The carbon dots accumulation ability at tumor site also displayed injection route dependence. Subcutaneous (sc) injection route gave the highest accumulation ability, thus exhibited the brightest emission. Intravenous (iv) group displayed a lower accumulation, but the light emission was still clear from the tumor. The lowest accumulation ability was observed from intramuscular (im) injection which showed the minimum PL intensity as seen figure 13b and 13c[8].

All the observations have great significance to the clinical applications. Carbon dots displayed no accumulation overtime for all normal organs in body and could be entirely removed from body via Kidney[8], which meets the requirement of The U.S. Food and Drug Administration (FDA). In addition, the unique tumor accumulation ability implied that carbon dots carried drug may exhibit better therapeutic effect, as discussed in the next sub-section. Moreover, the in vivo performance such as tumor targeting, blood circulation time *etc.* could be controlled by properly choosing the injection routes.

4.2 Drug delivery

The excellent bio-compatibility and clearance from body of carbon dots desirably meet the pre-requisition of in vivo applications. The rich and tunable function groups such as amino, carboxyl, or hydroxyl *etc.* endow carbon dots the ability to carry therapeutic agents, generating the theranostic nanomedicine[118-122]. The bright emission of carbon dots provide the opportunity to dynamically and real-time monitor the drug distribution and response. Carbon dots synthesized by thermal pyrolysis of citric acid and polyene polyamine have been employed by Zheng and co-workers to carry oxaliplatin[123], one of the platinum-based drug, where the platinum-based drugs are the most efficient anticancer drugs used in more than 50% chemotherapeutic treatment for clinical cancer patients. One of the oxaliplatin (IV) derivatives Oxa(IV)-COOH was employed to link with carbon dots, forming CD-Oxa, and the linkage was finished by the reaction between the amino groups on carbon dots surface and the activated COOH group of Oxa(IV)-COOH, where the COOH group was activated by using EDC/sulfo-NHS, as shown in figure 14a. The newly appeared Pt 4f XPS signal confirmed the successful bonding of Oxa(IV) to carbon dots. Inductively coupled plasma mass spectrometry (ICP-MS) analysis unveiled that the platinum element of carbon dots-Oxa was 1.5 wt. %, corresponding to a 4.2 wt. % oxaliplatin(IV). In addition, TEM data indicated that the size of carbon dots-Oxa was 2.71 ± 0.43 nm, larger than the diameter of pure carbon dots (2.28 ± 0.42 nm).

The synthesized Carbon dots-Oxa was injected into the hepatocarcinoma 22 cell line (H22) liver cancer of Chinese Kun Ming (KM) mice by means of intralesional injection[123], and the dynamical distribution of the drug was observed from in vivo optical imaging system using the blue light as the excitation source. At the instant of the exposure[123] (figure 14b), a highlight point was observed from the in vivo imaging due to the high concentration of carbon dots, and the following delivery of Carbon dots-Oxa resulted in the fluorescent intensity decrease of initial position and a broaden intensity distribution. After 24 h post-injection(figure 14e), the PL signal became much weak, which implied the decrease of the oxaliplatin(IV) drug, thus the second injection was carried out by the authors[123] and the PL intensity became strong again. Furthermore, the PL intensity declined over another 24 h (figure 14 g), and the PL signal totally disappeared when the time reached to 72 h (figure 14h), which implied that the carbon dots were cleared from the body entirely. The tumor size of mice continued to decrease along the time of therapy, from 6.5 cm^3 at the initial exposure time to 1.2 cm^3 within 2 times injection, as observed by the authors[123] (figure 14i). The dynamic drug distributions in tumor and body during the cure process were obtained by the fluorescence carbon dots, thus one can achieved the "personalized medicine", which means that the injection doses, time *etc.* can be controlled for individual patient.

Later, the charge-convertible carbon dots have also been fabricated for drug delivery by Feng *et al.* [124]. The carbon dot surface was negatively charged at pH= 7.4 which correspond to the normal physiological condition, while the surface reversed to positively charged when pH decreased to 6.8, mimicking the tumor microenvironment. Negatively charged carbon dot surface in the normal cell microenvironment suppressed the drug absorption of normal cells by means of electrostatic repulsion between the carbon dots surface and the negatively charged cell membrane, thus reducing the side effect. On the contrary, the positively charged carbon dots surface in tumor cell microenvironment could promote the internalization and cancer drug absorption because of the electrostatic interaction with negatively cell membrane (figure 14g). Both the in vitro and in vivo demonstration indicated[124] that carbon dots could be used as an effective imaging guided drug carrier with increased therapeutic efficiency and deceased side effect.

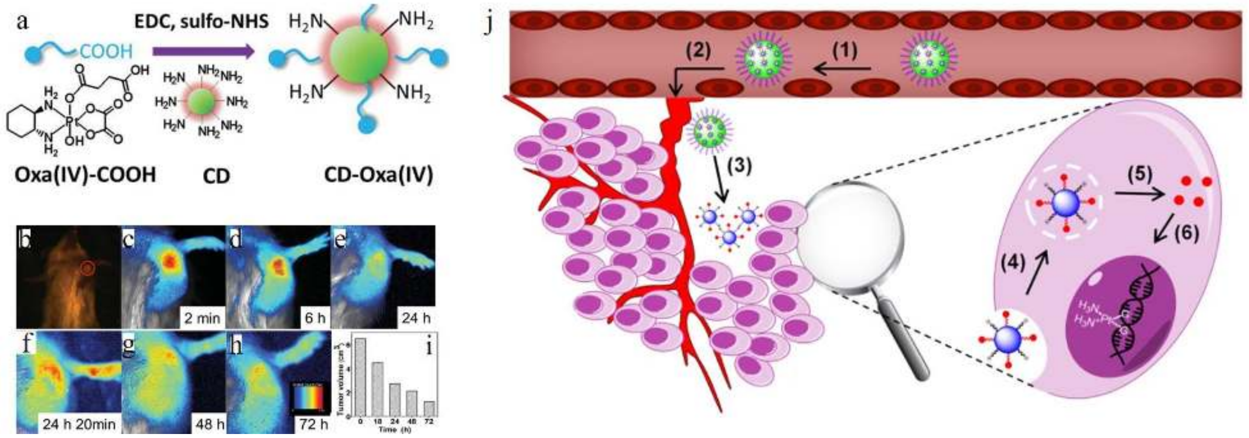

Figure 14 a) The Linkage illustration between the Oxa(IV)-COOH and carbon dots. b-h) In vivo imaging of H22 xenograft model mice for different period of times after intralesional injection. b) Injection time, red circle means the tumor site (white light view). c-e) Correspond to the time of 2 min, 6 h and 24 h. f) Second injection. f-g) The in vivo imaging for 48 h and 72 h. i) Tumor size of H22 xenograft model, it could be clearly seen that the tumor size continuously decrease. j) Illustration of the charge convertible carbon dots based drug delivery process. 1. Negative charged carbon dots extended the circulation time in blood. 2. The drug accumulated at the tumor position via the enhanced permeability and retention effect. 3. Drug response in the tumor micro-environment. 4. Drug uptake by the cancer cells. 5. Drug release from carbon dots carrier through proton sponge effect. 6. cisplatin attaching with DNA to display cancer cell cytotoxicity. a-i) Reproduced with permission[123]. Copyright 2014, Wiley-VCH. j) Reproduced with permission[124]. Copyright 2016, American Chemical Society.

4.3 Microfluidics marker

Microfluidic systems have become a superior platform for investigating the fluidic physics at microscale[125, 126]. The dramatically increased surface to volume ratio results in the surface tension and viscosity dominant over the inertial effects, thus makes the fluid easier to manipulate. The typical micro-fluidic cases are static laminar flows and dynamic droplet formation, and both of them possess various merits such as less reagents consumption, high sensitivity, high output *etc.*, which makes them find numerous applications in bio-assay, chemical reaction, drug delivery *etc*[127-129]. Most of the applications are based on the fluid flow visualization in the microfluidic circuit. However, the currently employed fluorescent materials cannot balance the bio-compatibility and low-cost, which is an urgent issue for microfluidic applications, especially for the bio-applications. To address this issue, carbon dots (synthesized from microwave heating of glucose and urea) have been firstly employed to visualize the micro fluid flows by Sun's group[130]. The authors have explored the mix dynamics of DI water and glycerol with the carbon dots dissolved DI water as the fluorescent marker. At t=0 s (figure 15a), the flat flow was determined by the hydrodynamic driving, the applied electric field (136.36kV/m) ruptured the interface and resulted in the complete mixing at t=3.76 s, as seen in figure 15a. The instability process was balanced by the pressure gradient, viscous dissipation and electric field induced body-force ruled by the ion species conversion law in each fluid. An electric field higher than a threshold shall rupture the interface and lead to the rapid mixing at microscale[131]. In addition to the laminar flow, mono-dispersed droplets also achieved by the authors[130] using the flow focusing configuration, where the carbon dots aqueous solution was the dispersed phase and the mineral oil acted as the continuous phase. The diameter of droplet followed an inverse relationship to the capillary numbers (Ca) defined as $Ca = \mu v/\gamma$, where the μ and v were the dynamic viscosity characteristic velocity of the mineral phase respectively, and γ represented the interfacial tension between the dispersed (carbon dots aqueous solution) and mineral oil continuous phases. The larger capillary numbers means higher interfacial shear force, thus the diameter of the droplets decreased. The results are shown in figure 15b and 15c, where the generated droplets changed from squeezing to dripping and finally reached jetting along with the increasing of capillary numbers (Ca). Besides, the multiple component droplet, merged droplet and double emulsion which possess the unique core-shell structure have also been demonstrated successfully by the authors[130] by making use of the superior carbon dots. To further quantitatively measure the velocity of the flow field, carbon dots fluorescent seeding particle was also been fabricated by stir-mixing the 3 μm porous polystyrene microparticle with carbon dots aqueous solution. The velocity field measured by the Micro-particle image velocimetry (μ-PIV) technique using carbon dots seeding particle was exhibited in figure 15d and 15e, which matched very well with the simulation results (figure 15f) [130]. All of the static and dynamic, qualitative and quantitative measurements unambiguously exhibited the high potential of applying carbon dots in microfluidics.

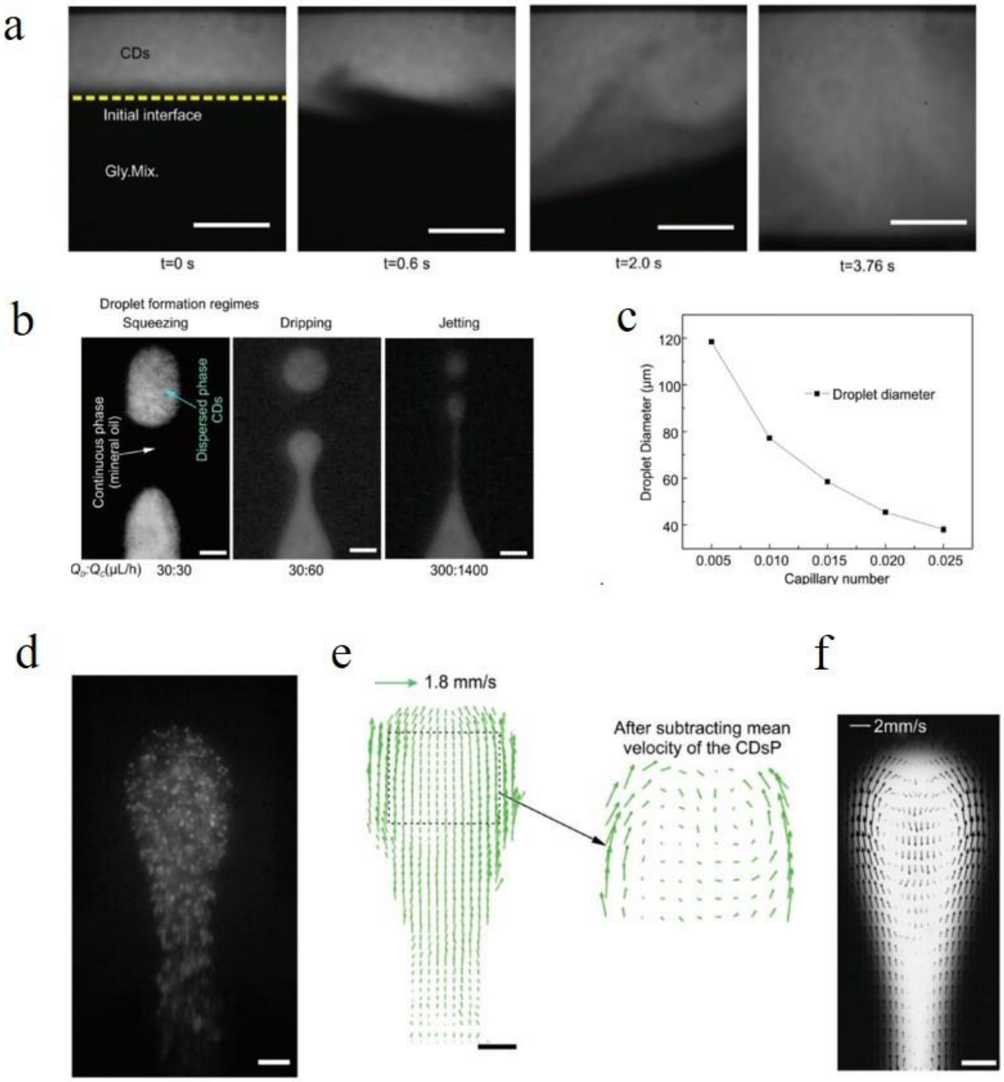

Figure 15 a) Mixing evolution of carbon dots aqueous solution and glycerol at an applied electric field of 136.36 kV/ m, scale bar 100 μm. b) Droplet formations in three typical regimes: squeezing, dripping, and jetting, which correspond to the different capillary number, scale bar 50 μm. c) Relationship between capillary number and droplet diameter. d-f) flow velocity field measurement using carbon dots based seeding particle. d) Florescent imaging of droplet generated with the carbon dots seeding particle distrusted in the dispersing phase. e) The measured velocity field by using the micro-PIV technique, scale bar 50μm. f) The simulation results of the velocity field of the droplet, which match very well to the measurement. For all experiments and simulations, the flow rate of dispersed phase and continues phase is 20: 100μL/h. Reproduced with permission[130]. Copyright 2017, Wiley-VCH.

4.4 LEDs

In 2010, Wang *et al*[39]. achieved the direct white light emission from carbon dots, which offered the possibility to fabricate carbon dots based white light emitting devices[132-135]. Later, they carried out the white light emitting devices by using the white light carbon dots as the emissive layer[136]. Briefly, the carbon dots were synthesized by thermal pyrolysis method using citric acid as the carbon source and 1-hexadecylamine as the surface passivation agent, which showed a relative high quantum yield of 60% with average diameter of 5 nm.

The device structure, energy alignment, and organic molecular structure adopted by the authors[136] were illustrated in figure 16a-c. The architecture of the device was constitutive of three layers. The buffer layer consisted of 40 nm poly (3,4-ethylenedioxythiophene) : poly(styrenesulfonate) (PEDOT : PSS) in anode, which have two functions: 1. Increase the work-function from 4.7 eV (ITO) to 5.0 eV. 2. Increase the smoothness of the anode. The carbon dots emissive layer was fabricated by spun-cast method with an optimized thickness of 20 nm. A thicker film *e.g.*35 nm shall lead to the bad charge transport in the carbon dot film, but a thinner film *e.g.*10 nm shall increase the density of voids, grain boundaries *etc.*, both of which shall decrease the device EL efficiency. AFM measurement indicated that the surface roughness of the carbon dot film was less than 3 nm, which implied good compatibility between the carbon dots and the buffer layer. The electron transport layer was employed by 40 nm thick 1,3,5-tris(N-phenylbenzimidazol-2-yl) benzene (TPBI) since its well behaved electron transport ability. The electrode was consist of 1 nm LiF and 120 nm Al fabricated by thermal evaporation.

The pure carbon dots exhibited broad PL with the excitation dependent emission feature, while the LED device displayed stable emission even if the voltage was increased to 10 V as shown in figure 16d[136]. The Commission International d'Eclairage (CIE) coordinates of the emitted light was (0.40, 0.43) ((0.33, 0.33) for pure white light), with a color-rendering index CRI of 82. The WLED had a turn on voltage of 6 V, with the maximum external quantum efficiency (EQE) reaching to 0.083% at a current density of 5 mA/cm^2, and the maximum brightness output was 35 cd/m^2 with the condition of current density 160 mA/ cm^2 and voltage 9 V.

By modifying the device structure, color-switchable CD LEDs were demonstrated using the same carbon dots by Zhang's group[137]. According to the excitation dependent PL and time resolved measurement, the authors claimed that there existed three emission channels whose lifetimes were 2 ns, 5-6 ns and 14-15 ns, contributing to 420 nm, 460 nm and 580 nm band emission respectively. In addition, the authors proposed[137] that the relaxation process for high energy emission was faster. Adopting this assumption to the carbon dot LED, different current injection shall lead to the following conclusion. When the injection current density is low, the hot carries will relax by means of the fast decay channel, resulting in the high energy emission *e.g.* 412 nm band or blue emission, while the high injected current density can stimulated all of three emission band. In addition, the highly populated excited states can feed the lower emission band *e.g.* 480 nm and 580 nm states, thus the lower band emission become dominant in the case of high current injection. So by adjusting the injection current, the authors achieved[137] the tunable color emission based on one kind of carbon dots.

The structure illustration of the CD LED device adopted by the authors is shown in figure 16e-g[137]. Briefly, the LED consisted of six layers: ITO anode, 25 nm hole injection layer, 40 nm hole transport layer (HTL), 20 nm carbon dots layer, 5 nm electron transport layer (ETL), and top cathode layer. Poly (ethylenedioxythiophene):polystyrene sulfonate (PEDOT:PSS) has been utilized as the hole injection layer. Poly-(N,N'-bis(4-butylphenyl)-N,N'-bis(phenyl) benzidine) (poly-TPD) was employed as the HTL because of its superior hole transport capability, the matched energy alignment between poly-TPD and PEDOT:PSS layer and easy to synthesize uniform thin film. The ETL and the cathode layer were designed for certain purpose. When choosing 1,3,5-tris(N-phenylbenzimidazol-2-yl) benzene (TPBI) as ETL and 1-nm LiF and 150-nm aluminum as the cathode double layer, the turn on voltage was 5 V and the injection current density could be tuned from relative low to relative high(reach to 600 mA/cm^2), as discussed above, different injection current density(or the corresponding applied voltage) shall result in different color emission, as can be seen figure 16h. The blue, cyan, magenta, and white light emission occurred at the voltage of 6 V, 7 V, 8 V, 9 V respectively, the Commission Internationale de I'Enclairage (CIE) coordinates for the four emission colors were (0.198, 0.151), (0.212,0.162), (0.260, 0.221), and (0.318, 0.320) [137].

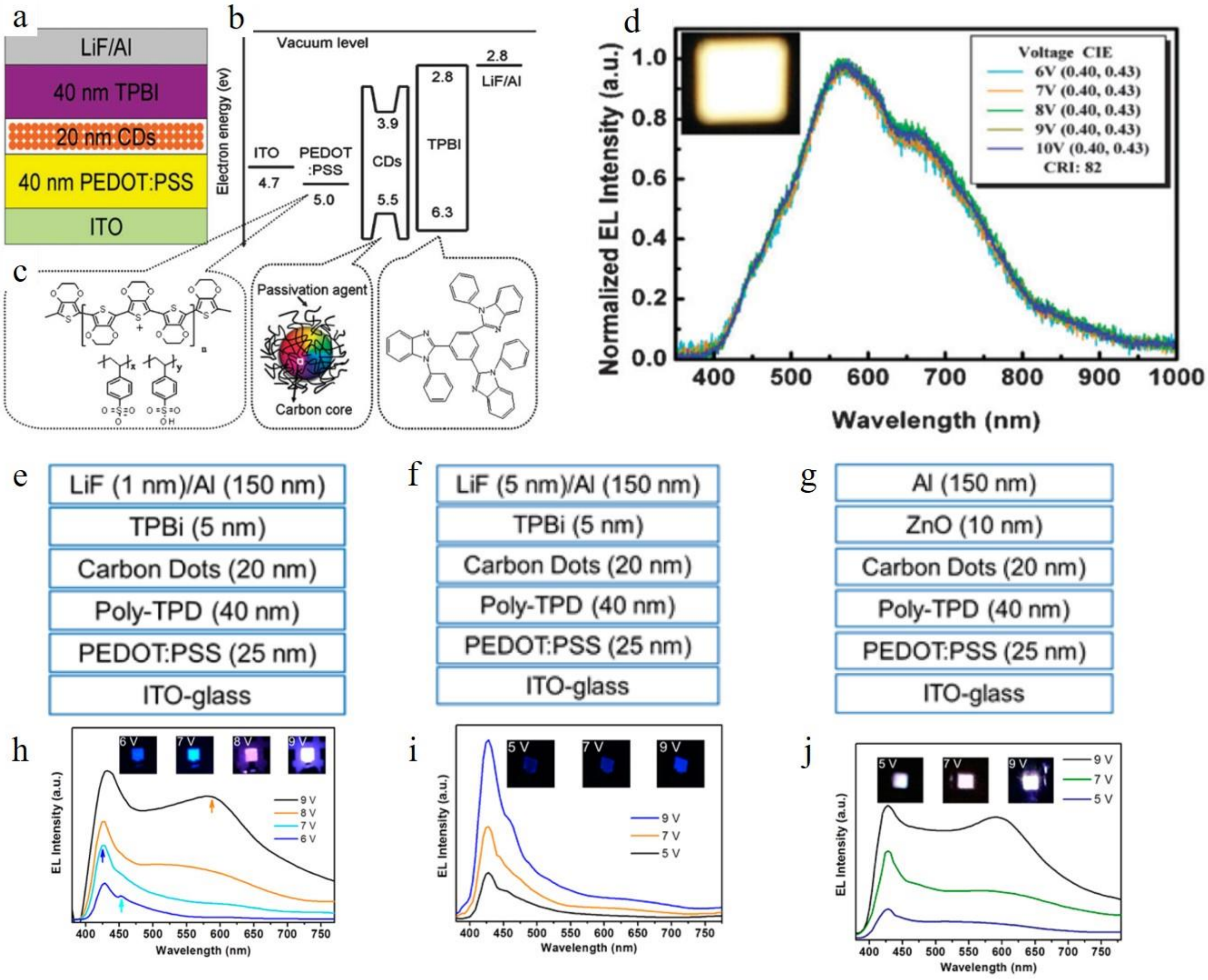

Figure 16 a-c) White light LED device structure illustration, energy alignment, and organic molecular structures. d) Normalized electroluminescence spectra of the carbon dots white light LED, inset is the photograph of the white light emission from the LED with a voltage of 9 V. e-g) The schematic diagrams of device structure for tunable EL light, blue light and white light emission LEDs respectively. h-j) The corresponding EL spectra for tunable, blue and white carbon dots LEDs, inserts are the photographs for the devices at different applied voltage. a-d) Reproduced with permission[136]. Copyright 2011, Royal Society of Chemistry. e-g) Reproduced with permission[137]. Copyright 2013, American Chemical Society.

To obtain the pure blue emission CD LED, the low current injection density was necessary, thus the authors[137] increased the thickness of LiF layer of cathode layer from 1 nm to 5 nm, as a result, the current density decreased to 150mA/cm^2 resulting in the pure blue CD LED with the turn on voltage 5 v and the maximum luminance 24 cd/m^2, as illustrated in figure 16i. Similarly, the high current density injection could result in the white light emission. Thus, ZnO nanoparticles have been utilized as the ETL and the cathode layer only contained 150 nm Al, the high electron mobility of ZnO nanoparticles ($2*10^{-3}$ cm^2 V^{-1} S^{-1} for ZnO, one order of magnitude higher than TPBI $1*10^{-4}$ cm^2 V^{-1} S^{-1}) endowed the high injection current density to the emissive layer, resulting in the white light emission as depicted in figure 16j. The white light CD LED possessed the maximum luminance of 90 cd/m^2 with a turn on voltage about 4.6 V.

Different from controlling the injection current density, carbon dots with excitation independent emission have also been proposed by Yang's group to fabricate mono color light emission LEDs[13]. The carbon dots were synthesized by means of hydrothermal methods. By controlling the carbon source (citric acid), nitrogen source (2,3-diaminonaphthalene or 1,5-diaminonaphthalene), surface passivation/carbonization(concentrated sulfuric acid) and reaction time, all the blue, green, yellow, orange, and red emission carbon dots have been achieved. All the carbon dots exhibited relative high quantum yield: 75% (B), 73% (G), 58% (Y), 53% (O), and 12% (R). The EL spectra of all carbon dots were consistent with the PL spectra with the peaks located at 455 nm (blue), 536 nm (green), 555 nm (yellow), 585 nm (orange), and 628 nm (red) and displayed voltage independent EL colors. The authors[13] attributed the tunable PL emission and voltage stable EL emission to the band emission of carbon dots with quantum confinement effect. The CIE coordinates, maximum luminance, current efficiency for the monochrome LEDs were[13] ((0.19, 0.20), 136 cd/m^2, 0.084 cd/A), ((0.31, 0.47), 93 cd/m^2, 0.045 cd/A), ((0.37, 0.52), 60 cd/m^2, 0.02 cd/A), ((0.46, 0.48), 65 cd/m^2, 0.027 cd/A), ((0.55, 0.41), 12 cd/m^2, 0.0028 cd/A) for blue, green, yellow, orange, and red LEDs respectively.

4.5 Sensing

The fluorescence intensity of carbon dots is closely related to the surrounding environment. The interaction between carbon dots and chemicals results in the quenching/enhancement of carbon dots emission. Thus carbon dots can be used as a king of florescent probe to detect the quantity of the items. Various sensors based on the florescence of carbon dots have been reported and can be generally categorized into the following groups: ion sensing[138-141] such as Eu^{3+}, Fe^{3+}, Fe^{2+}, F^-, Tl^+ (thallium) *etc.*, pH value sensing[142-145], bio-material sensing[145-148] such as Intracellular Lysine, Ascorbic Acid, guanosine 3′-diphosphate-5′-diphosphate (ppGpp), enzyme(e.g. Thioredoxin Reductase (TrxR)), DNA *etc.*, and temperature sensing[149-151]. However, the single fluorescent wavelength intensity change related sensing requires strict conditions. The fluctuation of the light source, concentration of fluorescence probes, different optical paths, and even the aggregation of the probes could devalue the reliability of the sensing results. Thus ratiometric sensing as an alternate has been proposed[143, 145, 152, 153], which simultaneously collected the intensity change of two separated emission bands. The intensity ratio of the two wavelength is the indicator of the sensing item and considered as the output. Compared to single emission sensor, the ratiometric sensing provide the self-calibration for both the light source and sensing environment, thus can vastly improve the sensing accuracy and reliability.

The carbon dots based ratiometric pH sensing was first proposed by Wen and co-workers[152], where the carbon dots was synthesized by thermal pyrolysis of citric acid with the 4,7,10-trioxa-1,13-tridecanediamine (TTDDA) as the surface passivation agent. Both pH-sensitive fluorescent fluoresceinisothiocyanate (FITC) and pH insensitive rhodamine B isothiocyanate (RBITC) have been utilized to post-treat the carbon dots, endowing the carbon dots two emission bands located at 515 nm and 575 nm(excited by 488 nm), respectively. The author's demonstration[152] indicated that as the pH value changed from 5 to 9 which covered the full range of physiological environment of human body, the intensity of 515 nm emission band increased substantially, while the 575 nm only increased a little, thus it was clearly shown that the carbon dots exhibited linear ratiometric response to pH input (figure 17a and 17b). In addition, the authors also demonstrated[152] that both the in intracellular genres (such as ions, saccharides and proteins) and redox substances (*e.g.* H_2O_2, ClO, reduced glutathione (GSH), GSH inhibitor (NEM), and GSH precursor (NAC)) have neglected effect on the carbon dots ratiometric response, which verified the selectivity of the carbon dots based ratiometric sensing.

The small molecular linked carbon dot ratiometric sensors possess the high accuracy, while the ease to photo-bleaching, and the leaching of small molecular from carbon dots also limited their practical applications. To overcome these issues, the label free carbon dots ratiometric pH sensor was proposed by Huang's group later[154]. The carbon dots was synthesized by hydrothermal treatment of citric acid and basic fuchsin where the fuchsin had the pH sensitive property. The carbon dots displayed two emission peaks located at 475 nm and 545 nm, respectively, when excited by 380 nm. The pH dependent experiments uncovered that as the pH values increased from 4.0 to 11.0, the intensity of 475 nm emission band continuously increased, while the intensity of 545 nm emission band manifested different performance which slightly increased from acid to neutral condition, further increasing the pH from 7 (neutral condition) to 14(alkaline condition) resulted in the decrease of the 545 nm emission band, as shown in figure 17c. The intensity ratio of 457 nm and 545 nm exhibited a linear relationship to the pH values in the range of 5.1 to 8.8, as can be seen in figure 17d[154], which implied that carbon dots could be used as the ratiometric pH sensor. The reproducibility experiments demonstrated that carbon dots emission could totally recover between the strong acidic environment (pH=4.0) and the strong alkaline condition (pH=11.0). In addition, the authors also substantiated[154] that both the metal ions (such as Fe^{3+}, $Cu2^{+}$, Hg^{2+} *etc.*), biothiol (e.g. GSH, Cys) and reactive oxygen species (ROS) (*e.g.* H_2O_2, HClO) had negligible influence to the ratiometric pH sensing, thus verified the selectivity of the sensing. The living HeLa cells were employed by the authors[154] to inspect the function and applicability of the carbon dots sensor. HaLa cells were treated by various buffered solutions which had different pH values (pH=5.01, 5.64, 6.46, 7.21, and 8.01). The results were displayed in figure 17e. As the pH values increased from 5.0 to 8.0, the blue emission corresponding to 475 nm band (465-495 nm, channel 1) increased, but the 545 nm yellow light (535-565 nm, channel 2) showed slightly decrease. The merged graphs of blue emission and yellow emission band exhibited a pronounced color change[154] as the pH value continued to increase, which could be clearly seen by the naked eyes. The fluorescence ratio imaging was accomplished by using imaging processing as illustrated in figure 17e. The calibrated Ratio-pH function was also obtained[154] by calculating the average PL intensity of the blue channel and yellow channel. Later, Song *et al*[145] also proposed another kind of dual emissive carbon dots (synthesized by hydrothermal treatment of o-phenylenediamine and phosphoric acid). The carbon dots exhibited two emission bands at 400 nm and 624 nm, where the 400 nm blue emission could be enhanced by the lysine while the 624 nm red emission band was inert to lysine. However, when the input changed to different pH values, the results were different: as the pH value increased from 1.5-5.0, the 400 nm blue band became stable, while the 624 red band emission decreased. In both cases, the intensity ratio of the two emission bands manifested linear relationship to the input items (lysine or pH), thus the authors advised[145] that the carbon dots could be used to sense both the lysine (linear performance in the range of 0.5-260μM with a detection limit of 98 nM) and pH value (linear performance in the range of 1.5 to 5) in a ratiometric manner, as seen in figure 17f-i.

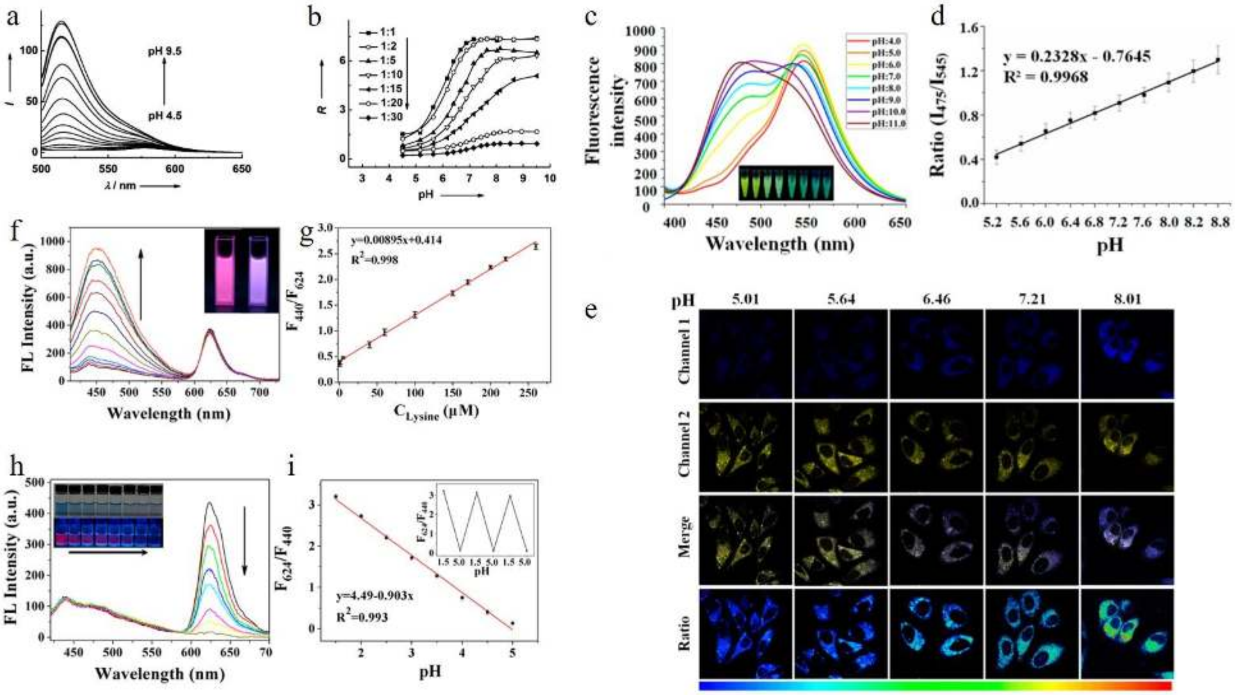

Figure 17 a) PL emission spectra of carbon dots in the pH range of 4.5-9. b) The relationship between the Intensity ratio (I_{515}/I_{575}) R and pH values. The carbon dots were surface passivated by FITC and RBITC with different molar ratio from 1:1 to 1:30. c) PL spectra of carbon dots in PBS buffer solution with different pH values (stimulated by 380 nm), inserted picture was the corresponding color change under 365 nm UV. d) Linear relationship between the intensity ratio and pH value. e) Confocal fluorescence images of HeLa cells. Channel 1: 465-495 nm band pass filter. Channel 2: 535-565 nm band pass filter. The ratio of the two band emission was obtained by imaging processing. All the samples were stimulated by 380 nm. f) PL emission spectra of carbon dots for different concentration of lysine: from 0.5-260μM in 100mM buffer solution with the pH value of 2. g) Linearly relationship between the intensity ratio (F_{440}/F_{624}) and the lysine concentration. h) PL emission spectra of carbon dots for buffer solutions at different pH values (in the range of 1.5-5.0), inserted were the photographs of the buffer solutions under white light (upper) UV light (lower) excitation respectively, left to right: pH value 1.5 to 5.0. i) The linearly relationship between the intensity ratio (F624/F440) and the pH values. a-b) Reproduced with permission[152]. Copyright 2012, Wiley-VCH. c-e) Reproduced with permission[154]. Copyright 2016, American Chemical Society. f-i) Reproduced with permission[145]. Copyright 2017, American Chemical Society.

4.6 Logic gates

The development of the molecular devices can help to achieve the multifunctional "lab-on-a-molecule"[155], and triggers the applications of molecular information processing, communication, molecular based bio-sensing *etc*[156]. All of the intriguing applications are based on the basic logic operations, and PL signal is regarded as the desirable logic gate readout due to the fast response, increased signal to noise ratio and high resolution. All those good merits of the florescent carbon dots make them an effective competitor in logic gates [157-162].

The pre-requisite to achieve the carbon dots chemical logic gate is to generate variable PL output, which could be realized by heavy metal ion caused PL quenching. Carbon dots aqueous solution synthesized by thermal pyrolysis of lemon juice have been adopted by Pal's group[15],which displayed two absorption bands located at 268 and 320 nm respectively. The authors[15] also discovered that increasing the pH value to 10.2 resulted in the enhanced 268 nm absorption and the appearance of a new broad band at longer wavelength. The pH dependent PL of carbon dots was also evaluated by the authors[15]. Exited by 360 nm, the PL intensity increased when the pH values increased from 1 to 7 with the PL peak nearly keeping the same (the absorption difference of 360 nm was eliminated by the authors[15] via normalizing the PL intensity to the relative absorption). On the contrary, continuously increasing the pH value from 7 to 10 leaded to the decreasing of the PL intensity, along with an intriguing PL spectral redshift. The authors[15] also discovered that different excitation wavelength in the range of 320-380 nm resulted in the same emission peak located at 445 nm for both acidic and basic condition. However, when the excitation wavelength increased to 400 nm, the PL spectra of carbon dots in alkaline condition shown red shift with the peak shifted to 465 nm, while nearly no PL signal could be observed from acidic carbon dots. Both the pH dependent absorption and emission spectra were completely reversible, which implied that both acidic and basic condition shall not degenerate the carbon dots.

Based on the opposite Zeta potential values measured from acidic ($\xi = 0.13$ mV for pH =2.6) and basic ($\xi = -7.8$ mV for pH=9) carbon dots, the authors[15] attributed the pH dependent spectral shift and intensity variation to the pH-triggered protonation and deprotonation. FTIR spectroscopy analysis implied that two stretching bonds at carbon dots surface gradually disappeared as the pH value increased from 2.5 to 10. One of the bonds was the C=O bond of the carboxylic acid with infrared absorption at 1725 cm^{-1}, along with the appearance of two new carboxylate categories at 1575 and 1390 cm^{-1}. The other disappeared function group was the C-OH stretching of phenolic category with absorption at 1220 cm^{-1} which converted to phenolate bond at 1278 cm^{-1}.

Generally, carboxylic function groups possess lower pK_a value in the range of 4-5 due to the relative acidic properties, while more basic phenolic function groups hold a higher pK_a value about 8-10. Considering that there was only one inflection point for the pH dependent absorption density and PL spectra shift, the authors[15] assumed that only one function group was involved in the emission of carbon dots. The fact that both the pH dependent absorption optical density (@400 nm) and PL peaks manifested a sigmoidal pattern with a similar inflection point at pH=7.9 leaded the authors to advocate that it was the phenolic function groups which contributed to the carbon dots PL redshift in high pH conditions. More specifically, the phenolic group was strong coupled with the emissive center located at the surface of carbon dots which could modify the energy level of the emissive states. Therefore, Pal et al[15] suggested the following pH dependent PL mechanism: The high pH value condition will lead to the deprotonation equilibrium of phenol ↔phenolate (coupling with phenol and phenolate will result in different energy states), namely the transformation between phenol and phenolate, which can tune the PL emission of carbon dots. The carboxylic function groups cannot affect the PL properties of carbon dots because there is no coupling between the emission center and carboxylic groups, even though the carboxylic ↔ carboxylate deprotonation equilibrium also exist. Thus the authors proposed[15] that tunable PL signal of carbon dots could be achieved by the proper control the surrounding environment *e.g.* pH and surface chemical modification *e.g.* the presence of Hg^{2+}, which offered the opportunity to perform the carbon dots based chemical logic gates.

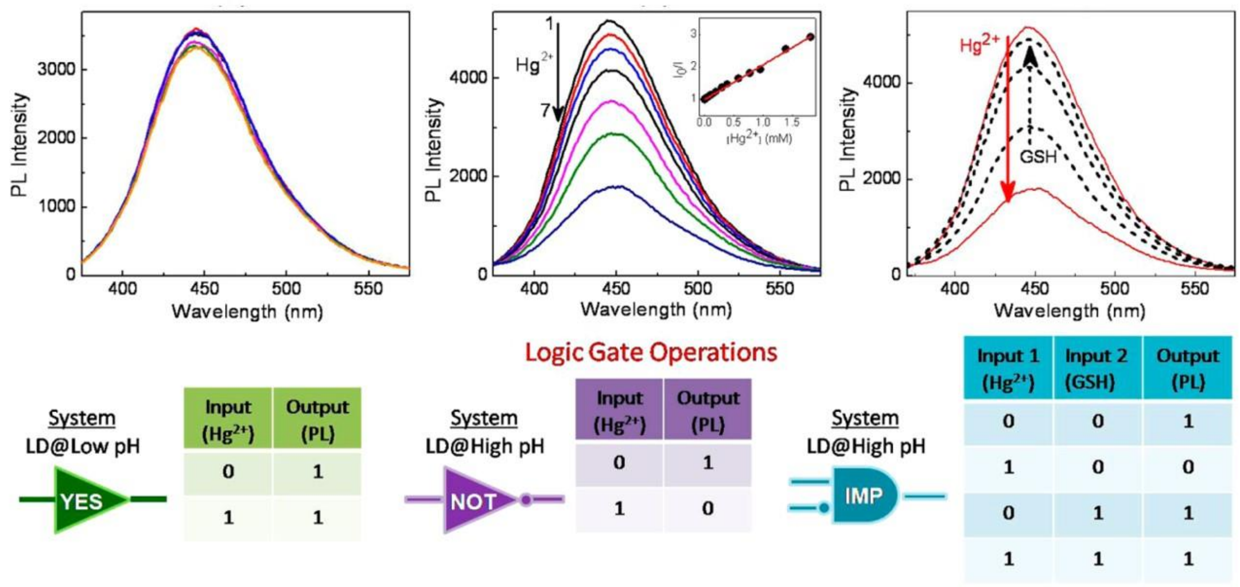

Input (Hg²⁺)	Output (PL)
0	1
1	1

Input (Hg²⁺)	Output (PL)
0	1
1	0

Input 1 (Hg²⁺)	Input 2 (GSH)	Output (PL)
0	0	1
1	0	0
0	1	1
1	1	1

Figure 18 PL spectra, corresponding logic gate and Truth tables for “YES”, “NOT” and “IMP” logic gate respectively. Reproduced with permission[15]. Copyright 2017, American Chemical Society.

As observed by the authors[15], In the condition of acidic environment *e.g.* pH=2.7, both the carboxylic (even the carboxylic group was not directly coupled with emissive states, it could also affect the PL quenching process by means of electrostatic interaction) and hydroxyl categories were absolute protonated, thus the Hg^{2+} could not quench the PL of carbon dots, as a result the authors suggested[15] that the YES logic gate could be realized if regarding the Hg^{2+} as the input and PL intensity as the output, as can be seen left part of figure 18. Increasing the pH value to 8.9 (basic environment) shall result in the deprotonation of both carboxylic and phenolic function groups, consequently, the surface of the carbon dots was negatively charged, which could interact with the Hg^{2+} leading the PL quenching. Therefore, the NOT gate was realized by the Pal *et al* [15] in the condition of basic environment when considering the Hg^{2+} as the input and PL intensity as the output (middle part of figure 18). The authors also discovered that the quenched PL could be recovered by adding the extra glutathione (GSH), as the thiol group in glutathione could combine with Hg^{2+} ion and release the carbon dots from the Hg^{2+} ion. But it should be noted pure glutathione could not affect the PL properties of carbon dots. Therefore, the implication logic gate was fulfilled by Choudhury and co-works[15] by using the Hg^{2+} ion and glutathione as the chemical input and the PL intensity as the output, as seen in right part of figure 18. If all the pH, $Hg^{2+,}$ and GSH were viewed as the chemical input and PL intensity as the readout, more complex logic gate could also be demonstrated.

Carbon dots synthesized by induction heater (500W, 100℃) of citric acid and ethylenediamine manifested pH stable PL in the range of 4-11, however it could be also used to realize chemical logic gate[157]. Chattopadhyay's group uncovered that the PL intensity (excited by 365nm, detected at 433 nm) of the carbon dots could be quenched by picric acid via static quenching. Additional mixture of acetonitrile, ethyl acetate and sodium chloride could transfer the picric acid to organic phase thus recovery the PL of carbon dots. Alternatively, the authors also discovered[157] that carbon dots could be quenched by Fe^{3+} through dynamic quenching, accomplished by ultrafast carriers transfer between the carbon dots and Fe^{3+} ions. The following treatment by ascorbic acid or cysteine shall reverse the PL quenching where the ascorbic acid could reduce the Fe^{3+} ion to Fe^{2+} ion and cysteine could yield complex with Fe^{3+}, both of them could consume the Fe^{3+} ion and release carbon dots emission. Diverse and multifunction logic gates were preferred by the authors[157] using the variable PL as output: The NOT logic gate has been realized by the using the picric acid (or Fe^{3+} ion) as the input (input logic 1); for the Fe^{3+} ion treated carbon dots system, the input of ascorbic acid (input logic 1) and cysteine (input logic 1) could result in the OR logic, as only when both of the input was 0 (both of ascorbic acid and cysteine were absent), the output was 0 (namely the PL intensity was low). By proper designing the system and chemical component input, even higher complex logical systems were demonstrated by Sk and co-workers[157].

4.7 Carbon dots chiral photonics

Chirality plays an important role in various practical application fields such as chiral drug recognition, chiral molecular biology, chiral chemistry and so on[163-165]. Thus the combination of carbon dots with chirality will give rise to the intriguing chiral optics based on carbon dots, which was first proposed by M. Va´zquez-Nakagawa et al[166]. In their pioneer work, the carbon dots were synthesized by means of chemical exfoliation (concentrated sulfuric acid and nitric acid) of graphite, and thionyl chloride was employed to convert the carbon dots surface carboxylic acid groups into acid chlorides. The simultaneous reaction between the acid chlorides and the (R) or (S)-2-phenyl-1-propanol (chiral molecular) resulted in the enantiomerically pure esters and formation of chiral carbon dots, as shown in figure 19a. The formation[166] of the enantiomerically esters and chiral carbon dots was confirmed by the ^{13}C-NMR and FTIR spectroscopy, where the appearance of 120–150 ppm in ^{13}C-NMR indicated the existence of the phenyl substituents and the 1731–1727 cm^{-1} (C=O stretch vibration), 1300 cm^{-1} (asymmetric stretching vibrations of C–

O–C) and 1200 cm^{-1} (symmetric stretching vibrations of C–O–C) signal in FTIR spectra implied the occurrence of ester groups.

The chiral carbon dots N-methylpyrrolidone (NMP) solution was prepared for the circular dichroism (CD) measurement. However, the authors discovered that[166] the chiral moieties at the carbon dots surface did not have obvious chiral absorption when the wavelength longer than 300 nm, thus pyrene molecular was introduced to the chiral carbon dots solution to form supermolecular, which could trigger the chiral property transfer from the chiral carbon dots to the supermolecular by means of strong π-π stacking forces, as observed from other carbon nano-forms[167-169]. Consequently, the pyrene/chiral carbon dots NMP solution displayed an obvious CD signal, as observed by the authors[166] (figure 19b). More specifically, the S-chiral carbon dots exhibited a positive Cotton effect in the absorption range of 320–350 nm, while the R-chiral carbon dots shown the opposite negative Cotton effect in the similar absorption range. The authors attributed[166] the small wavelength shift of CD signal for the R- and S- chiral carbon dots to the non-identical surface functionalization and organization.

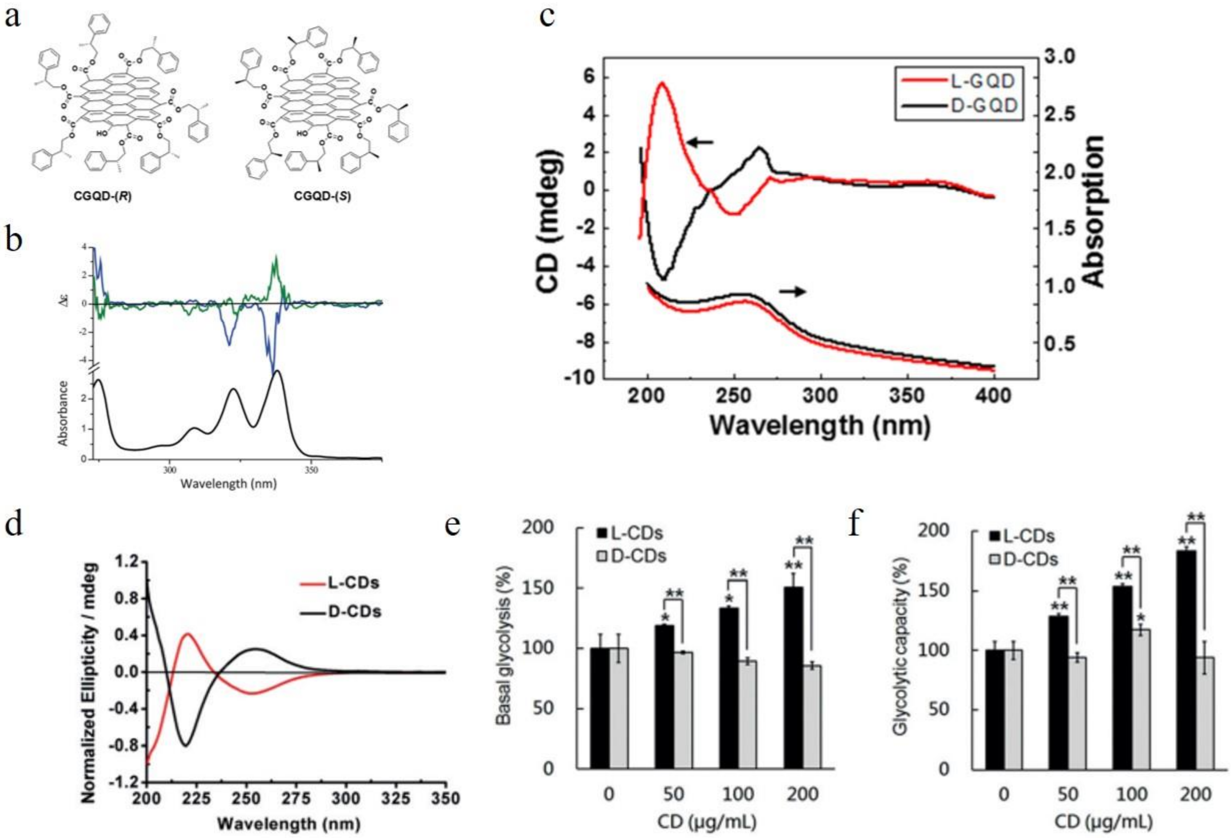

Figure 19 a,b) Chiral carbon dots synthesized by Martin's group. a) Structure illustration of Chiral carbon dots obtained from the (R) or (S)-2-phenyl-1-propanol. b) Upper: Circular dichroism spectra of chiral carbon dots-(R)/pyrene (blue) and chiral carbon dots-(S)/pyrene (green) in NMP solution. Bottom: UV-visible spectra of pyrene in NMP. c) Circular dichroism spectra of carbon dots synthesized by Nicholas A. Kotov's group[170]. d) Circular dichroism spectra of chiral carbon dots synthesized by Guangjun Nie's group[171]. e-f) The tunability of L- and D- carbon dots to ECAR (extracellular acidification rate) where the basal glycolysis and the glycolytic capacity are the indicators of the ECAR. a-b) Reproduced with permission[166]. Copyright 2016, Royal Society

of Chemistry. c) Reproduced with permission[170]. Copyright 2016, American Chemical Society. d-f) Reproduced with permission[171]. Copyright 2018, Royal Society of Chemistry.

In addition to the (R) and (S)-2-phenyl-1-propanol chiral molecules, L/D-cysteine chiral molecular also been adopted by Nozomu Suzuki *et al.*[170] to synthesize chiral carbon dots. Briefly, the carbon dots was synthesized by chemical exfoliation of carbon fiber in the presence of sulfuric acid and nitric acid, and the following carbodiimide/N-hydroxysuccinimide (EDC/NHS) cross-link method linked the L/D cysteine to the surface of carbon dots by means of covalently bonding the amine group in L/D cysteine with the carboxylic group in carbon dots, thus resulting in the chiral carbon dots, labeled as L-/D- carbon dots. Both pristine and chiral carbon dots exhibited the similar size distribution in the range of 2-7 nm and broaden XRD peak at $2\theta = 25°$. In addition, both the position and the relative intensity of the A_{1g} D band Raman signal at 1355 cm^{-1} and E_{2g} G band Raman signal at 1590 cm^{-1} were the same for pristine and chiral carbon dots. All of these indicated that the cysteine surface modification did not change the structure of the centre graphene carbon sheets as suggested by the authors[170]. The appearance of the S-H bond (2390 cm^{-1}) in FTIR spectra implied that the cysteine ligands was linked to the carbon dots successfully, and the linkage was finished via covalent bonding, which was verified by the newly formed C-N bond (830 cm^{-1}) in chiral carbon dots.

CD spectral measurement demonstrated[170] that both L and D chiral carbon dots exhibited two chiral bands, as seen in figure 19c, one was located at the high energy band of 210-220 nm, which was closed to the chiral band of the pure cysteine at 209 nm, the other was a lower energy chiral band located at 250-265 nm which have opposite sign compared to the chirality of cysteine used to modify the carbon dots. In addition, the lower energy (located at 250-265nm) chiral band manifested overlap with the absorption peak at 260 nm and displayed a relative high g factor of 1×10^{-4}. By using the combined calculation methods of semiempirical ZINDO algorithm, MMFF algorithm, DFT +ZINDO algorithms, and compared with the XPS and CD spectral data, the authors suggested[170] that the high energy chiral band originated from the hybridization of the atomic orbit of the cysteine chiral molecular and the molecular orbit of small segment or edge groups of the graphene sheet. The hybridization was caused by the symmetry-breaking triggered perturbation of the graphene surface edge states, due to the existence of the chiral ligands on the surface. Such a mechanism was termed as[170] local chirality induction. However, the authors also pointed out that local hybridization mechanism was not suitable for interpreting the longer wavelength chiral band (at 250-265 nm) because based on the theory, for the larger diameter of 10-15 nm carbon dots, no chiral band should be observed for wavelength longer than 220 nm even the local hybridization exist on the surface of the large diameter carbon dots. On the contrary, the authors[170] attributed the longer wavelength chiral band to the change of the conformation structure of the carbon dots itself. The cysteine ligand was linked to the carbon dots by means of noncovalent intermolecular interaction. Intermolecular interaction between the chiral molecular and the large carbon dots shall result in the buckling deformation, as a result, the equilibrium conformation of the carbon dots sustained a strong twist, more specifically, L-cysteine and D-cysteine shall result in right hand and left hand twist respectively, corresponding to the different twisted excitonic states. The twisted carbon dots could facilitate the electrons and holes to one of the excitonic states, resulting in the longer wavelength chiral excitonic band. It's clear that the chirality (i.e., rotatory handedness) of carbon dots was opposite to chirality of the modification chirality molecular, consistent with the authors' experiment observations[170].

In addition to surface chiral molecular modification[172, 173], chiral carbon dots could also be directly prepared by the chiral precursor Guanosine 5'-monophosphate, (5'-GMP)[174]. Briefly, the chiral molecular disodium salt of guanosine 5′-monophasphate, Na_2(5'-GMP) was heated by microwave at 160 °C for 5 minutes to synthesize chiral carbon dots. (HR)TEM analysis indicated that the carbon dots have an average diameter less than 5 nm, with a highly disordered amorphous carbon core. The amorphous carbon dots was also confirmed by the Raman spectroscopy due to the absence of the D band and G band signal for carbon dots. The synthesized chiral carbon dots displayed several chiral peaks including three positive peaks 218, 270 and 300 nm and two negative chiral peaks 230 nm and 260 nm. The similarity of the CD spectra of carbon dots and the 5'-GMP indicated that the chiral structure was converted during the carbon dots synthesis as suggested by the authors[174].

The most exciting news for chiral carbon dots are the recent achievements of the chiral control of the bio-reactions. Xin *et al*[175] demonstrated that D-glutamic acid (D-Glu)-carbon dots could drastically destroy both the Gramnegative and Gram-positive bacteria cell wall, resulting in the death of bacteria while its counterpart L-glutamic acid (L-Glu)-carbon dots manifested negligible effect to bacteria, which suggested that chiral carbon dots could be used as the chiral antimicrobial nanoagent. L and D cysteine based carbon dots have also been utilized to control the enzyme's chiral activity[176], *e.g.,* L cysteine carbon dots increased the laccase enzyme activity by 20.2% while D cysteine carbon dots exhibited opposite behavior suppressing the enzyme activity by 10.4%. Very recently, Li *et al.*[171] even discovered that the L/D cysteine based carbon dots could even affect the cellular energy metabolism. In the future, we believe that more chiral carbon dots based applications will be explored[177], and chiral carbon dots will become a new but fascinating field due to the huge practical applications.

5 Summary and prospect

Carbon dots as a new kind of carbon based fluorescent material have triggered numerous investigations. Various breakthrough have been obtained from fundamental optical-physical properties to potential applications. It's believed that carbon dots will play a more important role in various field in the future. Considering the excellent bio-compatibility, it's reasonable to predict that carbon dots will become an important platform for bio-applications. Thus, exploring the high quantum yield NIR emission carbon dots is urgent for bio-imaging, as the near IR light manifest high tissue penetration depth and deceased auto-fluorescent background. Carbon dots linked with proper moieties and therapeutic drugs offer the potential to identify the challenge of cancer heterogeneity and adaptation. However, as pointed out by Gao *et al.*[178], before the practical clinical applications of carbon dots, researchers should provide more evidences that carbon dots based drug deliver is better than the monoclonal antibody bonded anticancer drug[179] and biodegradable polymer linked drugs[180]. Consequently, the next step for carbon based nano-therapy is to explore carbon dots which can hugely reduce the non-specific uptake by normal cells, but increase the specific targeting capability, especially enhance the cancer cell specific targeting ability, and elongate blood circulation to increase to therapeutic effect. Namely to explore the carbon dots targeted nano–medicine to achieve the cancer targeted therapy. The carbon dots based targeted cancer therapy can vastly increase the therapeutic effect and decrease the side effect, thus may trigger the revolution on diagnose, treat and prevention of cancer[178].

Although carbon dots based optoelectronic applications have been demonstrated, *e.g.* in LEDs, the external quantum efficiency and the maximum luminance are still low, further improvement of the efficiency requires higher quantum yield carbon dots, proper device structure design. Both of them are related to a clear understanding of the optical physical properties of carbon dots. As we discussed above, researchers have paid much attentions to understand the emission essence of carbon dots, various breakthrough have been achieved in recent years, but there are still some debates and challenges. Even through different emission models proposed by researchers may contribute to different kinds of carbon dots emission, the fine structure (*e.g.* for the self-trapped exciton emission[84], the bond geometry configuration, bond length, bond angle, and local potential distribution *etc.*) of the emission center is still a big issue. Thus more theoretical and experiment methods need to be employed to uncover the mystery of carbon dots emission.

Carbon dots based sensing platform may play a more important role in the future, especially for the bio-sensing. The discovery of ratiometric sensing and the demonstration of in vitro pH mapping imply the high potential for practical sensing applications. However, to compete with the commercial sensors, carbon dots based sensing should further improve the sensitivity, selectivity and robustness. And to achieve the in vivo sensing and mapping will be also the future development of carbon dots based bio-sensing. Sun's group[130] have demonstrated the potential to apply carbon dots into microfluidic platform. Considering the widespread applications, especially the bio-applications of microfluidic platform, we believe that bright fluorescent carbon dots will light up the micro-channels and facilitate more applications based on microfluidic system such as bio-assay, drug delivery, bio-system mimic and so on.

We want to highlight the discovery of chiral carbon dots. A very exciting news is that the chiral carbon dots based applications also start to appear, for example, chirality controlled enzyme activity, and cellular energy metabolism *etc*[171, 175, 176]. We predict that more and more chiral carbon dots based applications will appear in biology, catalysis, optic electronic, and sensing. However, at current stage, the chiral carbon dots only hold UV range CD signal, which is caused by the chiral molecular, thus one of the future directions is to explore chiral carbon dots which possess the visible and even near IR range CD signal. Another big issue for chiral carbon dots is the circular polarized emission. Circular polarization emission have wide applications such as chiral sensing, chiral drug discovery, flat panel display, quantum communications *etc*[163, 181-183]. While it's still difficult to achieve circular polarized emission from carbon dots, which hugely hinders the applications of chiral carbon dots, future research efforts shall be paid to address this issue.

In summary, researchers have achieved gratifying progress for carbon dots in both fundamental aspects and practical applications in recent years, even though there still exist some debates and challenges. We believe that this kind of novel nanomaterial hold bright future. Someday, carbon dots may replace some currently used fluorescent material in various fields such as bio-imaging, drug delivery, nanomedicine, bio-sensing, LEDs and so on. Besides these traditional fields, carbon dots may find its place in the current urgent and pressing fields such as green chemistry and clean energy production.

Conflicts of interest

There are no conflicts to declare.

Acknowledgement

This work was supported by Ministry of Education Singapore through the Academic Research Fund under Projects RG105/16 and RG189/17.

References

1. X. Xu, R. Ray, Y. Gu, H. J. Ploehn, L. Gearheart, K. Raker and W. A. Scrivens, *Journal of the American Chemical Society*, 2004, **126**, 12736-12737.
2. Y.-P. Sun, B. Zhou, Y. Lin, W. Wang, K. S. Fernando, P. Pathak, M. J. Meziani, B. A. Harruff, X. Wang and H. Wang, *Journal of the American Chemical Society*, 2006, **128**, 7756-7757.
3. Y. Wang, X. Li, J. Song, L. Xiao, H. Zeng and H. Sun, *Advanced materials*, 2015, **27**, 7101-7108.
4. Y. Wang, X. Li, X. Zhao, L. Xiao, H. Zeng and H. Sun, *Nano letters*, 2015, **16**, 448-453.
5. R. Hardman, *Environmental health perspectives*, 2006, **114**, 165.
6. J. Geys, A. Nemmar, E. Verbeken, E. Smolders, M. Ratoi, M. F. Hoylaerts, B. Nemery and P. H. Hoet, *Environmental health perspectives*, 2008, **116**, 1607.
7. S.-T. Yang, X. Wang, H. Wang, F. Lu, P. G. Luo, L. Cao, M. J. Meziani, J.-H. Liu, Y. Liu and M. Chen, *The Journal of Physical Chemistry C*, 2009, **113**, 18110-18114.
8. X. Huang, F. Zhang, L. Zhu, K. Y. Choi, N. Guo, J. Guo, K. Tackett, P. Anilkumar, G. Liu and Q. Quan, *ACS nano*, 2013, **7**, 5684-5693.
9. M. Fu, F. Ehrat, Y. Wang, K. Z. Milowska, C. Reckmeier, A. L. Rogach, J. K. Stolarczyk, A. S. Urban and J. Feldmann, *Nano letters*, 2015, **15**, 6030-6035.
10. R. Schmidt, C. Krasselt, C. Göhler and C. von Borczyskowski, *ACS nano*, 2014, **8**, 3506-3521.
11. S. K. Das, Y. Liu, S. Yeom, D. Y. Kim and C. I. Richards, *Nano letters*, 2014, **14**, 620-625.
12. Y. Choi, B. Kang, J. Lee, S. Kim, G. T. Kim, H. Kang, B. R. Lee, H. Kim, S.-H. Shim and G. Lee, *Chemistry of Materials*, 2016, **28**, 6840-6847.
13. F. Yuan, Z. Wang, X. Li, Y. Li, Z. a. Tan, L. Fan and S. Yang, *Advanced materials*, 2017, **29**.
14. S. Sahu, B. Behera, T. K. Maiti and S. Mohapatra, *Chemical Communications*, 2012, **48**, 8835-8837.
15. S. Dutta Choudhury, J. M. Chethodil, P. M. Gharat and H. Pal, *The Journal of Physical Chemistry Letters*, 2017, **8**, 1389-1395.
16. B. Zhu, S. Sun, Y. Wang, S. Deng, G. Qian, M. Wang and A. Hu, *Journal of Materials Chemistry C*, 2013, **1**, 580-586.
17. K. Jiang, S. Sun, L. Zhang, Y. Lu, A. Wu, C. Cai and H. Lin, *Angewandte Chemie International Edition*, 2015, **54**, 5360-5363.
18. J. Peng, W. Gao, B. K. Gupta, Z. Liu, R. Romero-Aburto, L. Ge, L. Song, L. B. Alemany, X. Zhan and G. Gao, *Nano letters*, 2012, **12**, 844-849.
19. H. Liu, T. Ye and C. Mao, *Angewandte Chemie International Edition*, 2007, **46**, 6473-6475.

20. S.-L. Hu, K.-Y. Niu, J. Sun, J. Yang, N.-Q. Zhao and X.-W. Du, *Journal of Materials Chemistry*, 2009, **19**, 484-488.
21. V. Strauss, J. T. Margraf, C. Dolle, B. Butz, T. J. Nacken, J. Walter, W. Bauer, W. Peukert, E. Spiecker and T. Clark, *Journal of the American Chemical Society*, 2014, **136**, 17308-17316.
22. S. Zhu, Q. Meng, L. Wang, J. Zhang, Y. Song, H. Jin, K. Zhang, H. Sun, H. Wang and B. Yang, *Angewandte Chemie*, 2013, **125**, 4045-4049.
23. L. Tang, R. Ji, X. Li, G. Bai, C. P. Liu, J. Hao, J. Lin, H. Jiang, K. S. Teng and Z. Yang, *ACS nano*, 2014, **8**, 6312-6320.
24. L. Bao, C. Liu, Z. L. Zhang and D. W. Pang, *Advanced Materials*, 2015, **27**, 1663-1667.
25. H. Ding, S.-B. Yu, J.-S. Wei and H.-M. Xiong, *Acs Nano*, 2015, **10**, 484-491.
26. L. Tang, R. Ji, X. Cao, J. Lin, H. Jiang, X. Li, K. S. Teng, C. M. Luk, S. Zeng and J. Hao, *ACS nano*, 2012, **6**, 5102-5110.
27. X. Meng, Q. Chang, C. Xue, J. Yang and S. Hu, *Chemical Communications*, 2017, **53**, 3074-3077.
28. D. Zhou, D. Li, P. Jing, Y. Zhai, D. Shen, S. Qu and A. L. Rogach, *Chemistry of Materials*, 2017, **29**, 1779-1787.
29. X. Wang, L. Cao, F. Lu, M. J. Meziani, H. Li, G. Qi, B. Zhou, B. A. Harruff, F. Kermarrec and Y.-P. Sun, *Chemical Communications*, 2009, 3774-3776.
30. L. Cao, X. Wang, M. J. Meziani, F. Lu, H. Wang, P. G. Luo, Y. Lin, B. A. Harruff, L. M. Veca and D. Murray, *Journal of the American Chemical Society*, 2007, **129**, 11318-11319.
31. J. Zhou, C. Booker, R. Li, X. Zhou, T.-K. Sham, X. Sun and Z. Ding, *Journal of the American Chemical Society*, 2007, **129**, 744-745.
32. H. Li, X. He, Z. Kang, H. Huang, Y. Liu, J. Liu, S. Lian, C. H. A. Tsang, X. Yang and S. T. Lee, *Angewandte Chemie International Edition*, 2010, **49**, 4430-4434.
33. Q.-L. Zhao, Z.-L. Zhang, B.-H. Huang, J. Peng, M. Zhang and D.-W. Pang, *Chemical Communications*, 2008, 5116-5118.
34. L. Bao, Z. L. Zhang, Z. Q. Tian, L. Zhang, C. Liu, Y. Lin, B. Qi and D. W. Pang, *Advanced Materials*, 2011, **23**, 5801-5806.
35. Y. Li, Y. Hu, Y. Zhao, G. Shi, L. Deng, Y. Hou and L. Qu, *Advanced materials*, 2011, **23**, 776-780.
36. R. Ye, C. Xiang, J. Lin, Z. Peng, K. Huang, Z. Yan, N. P. Cook, E. L. Samuel, C.-C. Hwang and G. Ruan, *Nature communications*, 2013, **4**, 2943.
37. A. B. Bourlinos, A. Stassinopoulos, D. Anglos, R. Zboril, M. Karakassides and E. P. Giannelis, *small*, 2008, **4**, 455-458.
38. M. J. Krysmann, A. Kelarakis, P. Dallas and E. P. Giannelis, *Journal of the American Chemical Society*, 2011, **134**, 747-750.
39. F. Wang, M. Kreiter, B. He, S. Pang and C.-y. Liu, *Chemical Communications*, 2010, **46**, 3309-3311.
40. X. Guo, C.-F. Wang, Z.-Y. Yu, L. Chen and S. Chen, *Chemical communications*, 2012, **48**, 2692-2694.
41. S.-S. Liu, C.-F. Wang, C.-X. Li, J. Wang, L.-H. Mao and S. Chen, *Journal of Materials Chemistry C*, 2014, **2**, 6477-6483.
42. H. G. Baldovi, S. Valencia, M. Alvaro, A. M. Asiri and H. Garcia, *Nanoscale*, 2015, **7**, 1744-1752.
43. S. Qu, D. Zhou, D. Li, W. Ji, P. Jing, D. Han, L. Liu, H. Zeng and D. Shen, *Advanced Materials*, 2016, **28**, 3516-3521.
44. D. Pan, J. Zhang, Z. Li, C. Wu, X. Yan and M. Wu, *Chemical Communications*, 2010, **46**, 3681-3683.
45. C. Zhu, M. Yan, X. Shi, J. Fan and H. Bi, *RSC Advances*, 2016, **6**, 38470-38474.
46. X. Teng, C. Ma, C. Ge, M. Yan, J. Yang, Y. Zhang, P. C. Morais and H. Bi, *Journal of Materials Chemistry B*, 2014, **2**, 4631-4639.

47. J. Chen, X. Zhang, Y. Zhang, W. Wang, S. Li, Y. Wang, M. Hu, L. Liu and H. Bi, *Langmuir*, 2017, **33**, 10259-10270.
48. Z.-C. Yang, M. Wang, A. M. Yong, S. Y. Wong, X.-H. Zhang, H. Tan, A. Y. Chang, X. Li and J. Wang, *Chemical communications*, 2011, **47**, 11615-11617.
49. B. De and N. Karak, *Rsc Advances*, 2013, **3**, 8286-8290.
50. L. Wang and H. S. Zhou, *Analytical chemistry*, 2014, **86**, 8902-8905.
51. P.-C. Hsu and H.-T. Chang, *Chemical communications*, 2012, **48**, 3984-3986.
52. D. Pan, J. Zhang, Z. Li and M. Wu, *Advanced materials*, 2010, **22**, 734-738.
53. K. i. Holá, M. Sudolská, S. Kalytchuk, D. Nachtigallová, A. L. Rogach, M. Otyepka and R. Zbořil, *ACS nano*, 2017, **11**, 12402-12410.
54. L. Wang, Y. Wang, T. Xu, H. Liao, C. Yao, Y. Liu, Z. Li, Z. Chen, D. Pan and L. Sun, *Nature communications*, 2014, **5**, 5357.
55. G. Ren, M. Tang, F. Chai and H. Wu, *European Journal of Inorganic Chemistry*, 2018, **2018**, 153-158.
56. H. Zhu, X. Wang, Y. Li, Z. Wang, F. Yang and X. Yang, *Chemical Communications*, 2009, 5118-5120.
57. X. Zhai, P. Zhang, C. Liu, T. Bai, W. Li, L. Dai and W. Liu, *Chemical Communications*, 2012, **48**, 7955-7957.
58. S. Chandra, P. Das, S. Bag, D. Laha and P. Pramanik, *Nanoscale*, 2011, **3**, 1533-1540.
59. S. Qu, X. Wang, Q. Lu, X. Liu and L. Wang, *Angewandte Chemie*, 2012, **124**, 12381-12384.
60. J. Jiang, Y. He, S. Li and H. Cui, *Chemical communications*, 2012, **48**, 9634-9636.
61. S. Sun, L. Zhang, K. Jiang, A. Wu and H. Lin, *Chemistry of Materials*, 2016, **28**, 8659-8668.
62. R. Liu, D. Wu, S. Liu, K. Koynov, W. Knoll and Q. Li, *Angewandte Chemie*, 2009, **121**, 4668-4671.
63. A. B. Bourlinos, A. Stassinopoulos, D. Anglos, R. Zboril, V. Georgakilas and E. P. Giannelis, *Chemistry of Materials*, 2008, **20**, 4539-4541.
64. B. Wang, Y. Mu, H. Yin, Z. Yang, Y. Shi and J. Li, *Nanoscale*, 2018, **10**, 10650-10656.
65. Z. G. Gu, D. J. Li, C. Zheng, Y. Kang, C. Wöll and J. Zhang, *Angewandte Chemie International Edition*, 2017, **56**, 6853-6858.
66. H. Xu, S. Zhou, L. Xiao, H. Wang, S. Li and Q. Yuan, *Journal of Materials Chemistry C*, 2015, **3**, 291-297.
67. A. J. Amali, H. Hoshino, C. Wu, M. Ando and Q. Xu, *Chemistry-A European Journal*, 2014, **20**, 8279-8282.
68. Y. Yang, D. Wu, S. Han, P. Hu and R. Liu, *Chemical Communications*, 2013, **49**, 4920-4922.
69. T. Huang, T. Wu, Z. Zhu, L. Zhao, H. Ci, X. Gao, K. Liu, J. Zhao, J. Huang and Y. Yan, *Chemical Communications*, 2018.
70. N. Liu, J. Liu, W. Kong, H. Li, H. Huang, Y. Liu and Z. Kang, *Journal of Materials Chemistry B*, 2014, **2**, 5768-5774.
71. C. T. Chien, S. S. Li, W. J. Lai, Y. C. Yeh, H. A. Chen, I. S. Chen, L. C. Chen, K. H. Chen, T. Nemoto and S. Isoda, *Angewandte Chemie International Edition*, 2012, **51**, 6662-6666.
72. L. Wang, S.-J. Zhu, H.-Y. Wang, S.-N. Qu, Y.-L. Zhang, J.-H. Zhang, Q.-D. Chen, H.-L. Xu, W. Han and B. Yang, *ACS nano*, 2014, **8**, 2541-2547.
73. Y. Dong, H. Pang, H. B. Yang, C. Guo, J. Shao, Y. Chi, C. M. Li and T. Yu, *Angewandte Chemie International Edition*, 2013, **52**, 7800-7804.
74. Y. Chen, H. Lian, Y. Wei, X. He, Y. Chen, B. Wang, Q. Zeng and J. Lin, *Nanoscale*, 2018, **10**, 6734-6743.
75. S. Zhu, J. Zhang, X. Liu, B. Li, X. Wang, S. Tang, Q. Meng, Y. Li, C. Shi and R. Hu, *Rsc Advances*, 2012, **2**, 2717-2720.

76. F. Ehrat, S. Bhattacharyya, J. Schneider, A. Löf, R. Wyrwich, A. L. Rogach, J. K. Stolarczyk, A. S. Urban and J. Feldmann, *Nano letters*, 2017, **17**, 7710-7716.
77. S. Khan, A. Gupta, N. C. Verma and C. K. Nandi, *Nano letters*, 2015, **15**, 8300-8305.
78. E. v. Lippert, *Zeitschrift für Elektrochemie, Berichte der Bunsengesellschaft für physikalische Chemie*, 1957, **61**, 962-975.
79. N. Mataga, Y. Kaifu and M. Koizumi, *Bulletin of the Chemical Society of Japan*, 1956, **29**, 465-470.
80. N. Nemkovich, A. Rubinov and V. Tomin, *Journal*, 1991.
81. J. Lakowicz, *New York*, 1999.
82. A. Sciortino, E. Marino, B. v. Dam, P. Schall, M. Cannas and F. Messina, *The journal of physical chemistry letters*, 2016, **7**, 3419-3423.
83. C. J. Reckmeier, Y. Wang, R. Zboril and A. L. Rogach, *The Journal of Physical Chemistry C*, 2016, **120**, 10591-10604.
84. L. Xiao, Y. Wang, Y. Huang, T. Wong and H. Sun, *Nanoscale*, 2017, **9**, 12637-12646.
85. B. P. Zakharchenya, D. N. Mirlin, V. Perel' and I. Reshina, *Physics-Uspekhi*, 1982, **25**, 143-166.
86. V. Dymnikov, D. Mirlin, L. Nikitin, V. Perel, I. Reshina and V. Sapega, *Zh. Eksp. Teor. Fiz*, 1981, **80**, 1766-1778.
87. V. Dymnikov, M. D'yakonov and N. Perel, *Soviet Journal of Experimental and Theoretical Physics*, 1976, **44**, 1252.
88. H. Koyama, T. Oguro and N. Koshida, *Applied physics letters*, 1993, **62**, 3177-3179.
89. S. Kazaoui, R. Ross and N. Minami, *Physical Review B*, 1995, **52**, R11665.
90. C. Itoh, K. Tanimura and N. Itoh, *Journal of Physics C: Solid State Physics*, 1988, **21**, 4693.
91. M. Matus, H. Kuzmany and E. Sohmen, *Physical review letters*, 1992, **68**, 2822.
92. D. Emin, *Journal of Non-Crystalline Solids*, 1980, **35**, 969-973.
93. S. Ghosh, A. M. Chizhik, N. Karedla, M. O. Dekaliuk, I. Gregor, H. Schuhmann, M. Seibt, K. Bodensiek, I. A. Schaap and O. Schulz, *Nano letters*, 2014, **14**, 5656-5661.
94. A. I. Chizhik, A. M. Chizhik, D. Khoptyar, S. Bär and A. J. Meixner, *Nano letters*, 2011, **11**, 1131-1135.
95. T. Schmidt, A. I. Chizhik, A. M. Chizhik, K. Potrick, A. J. Meixner and F. Huisken, *Physical Review B*, 2012, **86**, 125302.
96. A. I. Chizhik, A. M. Chizhik, A. Huss, R. Jäger and A. J. Meixner, *The Journal of Physical Chemistry Letters*, 2011, **2**, 2152-2157.
97. A. P. Demchenko and M. O. Dekaliuk, *Nanoscale*, 2016, **8**, 14057-14069.
98. M. Kasha, H. Rawls and M. A. El-Bayoumi, *Pure and Applied Chemistry*, 1965, **11**, 371-392.
99. F. Würthner, T. E. Kaiser and C. R. Saha‐Möller, *Angewandte Chemie International Edition*, 2011, **50**, 3376-3410.
100. U. Rösch, S. Yao, R. Wortmann and F. Würthner, *Angewandte Chemie*, 2006, **118**, 7184-7188.
101. J. Gierschner, L. Lüer, B. a. Milián-Medina, D. Oelkrug and H.-J. Egelhaaf, *The Journal of Physical Chemistry Letters*, 2013, **4**, 2686-2697.
102. C. J. Reckmeier, J. Schneider, Y. Xiong, J. Häusler, P. Kasák, W. Schnick and A. L. Rogach, *Chemistry of Materials*, 2017.
103. A. Sharma, T. Gadly, A. Gupta, A. Ballal, S. K. Ghosh and M. Kumbhakar, *The journal of physical chemistry letters*, 2016, **7**, 3695-3702.
104. A. Sharma, T. Gadly, S. Neogy, S. K. Ghosh and M. Kumbhakar, *The journal of physical chemistry letters*, 2017, **8**, 1044-1052.
105. J. Zhang, L. Yang, Y. Yuan, J. Jiang and S.-H. Yu, *Chemistry of Materials*, 2016, **28**, 4367-4374.
106. Y. Malyukin, O. Viagin, P. Maksimchuk, M. Dekaliuk and A. Demchenko, *Nanoscale*, 2018, **10**, 9320-9328.

107. Y. Xu, Y.-H. Li, Y. Wang, J.-L. Cui, X.-B. Yin, X.-W. He and Y.-K. Zhang, *Analyst*, 2014, **139**, 5134-5139.
108. S.-T. Yang, L. Cao, P. G. Luo, F. Lu, X. Wang, H. Wang, M. J. Meziani, Y. Liu, G. Qi and Y.-P. Sun, *Journal of the American Chemical Society*, 2009, **131**, 11308-11309.
109. H. Zhang, B. Zhang, C. Di, M. C. Ali, J. Chen, Z. Li, J. Si, H. Zhang and H. Qiu, *Nanoscale*, 2018, **10**, 5342-5349.
110. F. Jia, S. Lv and S. Xu, *RSC Advances*, 2017, **7**, 53532-53536.
111. Y. Zhang, X. Liu, Y. Fan, X. Guo, L. Zhou, Y. Lv and J. Lin, *Nanoscale*, 2016, **8**, 15281-15287.
112. L. Pan, S. Sun, L. Zhang, K. Jiang and H. Lin, *Nanoscale*, 2016, **8**, 17350-17356.
113. Q. Liu, B. Guo, Z. Rao, B. Zhang and J. R. Gong, *Nano letters*, 2013, **13**, 2436-2441.
114. J. Liu, D. Li, K. Zhang, M. Yang, H. Sun and B. Yang, *Small*, 2018, 1703919.
115. L. Di, J. Pengtao, S. Lihuan, A. Yang, S. Xinyan, L. Xinghua, Z. Ding, H. Dong, S. Dezhen, Z. Yuechen, Q. Songnan, Z. Radek and R. A. L., *Advanced Materials*, 2018, **30**, 1705913.
116. H. S. Choi, W. Liu, P. Misra, E. Tanaka, J. P. Zimmer, B. I. Ipe, M. G. Bawendi and J. V. Frangioni, *Nature biotechnology*, 2007, **25**, 1165.
117. J. Chen, S. Li, Y. Zhang, W. Wang, X. Zhang, Y. Zhao, Y. Wang and H. Bi, *Advanced healthcare materials*, 2017, **6**, 1700746.
118. W.-Q. Li, Z. Wang, S. Hao, L. Sun, M. Nisic, G. Cheng, C. Zhu, Y. Wan, L. Ha and S.-Y. Zheng, *Nanoscale*, 2018, **10**, 3744-3752.
119. H. Wang, C. Liu, Z. Liu, J. Ren and X. Qu, *Small*, 2018, **14**, 1703710.
120. H.-J. Jian, R.-S. Wu, T.-Y. Lin, Y.-J. Li, H.-J. Lin, S. G. Harroun, J.-Y. Lai and C.-C. Huang, *ACS nano*, 2017, **11**, 6703-6716.
121. J. Tang, B. Kong, H. Wu, M. Xu, Y. Wang, Y. Wang, D. Zhao and G. Zheng, *Advanced materials*, 2013, **25**, 6569-6574.
122. Q. Wang, X. Huang, Y. Long, X. Wang, H. Zhang, R. Zhu, L. Liang, P. Teng and H. Zheng, *Carbon*, 2013, **59**, 192-199.
123. M. Zheng, S. Liu, J. Li, D. Qu, H. Zhao, X. Guan, X. Hu, Z. Xie, X. Jing and Z. Sun, *Advanced Materials*, 2014, **26**, 3554-3560.
124. T. Feng, X. Ai, G. An, P. Yang and Y. Zhao, *ACS nano*, 2016, **10**, 4410-4420.
125. Y. Huang, Y. Wang and T. Wong, *Lab on a Chip*, 2017, **17**, 2969-2981.
126. Y. Huang, J. Chen, T. Wong and J.-L. Liow, *Soft Matter*, 2016, **12**, 6206-6213.
127. J. Atencia and D. J. Beebe, *Nature*, 2004, **437**, 648.
128. M. P. Stewart, A. Sharei, X. Ding, G. Sahay, R. Langer and K. F. Jensen, *Nature*, 2016, **538**, 183.
129. H. Song, D. L. Chen and R. F. Ismagilov, *Angewandte chemie international edition*, 2006, **45**, 7336-7356.
130. Y. Huang, L. Xiao, T. An, W. Lim, T. Wong and H. Sun, *Small*, 2017, **13**.
131. H. Lin, B. D. Storey, M. H. Oddy, C.-H. Chen and J. G. Santiago, *Physics of Fluids*, 2004, **16**, 1922-1935.
132. W. Kwon, Y.-H. Kim, C.-L. Lee, M. Lee, H. C. Choi, T.-W. Lee and S.-W. Rhee, *Nano letters*, 2014, **14**, 1306-1311.
133. Z. Luo, G. Qi, K. Chen, M. Zou, L. Yuwen, X. Zhang, W. Huang and L. Wang, *Advanced Functional Materials*, 2016, **26**, 2739-2744.
134. F. Yuan, T. Yuan, L. Sui, Z. Wang, Z. Xi, Y. Li, X. Li, L. Fan, A. Chen and M. Jin, *Nature communications*, 2018, **9**, 2249.
135. Z. Zhou, P. Tian, X. Liu, S. Mei, D. Zhou, D. Li, P. Jing, W. Zhang, R. Guo and S. Qu, *Advanced Science*, 2018, 1800369.
136. F. Wang, Y.-h. Chen, C.-y. Liu and D.-g. Ma, *Chemical Communications*, 2011, **47**, 3502-3504.

137. X. Zhang, Y. Zhang, Y. Wang, S. Kalytchuk, S. V. Kershaw, Y. Wang, P. Wang, T. Zhang, Y. Zhao and H. Zhang, *ACS nano*, 2013, **7**, 11234-11241.
138. Y.-L. Zhang, L. Wang, H.-C. Zhang, Y. Liu, H.-Y. Wang, Z.-H. Kang and S.-T. Lee, *Rsc Advances*, 2013, **3**, 3733-3738.
139. H. X. Zhao, L. Q. Liu, Z. De Liu, Y. Wang, X. J. Zhao and C. Z. Huang, *Chemical Communications*, 2011, **47**, 2604-2606.
140. X. Lu, J. Zhang, Y.-N. Xie, X. Zhang, X. Jiang, X. Hou and P. Wu, *Analytical chemistry*, 2018, **90**, 2939-2945.
141. T.-H. Chen and W.-L. Tseng, *Analytical chemistry*, 2017, **89**, 11348-11356.
142. X. Jin, X. Sun, G. Chen, L. Ding, Y. Li, Z. Liu, Z. Wang, W. Pan, C. Hu and J. Wang, *Carbon*, 2015, **81**, 388-395.
143. H. Nie, M. Li, Q. Li, S. Liang, Y. Tan, L. Sheng, W. Shi and S. X.-A. Zhang, *Chemistry of Materials*, 2014, **26**, 3104-3112.
144. A. Chandra and N. Singh, *Chemical Communications*, 2018.
145. W. Song, W. Duan, Y. Liu, Z. Ye, Y. Chen, H. Chen, S. Qi, J. Wu, D. Liu and L. Xiao, *Analytical chemistry*, 2017, **89**, 13626-13633.
146. J. S. Sidhu, A. Singh, N. Garg, N. Kaur and N. Singh, *Analyst*, 2018, **143**, 1853-1861.
147. B. B. Chen, M. L. Liu, L. Zhan, C. M. Li and C. Z. Huang, *Analytical chemistry*, 2018.
148. L.-L. Feng, Y.-X. Wu, D.-L. Zhang, X.-X. Hu, J. Zhang, P. Wang, Z.-L. Song, X.-B. Zhang and W. Tan, *Analytical chemistry*, 2017, **89**, 4077-4084.
149. S. Qu, H. Chen, X. Zheng, J. Cao and X. Liu, *Nanoscale*, 2013, **5**, 5514-5518.
150. S. Kalytchuk, K. i. Poláková, Y. Wang, J. P. Froning, K. Cepe, A. L. Rogach and R. Zboril, *ACS nano*, 2017, **11**, 1432-1442.
151. H. K. Sadhanala, S. Senapati and K. K. Nanda, *Carbon*, 2018, **133**, 200-208.
152. W. Shi, X. Li and H. Ma, *Angewandte Chemie*, 2012, **124**, 6538-6541.
153. X. Sun, C. Brückner and Y. Lei, *Nanoscale*, 2015, **7**, 17278-17282.
154. J. Shangguan, D. He, X. He, K. Wang, F. Xu, J. Liu, J. Tang, X. Yang and J. Huang, *Analytical chemistry*, 2016, **88**, 7837-7843.
155. P. A. de Silva, N. H. Gunaratne and C. P. McCoy, *Nature*, 1993, **364**, 42.
156. L. Feng, A. Zhao, J. Ren and X. Qu, *Nucleic acids research*, 2013, **41**, 7987-7996.
157. M. P. Sk, S. K. Sailapu and A. Chattopadhyay, *ChemPhysChem*, 2015, **16**, 723-727.
158. C. Shen, Y. Zhao, H. Liu, Y. Jiang, N. Li, S. Lan, H. Bao, B. Yang and Q. Lin, *Polymer Chemistry*, 2018.
159. N. Dhenadhayalan and K.-C. Lin, *Scientific reports*, 2015, **5**, 10012.
160. W.-S. Zou, Q.-C. Zhao, W.-L. Kong, X.-F. Wang, X.-M. Chen, J. Zhang and Y.-Q. Wang, *Chemical Engineering Journal*, 2017.
161. M. Li, Z. Wang, J. Liang, H. Yao, L. Shen, H. Liu and L. Fan, *Nanoscale*, 2018.
162. J. Deng, Z. Tao, Y. Liu, X. Lin, P. Qian, Y. Lyu, Y. Li, K. Fu and S. Wang, *Chemical Communications*, 2018, **54**, 3110-3113.
163. F. P. Milton, J. Govan, M. V. Mukhina and Y. K. Gun'ko, *Nanoscale Horizons*, 2016, **1**, 14-26.
164. X.-L. Liu, S. Tsunega and R.-H. Jin, *Nanoscale Horizons*, 2017, **2**, 147-155.
165. R. Walker, D. Pociecha, J. Abberley, A. Martinez-Felipe, D. Paterson, E. Forsyth, G. Lawrence, P. Henderson, J. Storey and E. Gorecka, *Chemical Communications*, 2018, **54**, 3383-3386.
166. M. Vázquez-Nakagawa, L. Rodríguez-Pérez, M. Herranz and N. Martín, *Chemical Communications*, 2016, **52**, 665-668.
167. C. B. Kc, G. N. Lim and F. D'Souza, *Angewandte Chemie International Edition*, 2015, **54**, 5088-5092.

168. R. J. Chen, Y. Zhang, D. Wang and H. Dai, *Journal of the American Chemical Society*, 2001, **123**, 3838-3839.
169. E. M. Pérez and N. Martín, *Chemical Society Reviews*, 2015, **44**, 6425-6433.
170. N. Suzuki, Y. Wang, P. Elvati, Z.-B. Qu, K. Kim, S. Jiang, E. Baumeister, J. Lee, B. Yeom and J. H. Bahng, *ACS nano*, 2016, **10**, 1744-1755.
171. F. Li, Y. Li, X. Yang, X. Han, Y. Jiao, T. Wei, D. Yang, H. Xu and G. Nie, *Angewandte Chemie International Edition*, 2018, **57**, 2377-2382.
172. Y. Zhang, L. Hu, Y. Sun, C. Zhu, R. Li, N. Liu, H. Huang, Y. Liu, C. Huang and Z. Kang, *RSC Advances*, 2016, **6**, 59956-59960.
173. M. J. Deka and D. Chowdhury, *RSC Advances*, 2017, **7**, 53057-53063.
174. A. Ghosh, B. Parasar, T. Bhattacharyya and J. Dash, *Chemical Communications*, 2016, **52**, 11159-11162.
175. Q. Xin, Q. Liu, L. Geng, Q. Fang and J. R. Gong, *Advanced healthcare materials*, 2017, **6**,1601011.
176. L. Hu, H. Li, C. a. Liu, Y. Song, M. Zhang, H. Huang, Y. Liu and Z. Kang, *Nanoscale*, 2018,**10**,2333.
177. R. Butbul, S. Bhunia, S. Shaham-Niv, S. Kolusheva, E. Gazit and R. Jelinek, *Chemical Communications*, 2018, **54**.7762-7765.
178. S. Y. Lim, W. Shen and Z. Gao, *Chemical Society Reviews*, 2015, **44**, 362-381.
179. T. A. Waldmann, *Nature medicine*, 2003, **9**, 269.
180. N. Murthy, Y. X. Thng, S. Schuck, M. C. Xu and J. M. Frechet, *Journal of the American Chemical Society*, 2002, **124**, 12398-12399.
181. Y. Wang, X. Li, F. Li, W.-Y. Sun, C. Zhu and Y. Cheng, *Chemical Communications*, 2017, **53**, 7505-7508.
182. E. M. Sánchez-Carnerero, F. Moreno, B. L. Maroto, A. R. Agarrabeitia, M. J. Ortiz, B. G. Vo, G. Muller and S. d. l. Moya, *Journal of the American Chemical Society*, 2014, **136**, 3346-3349.
183. J. Han, P. Duan, X. Li and M. Liu, *Journal of the American Chemical Society*, 2017, **139**, 9783-9786.